UNIVERSIDAD **N**ACIONAL **A**UTÓNOMA DE **M**ÉXICO

PROGRAMA DE POSGRADO EN

CIENCIAS DE LA TIERRA

INSTITUTO DE GEOFISICA

LA CORDILLERA DE TEHUANTEPEC COMO UN LIMITE TECTÓNICO ENTRE EL NORTE DE LA PLACA DE COCOS Y LA CUENCA DE GUATEMALA: ESTRUCTURA Y ORIGEN

TESIS

Para obtener el grado de

DOCTORA EN GEOFÍSICA

(SISMOLOGÍA Y FÍSICA DEL INTERIOR DE LA TIERRA)

PRESENTA

Marina Manea

2004

A Dr. Vladimir Kostoglodov,

por todo el apoyo que me ha brindado desde mi llegada al

Departamento de Sismología

y

por haber puesto su confianza en mí.

Gracias por su amistad.

Agradecimientos

Agradezco a los coordinadores del programa de Posgrado, Drs. Blanca Mendoza Ortega y Oscar Campos-Enríquez, por todo el apoyo que me otorgaron.

Agradezco a mi comité de sinodales quienes lograron enriquecer este trabajo con sus comentarios muy atinados, a los Drs. Osvaldo Sánchez Zamora, Marco Guzmán Speziale, William Bandy, Luca Ferrari Pedraglio y Joann Stock.

Muchas gracias al Dr. Singh Krishna Singh por todo su apoyo que me ofreció a lo largo de todo el tiempo pasado en el Departamento de Sismología. Asimismo, quiero agradecer al Dr. Raúl Valenzuela Wong por todo su soporte que me brindo.

Quiero agradecer especialmente a la Dra. Joann Stock por todo su apoyo en la redacción de la tesis y para todas sus sugerencias que me ayudaron a mejorar la calidad del manuscrito.

Gracias a la beca que me otorgo la DGEP y al apoyo que me otorgaron PAEP, CONACYT (G25842-T, 37293-T), y PAPIIT (IN104801) pude finalmente concluir el doctorado con este trabajo de investigación.

Muchas gracias a Dr. Carlos Mortera Gutiérrez por todo el apoyo que me brindó y por su amistad.

Muchas gracias a Drs. Carlos Valdez y Raúl Valenzuela Wang por todo el apoyo y los buenos consejos que me dieron.

Muchas gracias a Dr. Arturo Iglesias que estuvo siempre cerca como buen compañero y amigo. Muchas gracias a ing. Manuel Velásquez por todo su apoyo en todos los problemas técnicos que ocurrieron y por su amistad.

Agradezco a Araceli y a Mónica del Posgrado en Ciencias de la Tierra y a Paty y Adriana del Departamento de Sismología, por toda su ayuda con los tramites burocráticos.

Sinceramente me siento afortunado por haber tenido la oportunidad de estudiar en el Posgrado en Ciencias de la Tierra de la UNAM y por haber convivido con excelentes profesores y compañeros.

INDICE

Resumen 1

I. Introducción 4

II. El relleno sedimentario de la trinchera Mesoamericana inferido de las anomalías de gravedad

Sediment fill in the Middle America trench inferred from gravity anomalies 18

III. Espesor elástico debajo de la cordillera de Tehuantepec

Elastic thickness of the Tehuantepec Ridge ……... 56

IV. ¿Es la cordillera de Tehuantepec una estructura compresional?

Tehuantepec Ridge: a compressional structure 87

V. Discusiones y Conclusiones 129

RESUMEN

Se utilizó una secuencia de perfiles de la anomalía de gravedad de aire libre a través de la Trinchera de Mesoamérica para modelar el relleno sedimentario de las facies sedimentarias no consolidadas pelágicas y hemipelágicas y del material parcialmente alterado del basamento. La diferencia entre los mínimos gravimétricos y batimétricos se utilizó en la estimación de la cantidad de los sedimentos de baja densidad. El efecto de la gravedad del relleno es relativamente pequeño, sugiriendo que el proceso mayor en la Trinchera de Mesoamérica es la subducción de sedimentos y el raspar de los sedimentos pelágicos desde la cima de la placa oceánica subducida. El volumen de los sedimentos en la trinchera tiende a incrementarse hacia el sur desde Jalisco hacia Oaxaca. Esta tendencia está menos evidente en la Cuenca de Guatemala. Hay una cierta correlación entre el monto del relleno sedimentario fresco y la velocidad de convergencia a la trinchera, excepto para los perfiles con una contribución terrígena de sedimentos o para las áreas de subducción de las entidades batimétricas importantes.

A continuación, se analizó la relación entre la batimetría y la anomalía de gravedad de aire libre, por medio del método de la admitancia para 7 perfiles que cruzan la Cordillera de Tehuantepec. La evaluación de la edad de la litosfera para el tiempo cuando se formó la Cordillera de Tehuantepec se calculó a través de los análisis de la admitancia experimental y del espesor elástico. Se calculó la admitancia, interpretada en términos del espesor elástico isotrópico de la placa de

Cocos debajo de la Cordillera de Tehuantepec. El modelo de compensación isostática más apropiado para ajustar los datos observados es el de una litosfera oceánica que se comporta como una placa elástica con un espesor de 10 $\pm$ 5 km. La forma de la admitancia (con valores bajos para longitudes de onda grandes) sugiere que la cordillera está compensada isostáticamente. La relación entre la edad de la litosfera oceánica y el espesor elástico para una temperatura de corte de 450 °C, da una estimación de ~ 8 +9/-6 Ma para el momento de formación de la Cordillera de Tehuantepec sobre la placa de Cocos.

A pesar del hecho de que la Cordillera de Tehuantepec es una de las más importantes entidades litosféricas sobre la placa de Cocos, su edad y mecanismo de formación han sido poco restringidos hasta ahora. Con base en un análisis morfo-estructural de la Cordillera y de la Cuenca de Guatemala y en las relaciones geodinámicas, en este estudio se proponen dos modelos genéticos para la Cordillera de Tehuantepec: uno que plantea la ideea de que la Cordillera de Tehuantepec se formó debido a los procesos de transpresión entre dos zonas de la placa de Cocos suponiendo que haya existido una tercer microplaca y el otro que da un modelo alternativo que prueba la respuesta de la zona de fractura a los cambios en el polo de rotación de Euler sin considerar una tercera microplaca.

El primer modelo propone que una disminución en la tasa de expansión en la Dorsal del Pacífico Este, al sur de la zona de fractura de Clipperton pudo haber determinado la formación de la cordillera. Esta disminución propuesta para el periodo después de ~ 12 - 14 Ma ha conducido a una deformación transpresional

a lo largo de la zona de fractura, resultando la Cordillera de Tehuantepec. El secundo modelo está basado en un análisis de unas estructuras similares con las estructuras asociadas a la cordillera de Tehuantepec, ubicadas a lo largo de la zona de fractura Kane, en el Océano Atlántico. Se supone que estas estructuras se formaron como parte de la respuesta a un cambio drástico en el movimiento relativo de las placas.

I. INTRODUCCIÓN

Una de las estructuras más importantes en la placa de Cocos es la Cordillera de Tehuantepec. Esta cordillera se considera similar a otras grandes zonas de fractura que se encuentran en el noreste del Pacífico (*Menard y Fisher, 1958*) y forma un borde estructural mayor sobre la placa de Cocos, separándola en dos regiones tectónicamente distintas (*DSDP 66 y 84; Manea et al., 2003*).

Hasta la fecha no se ha hecho una evaluación de los volúmenes de sedimentos ubicados a lo largo de toda la trinchera mesoamericana en México. Este estudio es muy importante para el estudio de la dinámica de los sedimentos pelágicos asociados al proceso de subducción, así como para conocer el cambio de las condiciones tectónicas a lo largo de la trinchera asociadas a la presencia de la cordillera de Tehuantepec sobre la placa de Cocos.

La Trinchera de Mesoamérica es aproximadamente paralela a la costa por más de 2,600 km, desde Jalisco hasta Costa Rica. La trinchera está asociada con mínimos gravimétricos y batimétricos. La parte norte de esta sección de la trinchera está separada de su parte sur más profunda por la Cordillera de Tehuantepec, que intercepta la trinchera cerca de 15˚N, 95˚W (*Menard y Fisher, 1958*). Al sur, la trinchera termina en la cordillera de Cocos.

La profundidad de la trinchera varía entre 4,500 y 6,500 m. Al noroeste de la Cordillera de Tehuantepec la trinchera es menos profunda que en la cuenca de Guatemala con ~ 1,000 m. En general, al noroeste de Acapulco, el perfil de la trinchera muestra una forma de U, con pendientes más pronunciadas hacia el

continente y con un basamento más comprimido, debido al relleno sedimentario (*Fisher, 1961*). Entre Acapulco y la Cordillera de Tehuantepec, la trinchera está dividida y forma una secuencia de cuencas profundas hasta 5,000 m. Al sureste de la Cordillera de Tehuantepec, la trinchera es más larga y más profunda hasta profundidades de 6,400 m en la parte oeste de la cuenca de Guatemala. En esta región, la forma de la trinchera, en sección es en "V". Asimismo se observa una asimetría y una batimetría irregulares. Estas entidades morfológicas pueden implicar que los montos de sedimentos en las regiones en forma de "V" sean más bajos que en las regiones en forma de "U" (*Fisher, 1961; Moore, 1981*).

Los estudios del relleno sedimentario para la parte norte de la trinchera son limitados (por ejemplo, *Ross, 1971, Renard et al., 1980, Mercier de Lépinay et al., 1997*). El proyecto de Deep Sea Drilling (DSDP) y el programa de Ocean Drilling (ODP) se restringen para algunas perforaciones en México y Guatemala a lo largo de la trinchera (*Underwood y Moore, 1995*). La velocidad de sedimentación observada en la pendiente de la trinchera hacia el continente (*DSDP sitio 486,* en frente de Acapulco) es de 1.46 km/Ma (*Ross, 1971*). Esto no es suficiente para mantener un equilibrio dinámico en la zona de subducción (*Mountney, 1997*).

Renard et al. (1980) observaron una serie de escarpes lineales, oblicuos a la trinchera. Las mediciones de multi-beam echo-sounder muestran que estos escarpes son paralelos a las líneas de las anomalías magnéticas, lo cuál se ha interpretado como fallas heredadas de la dorsal del Pacífico este y reactivadas en tanto se acercaron a la trinchera. La estimación del espesor máximo de los

sedimentos es ~ 400 m (*Renard et al., 1980*). No hay evidencia de acreción de sedimentos en la trinchera.

Hilde (1983) muestra que el modelo de graben es más desarrollado en la trinchera sobre la pendiente hacia el mar. Esto está de acuerdo con las observaciones previas de *Fisher (1961), Fisher y Hess (1963),* y *Renard et al. (1980). Hilde (1983)* considera que la subducción de sedimentos prevalece a la acreción para todas las zonas de subducción de la región circum-Pacífica.

Este estudio tiene sus orígenes en la observación de que los mínimos gravimétricos (típicos para las trincheras oceánicas profundas) no coinciden con los mínimos batimétricos a lo largo del eje de la trinchera. *Talwani (1968)* hizo esta observación para las anomalías de gravedad que cruzan las trincheras de las Aleutianas y de Japón. A lo largo de toda la trinchera de Mesoamérica, el mínimo gravimétrico está sobre la pendiente de la trinchera hacia el continente. La diferencia entre los mínimos batimétricos y gravimétricos sugiere que haya un relleno sedimentario de baja densidad, que puede ser estimado en algunos casos por el modelado gravimétrico. El propósito de este estudio es hallar una estimación de la cantidad de sedimentos acumulados y su distribución a lo largo de la Trinchera de Mesoamérica. Estas estimaciones son importantes, por ejemplo, en los estudios de la tectónica de la subducción y el balance de los sedimentos, el acoplamiento entre placas, el modelado térmico en las zonas de subducción, los terremotos tsunamigénicos de baja frecuencia, así como para ver el cambio de las condiciones tectónicas a lo largo de la trinchera asociadas a la presencia de la cordillera de Tehuantepec sobre la placa de Cocos.

El origen de la cordillera de Tehuantepec y su edad de formación son desconocidos. Pocos autores han intentado explicar el origen de la cordillera de Tehuantepec. Aunque *Klitgord y Mammerickx (1982)* propusieron una diferencia de edad entre las dos áreas separadas por la cordillera de Tehuantepec de ~ 12 Ma, la baja amplitud de las anomalías magnéticas en la Cuenca de Guatemala (*Anderson, 1974*) han hecho difícil la determinación de una edad confiable para la corteza. *Wilson (1996)* mencionó una diferencia de ~ 8 Ma, usando un fechamiento paleontológico par la identificación de las anomalías, mientras *Couch y Woodcock (1981)* dan una diferencia de ~ 10 Ma. Determinaciones de la edad de la placa de Cocos en la trinchera mesoamericana cerca de la cordillera de Tehuantepec han sido hechas por *Kanjorski (2003*), que obtuvo una edad de ~ 16 Ma para la parte noroeste, arriba de la cordillera. Otras estimaciones de la edad a lo largo de la trinchera han sido obtenidas por *Barckhausen (2001*), que calculó una edad de ~ 24 Ma para la placa de Cocos a lo largo de la trinchera, enfrente de Costa Rica. Estas estimaciones se utilizaron en este estudio para restringir la estimación de la edad en la trinchera a partir del modelo de enfriamiento de la placa oceánica con la edad (*Turcotte y Schubert, 2002*) y el modelo de *Gorbatov et al. (1997)*. Otras restricciones para la estimación de la edad en la cuenca de Guatemala vienen de *Wilson (1996*).

Una hipótesis acerca del origen de la cordillera de Tehuantepec viene de *Herron (1972),* que la considera como la traza de un “punto caliente”. La morfología asimétrica de la Cordillera de Tehuantepec sugiere que esta entidad tiene un origen tectónico más que volcánico. *Truchan y Larson (1973)* consideran

la cordillera como una falla de tijera que separa la placa de Cocos subducida debajo de la placa de Norteamérica al noroeste de la placa de Cocos subducida bajo la placa de Caribe al sureste. Otros estudios sismológicos (*Ponce et al., 1992; Bravo et al., 2004*) favorecen esta interpretación mostrando que la placa de Cocos aumenta su buzamiento hasta 45° y que la profundidad de los terremotos alcanza ~ 270 km al este de la intersección entre la cordillera de Tehuantepec y la trinchera de Mesoamérica. De todos modos, la ausencia de sismicidad descarta la posibilidad de que la cordillera sea producto de algún proceso de deformación continua. Un estudio de *Schilt et al. (1982)* sugiere que la cordillera de Tehuantepec se inició como una zona transformante dorsal-dorsal que pudo haber creado la zona de fractura de Clipperton.

El trabajo de *Couch y Woodcock (1981)* para esta área muestra una diferencia, entre las dos regiones, que define la forma de la cordillera sobre la placa de Cocos: la noroeste parece más antigua y más gruesa que la de sureste. Para esto, usaron un modelado gravimétrico sobre un perfil que cruza la cordillera. De todos modos, su modelo no está de acuerdo con la edad estimada para la placa de Cocos en la cuenca de Guatemala, usando la relación entre la profundidad del océano y la edad (*Parsons y Sclater, 1977*): la placa de Cocos subducida bajo la placa de Caribe es más vieja, más fría y por tanto más gruesa que la parte de la placa de Cocos subducida debajo de la placa de Norteamérica.

En este estudio se propone un mecanismo probable y una edad aproximada para la formación de la cordillera de Tehuantepec. Se hizo una interpretación gravimétrica, usándo un perfil promedio que cruza la cordillera y la

estructura ha sido analizada por el medio de las técnicas de la admitancia para inferir el espesor elástico de la placa oceánica debajo de la Cordillera de Tehuantepec. Los pocos estudios en el dominio de las técnicas de admitancia utilizadas para México, trataron de explicar si la parte continental norte y la península Yucatán están en equilibrio isostático (*Campos-Enríquez et al., 1997*) y trataron de averiguar el espesor elástico de la corteza oceánica enfrente de la trinchera mesoamericana, cerca de Acapulco (*Campos-Enríquez y Sánchez-Zamora, 2000*).

Un modelo gravimétrico bidimensional que cruza la Cordillera de Tehuantepec (*Manea et al., 2004*) ha encontrado una buena correlación entre las estimaciones edad/ profundidad y edad/ espesor de la litosfera oceánica. Este estudio muestra que la cordillera es un límite entre dos zonas, la sureste, más gruesa consecuentemente mas antigua que la noroeste. Usando la estimación del espesor elástico para la cordillera de Tehuantepec, *Manea et al. (2004)* sugieren una edad de formación para la cordillera de ~ 10 $\pm$ 7 Ma. Usando anomalias magneticas, *Kanjorski (2003)* muestra que la placa de Cocos sufrió en la zona noroeste un cambio importante en la velocidad de dispersión hace ~ 12 Ma. La velocidad de la placa Cocos bajó desde 7.8 cm /año hasta 4.8 cm/ año.

En este estudio se propone que la cordillera de Tehuantepec pudo haber sido el resultado de una deformación transpresional. Se muestra que una disminución de la velocidad de expansión para un segmento de la dorsal del Pacífico Este al sur de la cordillera entre ~ 14 y ~ 3.5 Ma ha resultado en un

movimiento diferencial entre las dos zonas de la placa de Cocos, que pudo haber producido un cabalgamiento oblicuo progresivo a lo largo de la cordillera.

Según la teoría clásica de las placas tectónicas, los bordes transformantes entre las placas son caracterizados por áreas de deformación transformante estrechas y paralelas al círculo menor alrededor del polo relativo de rotación de Euler, entre las dos placas. En algunos casos, la deformación puede cambiar de fallamiento de rumbo puro de tal manera que las fallas transformantes pueden acomodar la componente compresional de la deformación (por ejemplo *Sonder y Pockalny, 1999)*. En este estudio se analiza el caso de la cordillera de Tehuantepec, ubicada sobre la placa de Cocos al límite oriental de la prolongación de la zona de fractura de Clipperton. Mientras otras zonas de fractura que conectan la dorsal del Pacífico este con la Trinchera mesoamericana (por ejemplo, Orozco y O'Gorman) presentan una forma curvilínea, la Cordillera de Tehuantepec se destaca por su linealidad y la ausencia de sismicidad. Algunos trabajos reconocen que la cordillera separa la placa de Cocos en dos partes con regímenes tectónicos y edades diferentes (*DSDP 66 y 84; Wilson, 1996; Couch y Woodcock, 1981; Klitgord y Mammerickx, 1982; Manea et al., 2003*). Según estos trabajos, la diferencia de edades varía entre 8 y 12 Ma. Por otro lado, la diferencia de edades a través de la zona de Fractura de Clipperton, al lado oriental de la dorsal del Pacífico este es de nada mas 1.6 Ma *(Pockalny, 1997).* Esto muestra un movimiento diferencial entre las dos zonas de la placa de Cocos en algunos momentos dados, en el pasado.

Las metas principales del presente estudio son:

-Estimar el volumen especifico del relleno sedimentario en la trinchera mesoamericana;

-Mostrar la diferencia de régimen tectónico que hay entre las dos zonas de la placa de Cocos separadas por la cordillera de Tehuantepec, usando las estimaciones del volumen especifico del relleno sedimentario en la trinchera;

-Modelar un perfil gravimétrico en dos dimensiones, promedio, que cruce la cordillera de Tehuantepec;

-Calcular el espesor elástico de la litosfera oceánica debajo de la cordillera de Tehuantepec, usando datos batimétricos y de anomalía gravimétrica de aire libre, usando el método de la admitancia;

-Estimar la edad aproximativa de formación de la cordillera usando la correlación entre el espesor elástico y el enfriamiento de la placa oceánica con el tiempo;

-Calcular las edades teóricas en la cuenca de Guatemala usando los modelos de enfriamiento de la placa (la relación entre la profundidad del océano y la edad);

-Proponer unos modelos genéticos como posible explicación tectónica para la génesis de la cordillera de Tehuantepec.

En el capítulo II de esta tesis se presenta un estudio que determina el volumen especifico del relleno sedimentario en la trinchera mesoamericana y la relación entre este y el régimen tectónico a lo largo de la trinchera. Para esto se usan modelados gravimétricos 2D de los perfiles perpendiculares a la trinchera. El

capitulo III se enfoca en la estimación del espesor elástico de la litosfera oceánica debajo de la cordillera de Tehuantepec. Se usan perfiles conjuntos de datos batimétricos y de anomalía gravimétrica de aire libre sobre los cuales se aplican el método de la análisis espectral de la admitancia. En el capítulo IV se calculan las edades en la cuenca de Guatemala usando el modelo de enfriamiento de la placa oceánica con el tiempo. Asimismo se proponen dos modelos que presentan los mecanismos que probablemente pudieron originar la cordillera de Tehuantepec. En el capítulo V se presentan las discusiones y las conclusiones de los tres capítulos anteriores.

REFERENCIAS

Barckhausen, U., Ranero, C.R., von Huene, R., Cande, S.C., and Roeser, H.A., 2001. Revised tectonic boundaries in the Cocos Plate off Costa Rica: implication for the segmentation of the convergent margin and for plate tectonic models. *Journal of Geophysical Research, vol. 106, no. B9, pp. 19,207-19,220.*

Bravo H., Rebollar C., Uribe A., Jimenez O., 2004. Geometry and state of stress of the Wadati-Benioff zone in the Gulf of Tehuantepec, Mexico. *Journal of Geophysical Research, v. 109, 10.1029/2003JB002854*

Campos-Enriquez, J.O., Arzate, J.A., Urrutia-Fucugachi, J., and Delgado-Rodriguez, O., 1997. The subsurface structure of the Chicxulub crater (Yucatán, México): Preliminary results of a magnetotelluric study. *The Leading Edge, vol. 16, no. 12, p. 1,774-1,777.*

Campos-Enriquez, J.O., and Sánchez-Zamora, O., 2000. Crustal structure across southern México inferred from gravity data. *Journal of South American Earth Sciences, 13, 479-489.*

Couch, R. and Woodcock, S., 1981. Gravity structure of the continental margins of southwestern Mexico and northwestern Guatemala. *Journal of Geophysical Research, 86, 1829-1840.*

DSDP Leg 66. Shipboard party, 1979, Middle America Trench. *Geotimes, v. 24, p. 20-22.*

DSDP Leg 84. Shipboard party, 1982, Challenger drills again off Guatemala. *Geotimes, v. 27, p. 23-25*.

Fisher, R.L., 1961. Middle America Trench: topography and structure. *GSA Bulletin, 72, 703-720.*

Fisher, R.L., and Hess, H.H., 1963. Trenches, In: M.N. Hill (Ed.). *The Sea, 3, Wiley, New York, 411-436.*

GEODAS v. 4.0, Marine Trackline Geophysics, U.S. Department of Commerce, National Oceanic and Atmospheric Administration.

Gorbatov, A., and Kostoglodov, V., 1997. Maximum depth of seismicity and thermal parameter of the subducting slab: general empirical relation and its application. *Tectonophysics, v. 277, p. 165-187.*

Herron, E.M., 1972. Sea-floor spreading and the Cenozoic history of the east-central Pacific. *GSA Bullettin, v. 83, p. 1671-1692*.

Hilde, T.W.C., 1983. Sediment subduction versus accretion around the Pacific. *Tectonophysics, 99, 381, 397.*

Kanjorski, M.N., 2003. Cocos Plate structure along the Middle America subduction zone off Oaxaca and Guerrero, Mexico: influence of subducting plate morphology on tectonics and seismicity. *PhD thesis, University of California, San Diego.*

Klitgord, K.D. and Mammerickx, J., 1982. Northern east Pacific Rise; magnetic anomaly and bathymetric framework. *Journal of Geophysical Research, 87, no.138, 6725-6750.*

Manea, M., Manea, V.C., and Kostoglodov, V., 2003. Sediment Fill of the Middle America Trench Inferred from the Gravity Anomalies. *Geofisica Internacional, vol. 42, Num. 4, pp. 603-612.*

Manea, M., Manea, V.C., Kostoglodov, V., and Guzman-Speziale, M., 2004, Elastic Thickness of the Lithosphere below the Tehuantepec Ridge. *accepted Geofisica Internacional.*

Menard, H.W., and Fisher, R. L., 1958. Clipperton fracture zone in the northeastern equatorial Pacific. *Journal of Geology, 66, no. 3: 239-253.*

Mercier de Lépinay, B., F. Michaud, T. Calmus, J. Bourgois, G. Poupeau, P. Saint-Marc, 1997. Large Neogene subsidence event along the Middle America Trench off Mexico (18°–19°N): Evidence from submersible observations. *Geology, 25, 387-390.*

Michaud, F., Dañobeitia, J.J., Carbonell, R., Bartolomé, R., Córdoba, D, Delgado, L., Nuñez-Cornu, F., and Monfret, T., 2000. New insights about the oceanic crust entering the Middle America trench off western Mexico, (17°–19°N). *Tectonophysics, 318, 187-200.*

Moore, J.C., Watkins, J.S., and Shipley, T.H., 1981. Summary of accretionary process, Deep Sea Drilling Project Leg 66: Offscraping, underplating and deformation of the slope apron, in Watkins, J.S., Moore, J.C., et al., Initial reports of the Deep Sea Driling Project, Volume 66: Washington, D.C., U.S. Government Printing Office, 825-836.

Mountney, N.P., 1997. Dynamic equilibrium within oceanic trenches: A useful analytical tool. *Geology, 25, 151-154.*

Parsons, B. and Sclater, J.G., 1977. An analysis of the variations of ocean floor bathymetry with age. *Journal of Geophysical Research, 82, 803-827.*

Pockalny, R. A., 1997. Evidence of transpression along the Clipperton transform: Implications for processes of plate boundary reorganization. *Earth and Planetary Science Letters, v. 146, p. 449–464.*

Ponce L., Gaulon R., Suarez G., Lomas E., 1992. Geometry and state of stress of the downgoing Cocos plate in the Isthmus of Tehuantepec, Mexico. *Geophysical Research Letters, v. 19, p. 773-776.*

Renard, V., Aubouin, J., Lonsdale, P., and Stephan, J.F., 1980. Premiers resultants d'une etude de la fose d'Amerique Central au sondeur multifaisceaux (Seabeam). *Geologie Marine, C.R.Acad. Sci., 291, Sér. D, 137-142.*

Ross, D.A., 1971. Sediments in the northern Middle America trench. *GSA Bulletin, 82, 303-322.*

Schilt, F.S., Karig, D.E., and Truchan, M., 1982. Kinematic Evolution of the Northern Cocos Plate. *Journal of Geophysical Research, v. 87, no. B4, p. 2958-2968.*

Sonder L.J., and Pockalny R. A., 1999. Anomalous rotated abyssal hills along active transforms: distributed deformation of oceanic lithosphere. *Geology, v. 27, p. 1003-1006.*

Talwani, M., 1968. Gravity in the Sea, 4. *New Concepts of the Sea Floor Evolution, Part I, 1970, 251-297.*

Truchan, M. and Larson, R.L., 1973. Tectonic lineaments on the Cocos Plate. *Earth and Planetary Science Letters, v. 17, p. 46-432.*

Turcotte, D.L., and Schubert, G., 2002, Geodynamics, 2nd edition, Cambridge University Press, New York.

Underwood, M.B., and Moore, G.F., 1995. Trenches and trench-slope basins, in Busby, C.J., and Ingersoll, R.V., eds., *Tectonics of sedimentary basins, Cambridge, Massachusetts, Blackwell Science, 179-219.*

Wilson, D.S., 1996. Fastest known spreading on the Miocene Cocos-Pacific plate boundary. *Geophysical Research Letters, v. 23, p. 3003–3006.*

II. EL RELLENO SEDIMENTARIO DE LA TRINCHERA MESOAMERICANA INFERIDO DE LAS ANOMALIAS DE GRAVEDAD

Geofisica Internacional, vol. 42, no. 4, pp. 603-612

SEDIMENT FILL IN THE MIDDLE AMERICA TRENCH INFERRED FROM GRAVITY ANOMALIES

Marina Manea, Vlad C. Manea and Vladimir Kostoglodov

Instituto de Geofísica, Universidad Nacional Autónoma de México, México D.F., México

ABSTRACT

A sequence of free-air gravity anomaly profiles across the Middle America trench is used to model the sediment fill of unconsolidated pelagic and hemipelagic sediment facies, and partially altered bedrock material. The shift of the free-air forearc low from the bathymetric minimum in the trench is used to estimate the amount of low-density sediment. The gravity effect of the fill is relatively small, suggesting that the dominant processes in the Middle America trench are sediment subduction and scraping of unconsolidated pelagic sediments from the top of the subducting oceanic plate. The sediment volume in the trench tends to increase southward from Jalisco to Oaxaca. In the Guatemala basin, this tendency is less

clear. There is some correlation between the amount of fresh sediment fill and the convergence rate at the trench, except for the profiles with an extensive terrigenous sediment contribution or the areas of subduction of prominent bathymetric features.

Keywords: Subduction; trench sediment fill; gravity anomalies; Middle America Trench; Mexico.

INTRODUCTION

The Middle America Trench (MAT) is approximately parallel to the coast for more than 2,600 km, from Jalisco to Costa Rica. This trench is associated with gravity and bathymetry minima. The northern section of the MAT is separated from its deeper southern section by the Tehuantepec Ridge that intersects the trench near 15˚N, 95˚W (*Menard and Fisher, 1958*). To the south, the MAT stops at the northeast trending Cocos Ridge.

The depth of the MAT varies between 4,500 and 6,500 m. Northwest of the Tehuantepec ridge, the MAT is shallower than in the Guatemala basin by approximately 1,000 m. Northwest of Acapulco, the MAT is generally U-shaped in cross section, with a steeper landward slope and a flat bottom due to sedimentary fill (*Fisher, 1961*). Between Acapulco and the Tehuantepec ridge, the trench is segmented and forms a sequence of deeper basins up to 5,000 m depth (*Fig. 1*). Southeast of the Tehuantepec ridge, the MAT is wider and deepens to a maximum depth of 6,400 m in the western Guatemala basin. The MAT is V-shaped here; it is also asymmetric with an irregular bathymetry. These morphological features may imply that the amount of sediments in the V-shaped trench regions is less that in the U-shaped MAT (*Fisher, 1961; Moore, 1981*).

Studies of the sediment fill in the northern part of the MAT are limited (e.g., *Ross, 1971; Renard et al., 1980; Mercier de Lépinay et al., 1997*). The Deep Sea Drilling Project (DSDP) and the Ocean Drilling Program (ODP) are restricted in Mexico and Guatemala to a few drilling clusters along the MAT (*Underwood and*

Moore, 1995). The observed sedimentation rate on the landward slope of the MAT (*DSDP site 486*, in front of Acapulco) is 1.46 km/Ma (*Ross, 1971*), which is not sufficient to maintain a dynamic equilibrium in the subduction zone (*Mountney, 1997*).

Renard et al. (1980) observed a series of linear scarps, oblique to the MAT. The multi-beam echo-sounder survey shows that these scarps are parallel to the linear magnetic anomalies. They are interpreted as faults inherited from the East Pacific Rise and reactivated as they approached the trench. The estimate of maximum sediment thickness is ~ 400 m (*Renard et al., 1980*). There is no evidence of sediment accretion in the MAT.

Hilde (1983) showed that the graben-type pattern is well developed on the seaward slope of the MAT. This agrees with previous observations by *Fisher (1961), Fisher and Hess (1963), and Renard et al. (1980). Hilde (1983)* states that it is likely that sediment subduction prevails over accretion for the entire chain of Circum-Pacific subduction zones.

The present study originates from the observation that the gravimetric minimum, which is typical for deep oceanic trenches, does not coincide with the bathymetric minimum at the trench axis. *Talwani (1968)* made this observation for the gravity anomalies across the Aleutian and Japan Trenches. All along the MAT, the gravimetric minimum is located over the landward slope of the trench. The offset between gravimetric and bathymetric minima suggests that there is a low-density sedimentary fill, which can be estimated in some cases by gravity anomaly modelling (*Fig. 2*). The goal of this study is to estimate the amount of

unconsolidated sediments accumulated in the MAT and its distribution along the trench. Such estimates are important, for example, in studies of subduction tectonics and sediment balance, interplate coupling, thermal modelling of subduction zones, and low-frequency tsunamigenic earthquakes.

SEDIMENTS IN SUBDUCTION ZONES

In addition to sedimentation, three principal tectonic processes control the trench fill at convergent plate boundaries: subduction accretion, sediment subduction, and tectonic erosion. Which of these processes is dominant depends on the state of stress at the subduction zone. Sediment subduction prevails when the interplate coupling or normal stress across the subduction zone is relatively low, and either accretion or tectonic erosion occurs when coupling is high (*Uyeda and Kanamori, 1979; Dewey, 1980; Uyeda, 1982 and 1983*).

Isacks et al. (1968) first suggested that normal fault structures or grabens that develop on subducting oceanic plates might facilitate sediment subduction. Normal faults are common on the seaward slope of trenches *(Hilde, 1983; Renard et al., 1980)*. These faults are associated with tension acting on the subducting plate. Graben formation occurs initially near the outer topographic high, in front of the trench. Graben depth increases as the oceanic plate moves down for some 400 m or more towards the trench. Graben-type structures provide traps on the subducting plate where trench sediments are captured and subducted (*Fig. 3*).

In general the terrigenous input to the MAT is insufficient for a dynamic trench fill balance. The continuous supply of sediments to the trench is balanced by the removal of sediments from the inner trench wall by subduction or accretion when the equilibrium is maintained *(Mountney, 1997).* Thus, the sediment facies should be normally small in the trench fill complex. We would expect that unconsolidated pelagic facies are the main source of trench fill material, which is

scraped off the top of the oceanic plate as it is subducting into the trench. Higher density, consolidated pelagic sediments must be totally subducted, otherwise the total sediment fill within the MAT should be ~ 10 times higher than the observed values.

In non-accretional subduction zones, the volume of subducted sediments should depend on the pelagic sedimentation rate and the sedimentation duration, which is proportional to the A, age of the oceanic lithosphere in the trench. The convergence rate, *V* (km/yr), may also be an important parameter for the sediment subduction (e.g., *Kostoglodov, 1988; Mountney, 1997*).

This study is concerned with the unconsolidated, lower density phase of trench sediments, which develops from the removal of relatively fresh top cover of the pelagic sediments, *h*, plus some terrigenous component. The specific volume of unconsolidated sediment fill is the volume of a unit length (1 km) of sediment fill, *SVSF*, which produces the observed gravity effect. It depends on the fresh sediment input into the MAT, the sediment consolidation rate, V_c (km/yr) and the sediment subduction flux:

$$SVSF \sim [(hV + S_t w) - V_c w]^* t, \quad (1)$$

where *h* (km) is the mean thickness (assumed constant) of the soft pelagic sediment cover scraped off the top of the subducting plate; S_t (km/yr) is the average terrigenous sedimentation rate in the MAT, which may depend on the

coast-trench distance and on the proximity to the estuaries of large rivers; *w* (km) is the trench width and *t* (yr) is the time (see *Fig. 3*).

DATA

The gravity data (*Δg*) used in this study are free-air anomalies from the Geophysical Data System (*GEODAS*) provided by the National Geophysical Data Center (NGDC) (*Marine Trackline Geophysics, v 4.0*). These data have an accuracy of 3 - 7 mGal. The bathymetric data utilized for the modelling are retrieved from the Geodas bathymetric database (*Marine Trackline Geophysics, v 4.0*).

The study area (*Fig. 1*) is a rectangle of 20°N, 105°W to 12°N, 91°W. We selected 17 profiles perpendicular to the trench axis from a total of 21 profiles available. The distance between profiles is 0.5° to 1°. The length of the profiles is 100 to 250 km. Profiles 2 - 4 cross a tectonically complex zone traversed by the Lazaro Cardenas Canyon and the Orozco Fracture Zone. The Balsas River discharges a large amount of terrigenous sediments into this area. Therefore, the data along these profiles are dispersed and the sediment fill modelling is problematic.

Seismic record data and isopach maps from the IOC Geological/Geophysical Atlas of the Pacific (GAPA) project (*Ladd et al., 1985*) are used to develop the modelling results. Some reliable seismic data can be found along the northern part of the MAT, off Colima and Jalisco (*Michaud et al., 2000*) where a prominent horizontally layered sedimentary wedge was found. It should be noted that seismic methods detect only the unconsolidated wedge sediments and the acoustic basement may not actually represent the base of the sediment cover

(*World Data Center for Marine Geology & Geophysics*). *Fig. 4* shows seventeen analysed profiles of free-air gravity anomalies and bathymetry over the MAT. These profiles are subdivided into two groups: the northwestern part of the MAT (NW off the Tehuantepec Ridge), and the southeastern part (Guatemala Basin). From *Fig. 4*, in all profiles, the *Δg* minimum is located over the landward slope of the trench.

The shallower dip of the Wadati-Benioff zone is constrained by seismicity data (e.g., *Kostoglodov et al., 1996; Bandy et al., 1999*). The thermal thickness of the subducting slab at the trench, *H,* is estimated from the age ~ *H* relation and the age of the oceanic crust (*Klitgord and Mammerickx, 1982*), using the geomagnetic polarity time scale by *Cande and Kent (1995).*

MODELLING SEDIMENT FILL

A strong, 100 - 162 mGal negative free-air gravity anomaly over the trench and the inner trench wall is observed (*Fig. 4*). It is attributed to a mass deficit at the trench and low-density sediment fill. We are interested in determining the specific volume of the sediment fill, *SVSF*, along the MAT. The main trench features are the bathymetric and gravimetric minima. The difference between their locations, ξ, may be expressed in terms of the low-density, unconsolidated sedimentary fill which consists of the pelagic and hemipelagic sediment facies, and partially altered bedrock material. Gravity modelling helps to reveal the thickness and lateral extension of these sediments within the trench.

We assume the same average densities of the rock and sedimentary material for all modelled profiles. Only the shapes of the layers are adjusted to fit Δg. The basic structure of modelled profiles is: 1) the oceanic water layer, 2) the continental crust of the overriding North American and Caribbean Plates, 3) the oceanic crust of the Cocos Plate and 4) the upper mantle.

The oceanic crust of 11 km thick (*Sandwell, 2001*) is modelled consisting of 3 layers: sediments, basalts and gabbros with the densities of 2.15, 2.5 and 2.8 g/cm^3 respectively (*Sandwell, 2001; Morisson et al., 2001*). The continental crust in the subduction zone consists of a thin sedimentary layer, 2.2 g/cm^3, in the continental slope region, an upper crustal layer of weathered granite, 2.75 g/cm^3, and a lower crustal layer, 2.9 g/cm^3. The sedimentary layer is formed from pelagic

and hemipelagic sediments and from weathered granite fragments. The underlying upper mantle is of peridotite composition, 3.2 g/cm^3.

The gravity effect of the deep layers (e.g., upper mantle) is small and relevant only for the long wavelength regional modelling but not for relatively short, 10 - 15 km wavelength free air gravity anomalies. Our models are constrained by the seismic estimates of the top of the basement and hence the thickness of the sediments for several profiles in the Southern Mexico and Guatemala margins (*von Huene, 1985*).

In order to express the accuracy of the modelling results, the mean difference, $< \Delta g - \Delta g_m >$, and its standard deviation, between the observed, Δg, and modelled, Δg_m, anomalies are shown in *Fig. 5*. The standard deviation of the mean difference between the observed and modelled free-air anomalies is 1 - 4 mGal, which is within the accuracy range of the observed Δg data (*GEODAS*) of 3 - 7 mGal.

The difference in locations between the bathymetric and gravimetric minima, ξ, suggests the lateral extension of the trench fill. After the maximum depth and extension of the trench sediment fill is obtained from the gravity modelling, the estimate of the specific volume of the sedimentary fill, *SVSF*, is done using a simple geometric approximation shown in *Fig. 6.* We assume that the sediment fill is symmetric in the V-shaped trench basement. The *SVSF* in the trench is roughly proportional to ξ, hence the smaller is ξ the less is the sediment fill. In fact this relation comes out from the previous studies by *Menard and Fisher (1958), Fisher and Hess (1963), Renard et al. (1980), and Hilde (1983).*

RESULTS AND DISCUSSION

The minimum free-air gravity anomaly across the MAT does not coincide with the bathymetric minimum. In the northwestern part of the MAT (*Fig. 7-A*), the difference, ξ, between locations of the bathymetric minimum (trench axis) and the gravimetric minimum is small, ξ = 0.44 - 0.80 km, (see profiles 1-4 in Jalisco and Michoacan, *Fig. 1*). This difference systematically increases up to ξ = 2.05 - 9.19 km in the central part of the MAT (profiles 6 - 9, 11,12 in Guerrero and Oaxaca, *Figs. 1 and 7B - 7D*), but it noticeably decreases, ξ = 0.5 - 2.18 km, in front of the Tehuantepec Ridge (profiles 13 - 15, *Fig. 1*). In the Guatemala basin, southeast of the MAT (*Fig. 7E,F*), the difference between the gravimetric minimum and the trench axis is approximately constant along the entire trench. This difference is relatively small, ξ = 2.73 - 4.80 km (profiles 16-21, *Fig. 1*). Profile 19 is an exception, ξ = 5.75 km, probably due to higher local terrigenous sedimentation. Profile 10 (*Fig. 8*) has an anomalously high ξ = 9.18 due to a large amount of terrigenous sediments supplied to the trench by the Verde River. This suggests that an important amount of terrigenous sediments might be focused mainly in front of the large rivers.

Estimates of ξ for profiles 10, 13 and 14 are apparently outliers, caused by some local effects (e.g., contribution of high terrigenous sedimentation and probable tectonic erosion or lesser sediment fill over the subducting Tehuantepec ridge, profiles 13 - 16). The SVSF and the age of the oceanic lithosphere do not change noticeably in the Guatemala basin trench (except maybe for Profile 19

where ξ is higher because of the strong terrigenous contribution). Note that the mean SVSF in the Guatemala basin is lower than that for the northwestern part of the MAT.

The plot of SVSF as a function of V (*Fig. 9*) shows that there is a general tendency of augmenting the SVSF as the convergence rate is increasing. This trend is more distinct for the northwestern part of the MAT and is not so clear in the Guatemala basin where the boundary and convergence rate between the Caribbean and the Cocos plate are very poorly known. It is possible that there are two distinct sedimentary regimes in the northwest and southeast segments of the MAT. The average terrigenous sedimentation rate, S_t, within the Guatemala basin trench is expected to be lower than that in the northwestern part of the MAT, which could be merely an effect of a drastic change in the coast-trench distance across the Tehuantepec ridge. The longer transportation distance should diminish the terrigenous sedimentation rate at the MAT.

A difference in the plate coupling is also a conceivable factor, which has some bearing on the scraping and accretion of the sediments from the subducting oceanic plate. We may suspect the higher interplate coupling to the northwest of the Tehuantepec ridge, where the Cocos plate is relatively younger, $A < 16$ Ma.

A relatively small overall value of the *SVSF* estimated from the free-air anomaly modelling is the strongest argument for sediment subduction. The volumes of accreted wedge sediments are incomparably less than these volumes calculated under the assumption that all deposits transported with the oceanic lithosphere to the trench have been accreted (*Scholl et al., 1977*). However, an

accurate evaluation of the sediment subduction/accretion balance is not yet possible at the MAT (as well as on the global scale) because of the lack of reliable data. Thus, some seismic profiles normal to the MAT are needed in order to provide the depth of the acoustic basement surface and thickness of slope deposits for a better evaluation of the *SVSF*.

CONCLUSIONS

The estimated specific volume of the fresh sediment fill, *SVSF*, increases gradually along the MAT from *SVSF* ~ 0 km^2 in Jalisco up to *SVSF* ~ 7 km^2 in Oaxaca. The *SVSF* is contaminated in a few cases by a bulky terrigenous sediment contribution from large rivers (e.g., Profiles 10, 19) or a probable tectonic erosion process (e.g., Profiles 13-16). A roughly linear relation is observed between the convergence rate, *V*, and the *SVSF*. This relation is more distinct in the northwestern part of the MAT, where Cocos plate is relatively young, *A* < 16 Ma. The *SVSF = f(V)* relation is ambiguous in the Guatemala basin segment of the MAT. The average *SVSF* in the Guatemala basin is lower than the SVSF within the northwestern part of the MAT. This observation indicates that the tectonic regimes are different in these segments of the MAT (see *DSDP 66* and *DSDP 84*). A relatively small estimated amount of the *SVSF* suggests that sediment subduction is the dominant tectonic process along the Mexican part of the MAT.

REFERENCES

Aubouin, J., von Huene, R., Arnott, R., Bourgois, J., Filewicz, M., 1982. Subduction without accretion: Middle America Trench off Guatemala. *Nature, v.94, 458-460.*

Aubouin, J., Bourgois, J., and Azema, J., 1984. A new type of active margin: The convergent-extensional margin, as exemplified by the Middle America Trench off Guatemala. *Earth and Planetary Science Letters, v.67, 211-218.*

Bandy, W., Kostoglodov, V., Hurtado-Díaz, A. and Mena, M., 1999. Structure of the southern Jalisco subduction zone, México, as inferred from gravity and seismicity. *Geofísica Internacional, 38, no. 3, 127-136.*

Cande, S.C. and Kent, D.V., 1995. Revised calibration of the geomagnetic polarity time scale for the late Cretaceous and Cenozoic. *Journal of Geophysical Research, 100, 6093-6095.*

Dewey, J.F., 1980. Episodicity, sequence and style at convergent plate boundaries, D.W. Straugway (Ed.), The Continental Crust and its Mineral Deposits. *Geological Association of Canada, Special Paper, 20, 553-573.*

Fisher, R.L., 1961. Middle America Trench: topography and structure. *GSA Bulletin, 72, 703-720.*

Fisher, R.L., and Hess, H.H., 1963. Trenches, In: M.N. Hill (Ed.). *The Sea, 3, Wiley, New York, 411-436.*

GEODAS v. 4.0, Marine Trackline Geophysics, U.S. Department of Commerce, National Oceanic and Atmospheric Administration.

Hilde, T.W.C., 1983. Sediment subduction versus accretion around the Pacific. *Tectonophysics, 99, 381, 397.*

Isacks, B., Oliver, J. and Sykes, R.L., 1968. Seismology and the new global tectonics. *Journal of Geophysical Research, 73, 5855-5899.*

Klitgord, K.D. and Mammerickx, J., 1982. Northern east Pacific Rise; magnetic anomaly and bathymetric framework. *Journal of Geophysical Research, 87, no.138, 6725-6750.*

Kostoglodov V., 1988. Sediment subduction: a probable key for seismicity and tectonics at active plate boundaries. *Geophysical Journal, 94, 65-72.*

Kostoglodov V., Bandy, W., Domínguez, J., and Mena, M., 1996. Gravity and seismicity over the Guerrero seismic gap, Mexico. *Geophysical Research Letters, 23, 3385-3388.*

Kostoglodov V., Guzman-Speziale, M., and Bandy, W. 1996. Seismotectonic constraints on the age of the lithosphere in the Guatemala basin. *EOS, AGU Transactions, 77, No.46, F646.*

Ladd, J. W., and Buffler, R. T. (eds.), 1985. Middle America Trench of western Central America, Atlas 7, Ocean Margin Drilling Program, *Regional Atlas Series, Marine Science Internacional, Woods Hole, MYR, 21 sheets.*

Menard, H.W., and Fisher, R. L., 1958. Clipperton fracture zone in the northeastern equatorial Pacific. *Journal of Geology, 66, no. 3: 239-253.*

Mercier de Lépinay, B., F. Michaud, T. Calmus, J. Bourgois, G. Poupeau, P. Saint-Marc, 1997. Large Neogene subsidence event along the Middle America

Trench off Mexico (18°–19°N): Evidence from submersible observations. *Geology, 25, 387-390.*

Michaud, F., Dañobeitia, J.J., Carbonell, R., Bartolomé, R., Córdoba, D, Delgado, L., Nuñez-Cornu, F., and Monfret, T., 2000. New insights about the oceanic crust entering the Middle America trench off western Mexico, (17°–19°N), *Tectonophysics, 318, 187-200.*

Morrison, F., Gasperikova, E., and Washbourne, J., 2001. The Berkeley Course in Applied Geophysics, *http://socrates.berkeley.edu:7057/gravity/.*

Moore, J.C., Watkins, J.S., and Shipley, T.H., 1981. Summary of accretionary process, Deep Sea Drilling Project Leg 66: Offscraping, underplating and deformation of the slope apron, in Watkins, J.S., Moore, J.C., et al., Initial reports of the *Deep Sea Driling Project, Volume 66: Washington, D.C., U.S. Government Printing Office, 825-836.*

Mountney, N.P., 1997. Dynamic equilibrium within oceanic trenches: A useful analytical tool. *Geology, 25, 151-154.*

Renard, V., Aubouin, J., Lonsdale, P., and Stephan, J.F., 1980. Premiers resultants d'une etude de la fose d'Amerique Central au sondeur multifaisceaux (Seabeam). *Geologie Marine, C.R.Acad. Sci., 291, Sér. D, 137-142.*

Ross, D.A., 1971. Sediments in the northern Middle America trench. *GSA Bulletin, 82, 303-322.*

Sandwell, D.T., 2001. Crustal Structure, Isostasy and Rheology. web: *http://topex.ucsd.edu/geodynamics/08crust_rheology.pdf*

Scholl, D.W., Marlow, M.S., and Cooper, A.K., 1977. Sediment subduction and offscraping at Pacific margins. In: M. Talwani and W.C. Pitman III (Editors), Island Arcs, Deep Sea Trenches, and Back-Arc Basins. *Maurice Ewing Series, AGU, 1: 199-210.*

Talwani, M., 1968. Gravity in the Sea, 4. *New Concepts of the Sea Floor Evolution, Part I, 1970, 251-297.*

Underwood, M.B., and Moore, G.F., 1995. Trenches and trench-slope basins, in Busby, C.J., and Ingersoll, R.V., eds., *Tectonics of sedimentary basins, Cambridge, Massachusetts, Blackwell Science, 179-219.*

Uyeda, S., and Kanamori, H., 1979. Back-arc opening and the mode of subduction. *Journal of Geophysical Research, 84, 1049-1061.*

Uyeda, S., 1982. Subduction zones: an introduction to comparative subductology. *Tectonophysics, 81: 133-159.*

Uyeda, S., 1983. Comparative subductology. *Episodes, 2: 19-24.*

Von Huene, R., 1985. Top of acoustic basement and thickness of sediments southern Mexico and Guantemala margin. In: Ladd, J. W., and Buffler, R. T. (eds.), Middle America Trench of western Central America, Atlas 7, Ocean Margin Drilling Program, Regional Atlas Series, *Marine Science International, Woods Hole, MYR, 21 sheets.*

Von Huene, R., and Scholl, D.W., 1991. Observations at convergent margins concerning sediment subduction, subduction erosion and the growth of continental crust. *Reviews of Geophysics, 29, pp. 279-316.*

World Data Center for Marine Geology & Geophysics, Boulder. Total Sediment Thickness of the World's Oceans & Marginal Seas, web: *http://www.ngdc.noaa.gov/mgg/sedthick/sedthick.html*.

FIGURE CAPTIONS

Figure 1. The study area with the locations of the modelled profiles along the MAT. Thin dashed lines indicate the tectonically complex profiles. These profiles are not modelled in this study. Thick dashed MAT lines indicate subduction-erosion off Jalisco (*Mercier de Lepinay et al., 1997*) and off Guatemala (*Aubouin et al., 1982; Aubouin et al., 1984*). A segment of the MAT shown by solid line indicates the subduction-accretion region (*Moore et al., 1981*). Solid lines on the continent show the main rivers.

Figure 2. Example of the free-air gravity anomaly, Δg, and bathymetry profiles across the Middle America trench. The minimum of Δg does not coincide with the trench axis. This implies the presence of low-density sediment fill in the trench.

Figure 3. Trench model with the sediment fill and graben structures on the subducted oceanic plate. V (km/yr) is the convergence rate, V_c (km/yr) is the sediment consolidation rate, h (km) is the mean thickness (assumed constant) of the soft pelagic sediment cover scraped off the top of the subducting plate; S_t (km/yr) is the average terrigenous sedimentation rate in the MAT, which may depend on the coast-trench distance and on the proximity to the estuaries of large rivers; w (km) is the trench width.

Figure 4. Seventeen profiles of free-air gravity anomalies (*Δg*) and bathymetry crossing the MAT.

(A) Profiles 1 and 5-14, located northwest of the Tehuantepec ridge.

(B) Profiles located to the southeast of the Tehuantepec ridge (Guatemala basin). The circle marks on the free-air gravity anomaly curves show the positions of *Δg* minima.

Figure 5. Mean difference between the observed and modeled free-air anomalies for each profile. The accuracy range of the observed *Δg* data (*GEODAS*) is 3 - 7 mGal (dashed lines) and the standard deviation of the mean difference between the observed and modelled free-air anomalies is 1 - 4 mGal.

Figure 6. Geometric approximation of the specific sediment fill volume. Grey triangle, representing the sediment fill, is determined using the difference between the locations of gravimetric and bathymetric minima and the modeled ocean floor surface. *W/2* is half width of the sedimentary fill.

Figure 7. Examples of the free-air gravity anomaly profiles and the gravity models at the northwestern part (A - D) and of the southeastern part (E, F) of the MAT. The modelling was done for the entire length of the profiles (100 - 250 km) while only the trench segments of the profiles are shown. Vertical exaggeration is 1.21. The distance between the arrows is *w/2* (half width of the sediment fill). *ρ* is the density in g/cm^3.

Figure 8. Profile 10 has an “anomalously” wide difference between the position of the gravity and bathymetry minima (*w/2*) due to a large amount of terrigenous sediments supplied by the Verde River to the trench.

Figure 9. The plot of the *SVSF* as a function of *V*. Circles represent the *SVSF* northwest of Tehuantepec; triangles show the *SVSF* near the Tehuantepec ridge and the diamonds the SVSF in the southeastern part; a linear relationship between *SVSF* and the convergence rate might be observed in the northwestern part. The outlier (profile 10) can be excluded from this analysis due to large terrigenous influence. The trend observed in the northewestern MAT is not valid for the Guatemala basin, where the boundary between the Caribbean and Cocos plate and hence the convergence rate are very poorly known.

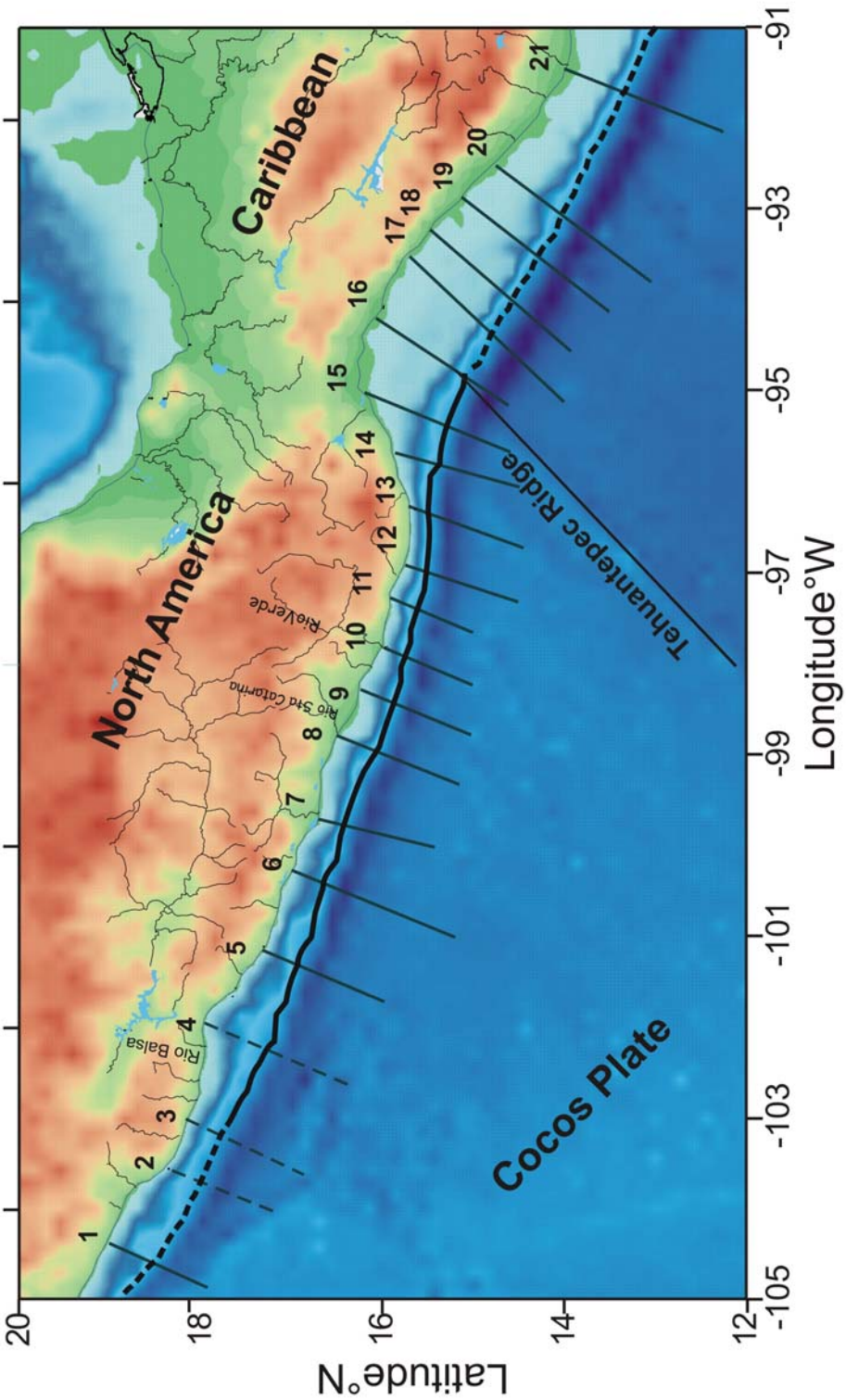
Caribbean
North America
Cocos Plate
Tehuantepec Ridge
Río Balsa
Río Verde
Río Sta Catarina
1
2
3
4
5
6
7
8
9
10
11
12
13
14
15
16
17
18
19
20
21
20
18
16
14
12
Latitude°N
-105
-103
-101
-99
-97
-95
-93
-91
Longitude°W

Figure1

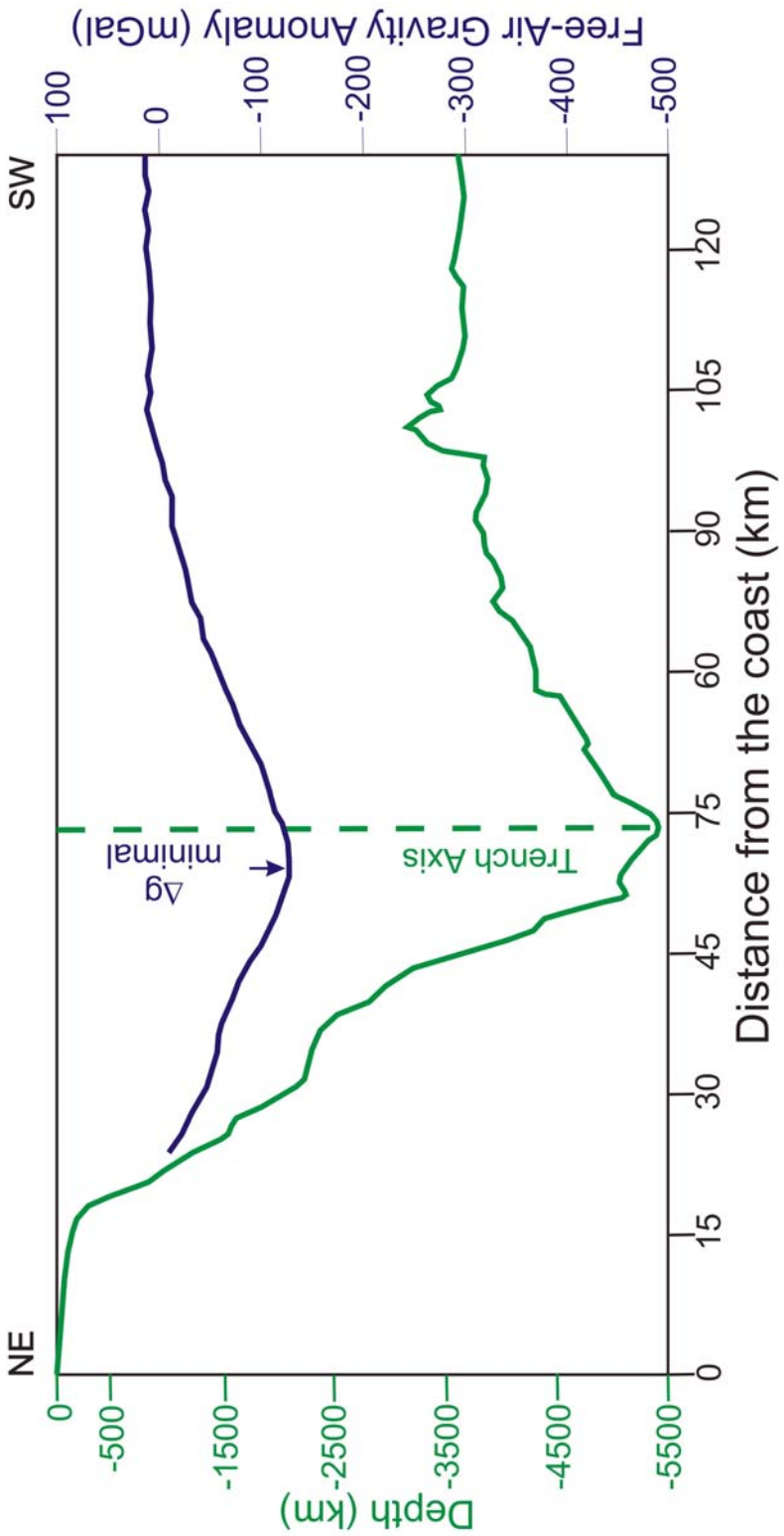
Free-Air Gravity Anomaly (mGal)
100
0
-100
-200
-300
-400
-500
SW
NE
Δg
minimal
Trench Axis
Depth (km)
0
-500
-1500
-2500
-3500
-4500
-5500
0
15
30
45
60
75
90
105
120
Distance from the coast (km)

Figure 2

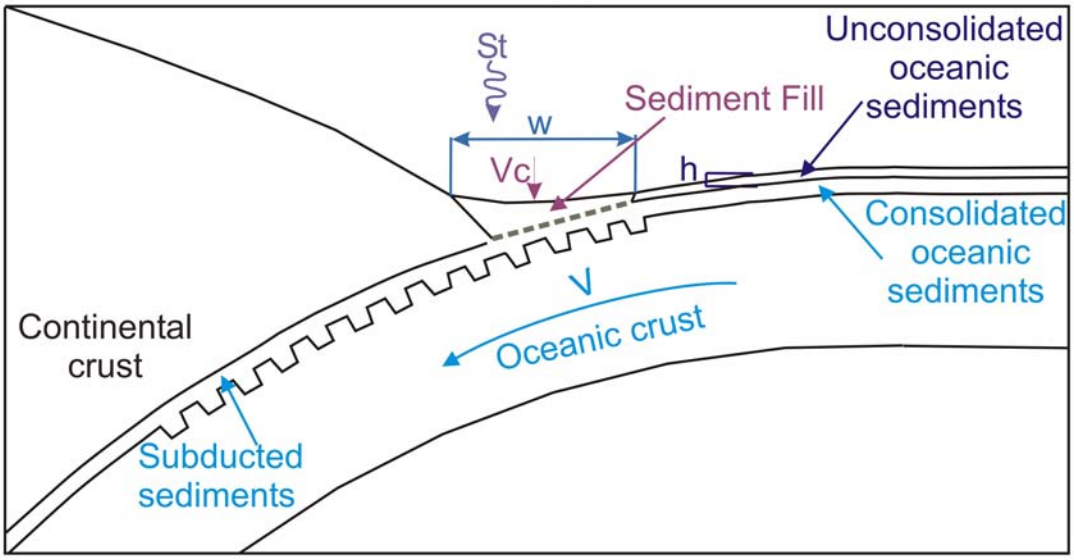
St
w
Vc
Sediment Fill
h
Unconsolidated
oceanic
sediments
Consolidated
oceanic
sediments
V
Oceanic crust
Continental
crust
Subducted
sediments

Figure 3

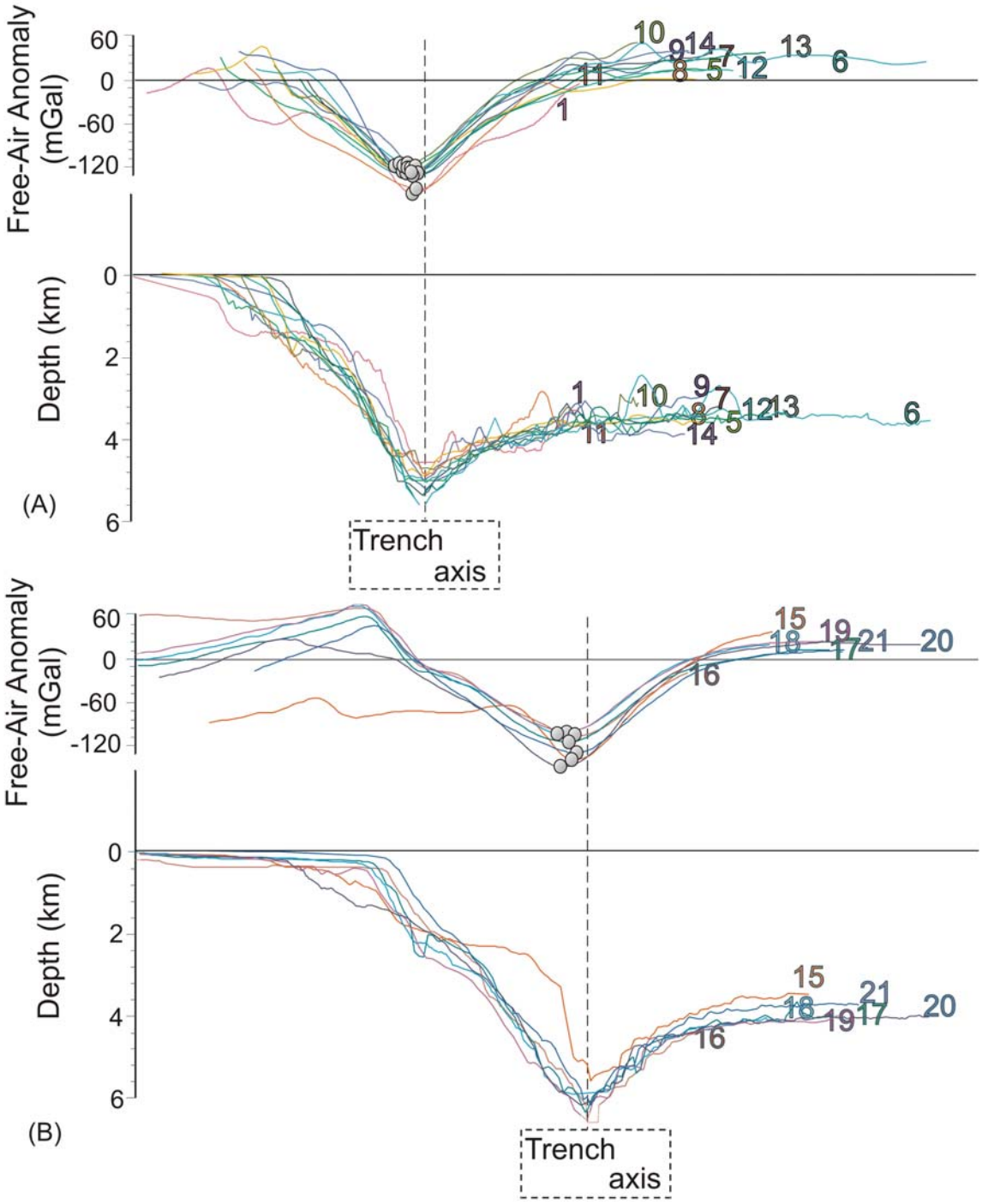
Free-Air Anomaly (mGal)
60
0
-60
-120
Depth (km)
0
2
4
6
(A)
Trench axis
Free-Air Anomaly (mGal)
Depth (km)
(B)
Trench axis

Figure 4

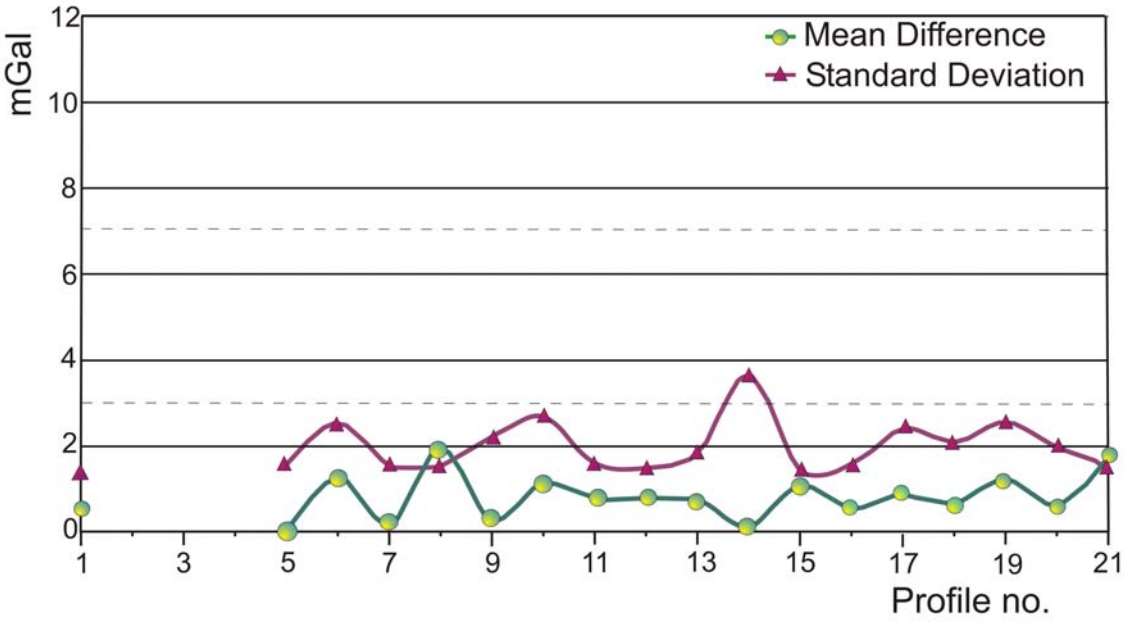
mGal
12
10
8
6
4
2
0
Mean Difference
Standard Deviation
1
3
5
7
9
11
13
15
17
19
21
Profile no.

Figure 5

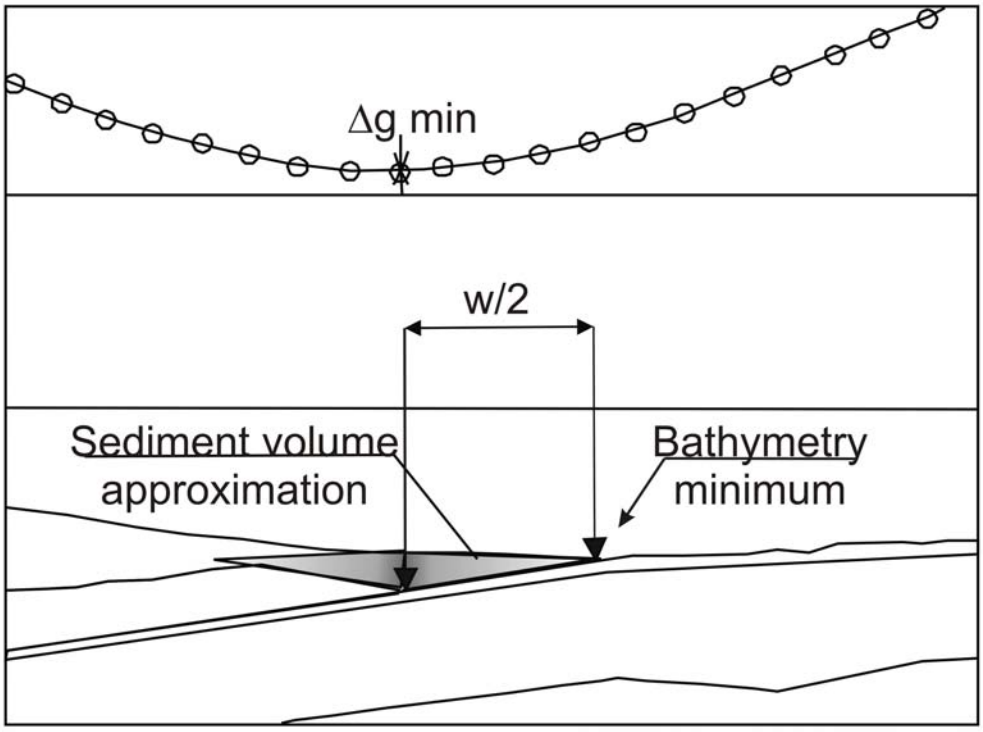
Δg min
w/2
Sediment volume approximation
Bathymetry minimum

Figure 6

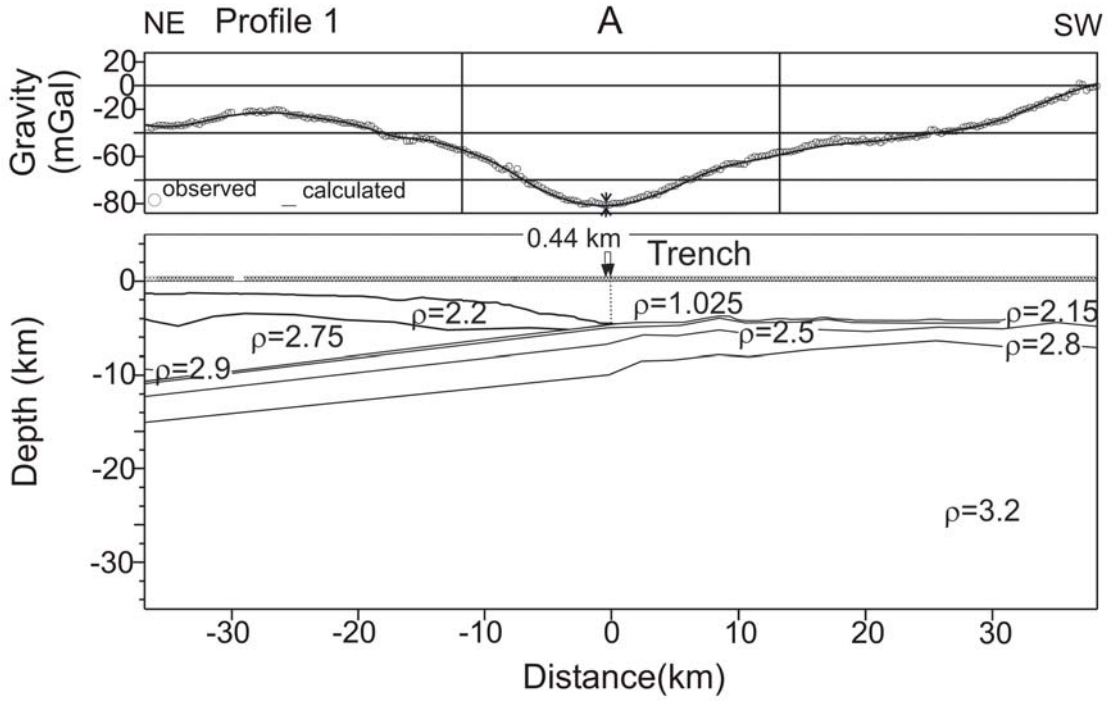
NE
Profile 1
A
SW
Gravity (mGal)
20
0
-20
-60
-80
observed
calculated
0.44 km
Trench
Depth (km)
0
-10
-20
-30
ρ=2.2
ρ=1.025
ρ=2.15
ρ=2.75
ρ=2.5
ρ=2.8
ρ=2.9
ρ=3.2
-30
-20
-10
0
10
20
30
Distance(km)

Figure 7A

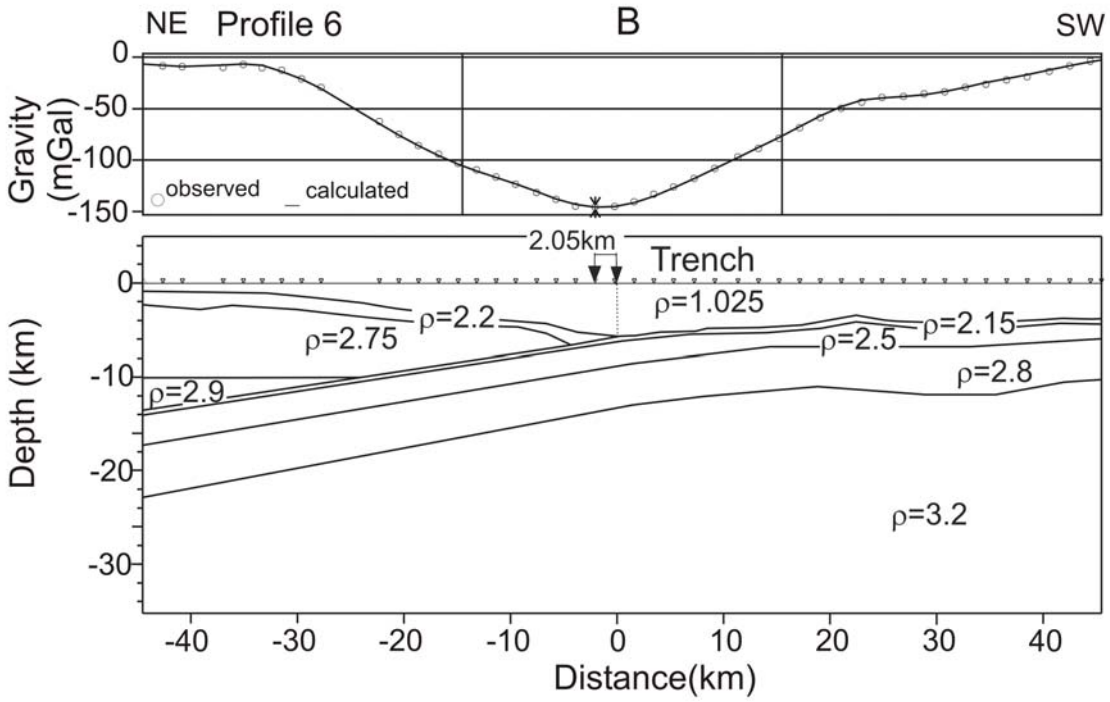
NE
Profile 6
B
SW
Gravity (mGal)
0
-50
-100
-150
observed
calculated
2.05km
Trench
Depth (km)
0
-10
-20
-30
ρ=2.2
ρ=1.025
ρ=2.75
ρ=2.5
ρ=2.15
ρ=2.8
ρ=2.9
ρ=3.2
-40
-30
-20
-10
0
10
20
30
40
Distance(km)

Figure 7B

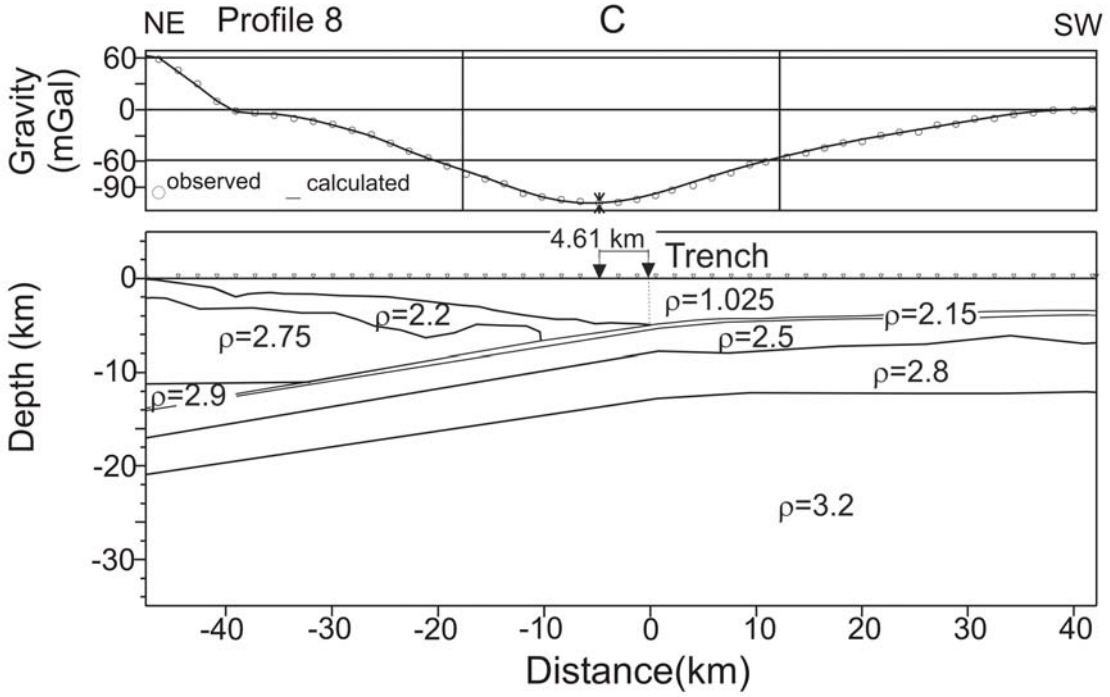
NE
Profile 8
C
SW
Gravity (mGal)
60
0
-60
-90
observed
calculated
4.61 km
Trench
Depth (km)
0
-10
-20
-30
ρ=2.75
ρ=2.2
ρ=1.025
ρ=2.15
ρ=2.5
ρ=2.8
ρ=2.9
ρ=3.2
-40
-30
-20
-10
0
10
20
30
40
Distance(km)

Figure 7C

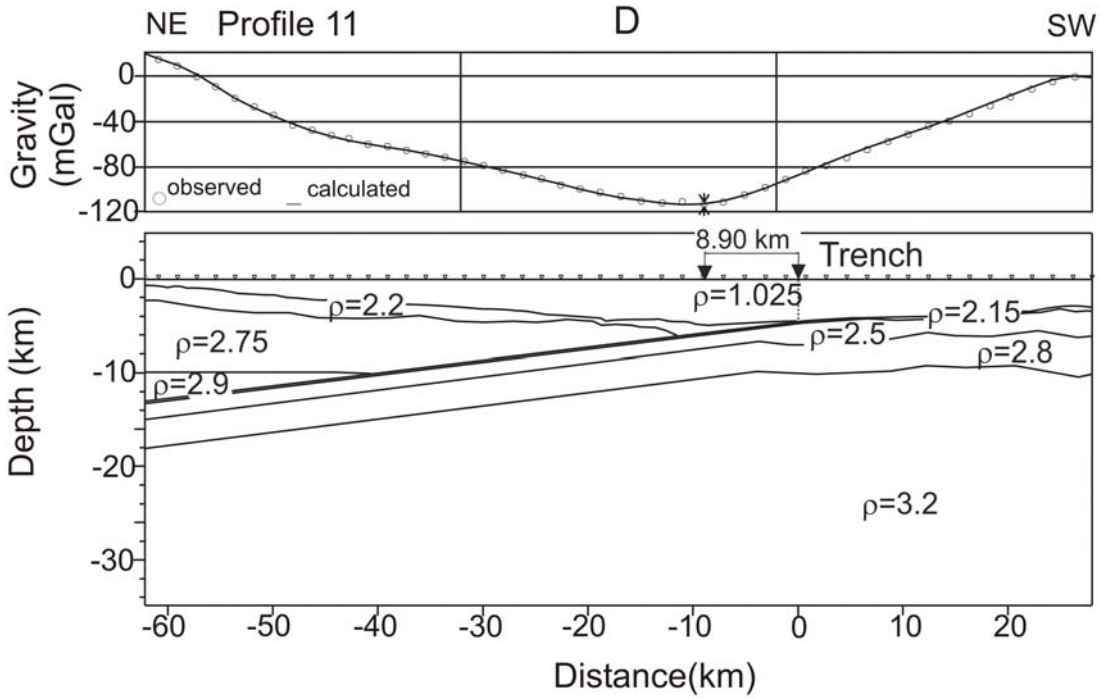
NE
Profile 11
D
SW
Gravity (mGal)
0
-40
-80
-120
observed
calculated
8.90 km
Trench
Depth (km)
0
-10
-20
-30
ρ=2.2
ρ=1.025
ρ=2.15
ρ=2.75
ρ=2.5
ρ=2.8
ρ=2.9
ρ=3.2
-60
-50
-40
-30
-20
-10
0
10
20
Distance(km)

Figure 7D

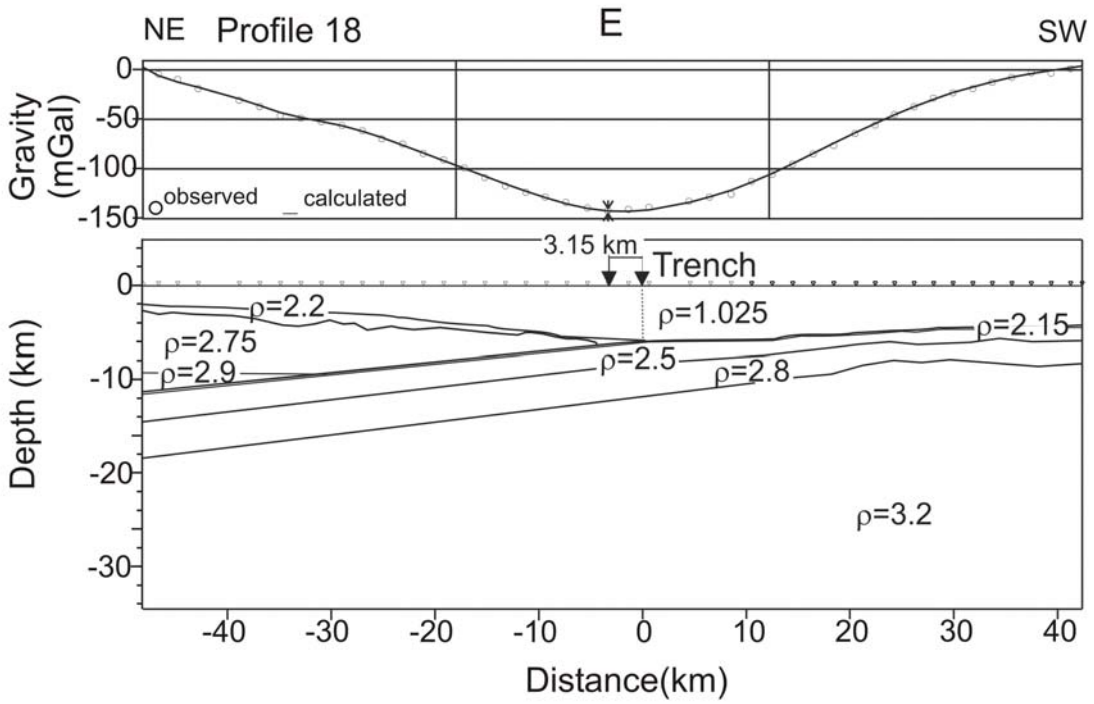
NE
Profile 18
E
SW
Gravity (mGal)
0
-50
-100
-150
observed
calculated
3.15 km
Trench
Depth (km)
0
-10
-20
-30
ρ=2.2
ρ=2.75
ρ=2.9
ρ=1.025
ρ=2.5
ρ=2.8
ρ=2.15
ρ=3.2
-40
-30
-20
-10
0
10
20
30
40
Distance(km)

Figure 7E

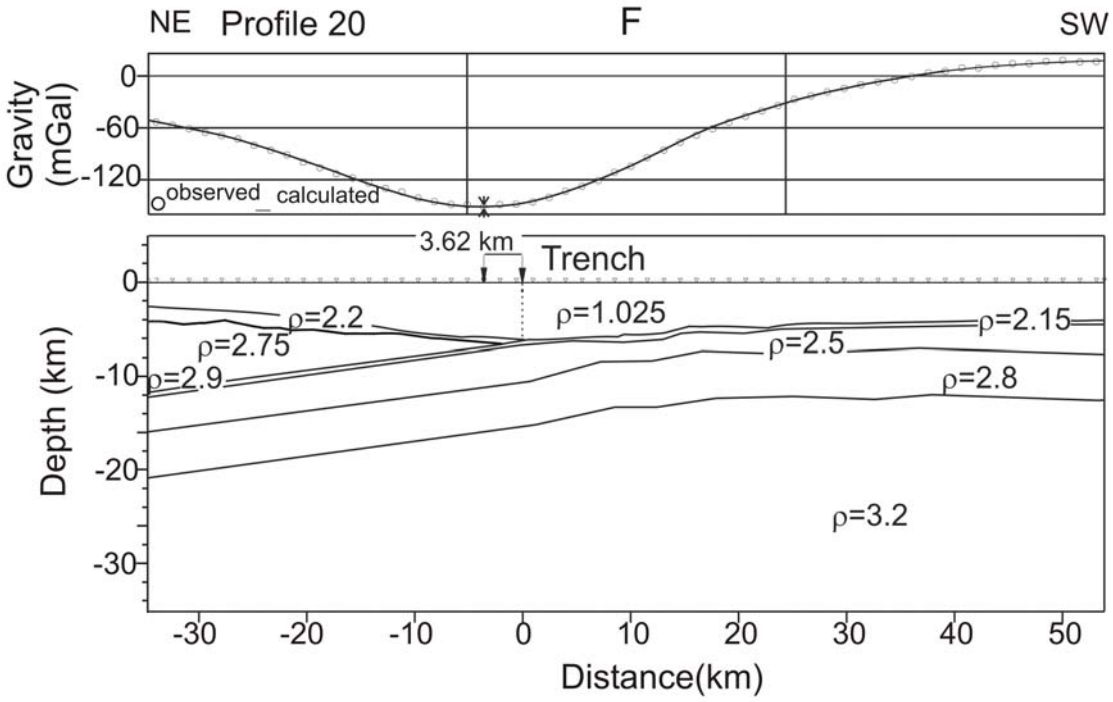
NE
Profile 20
F
SW
Gravity (mGal)
0
-60
-120
observed
calculated
3.62 km
Trench
Depth (km)
0
-10
-20
-30
ρ=2.2
ρ=1.025
ρ=2.15
ρ=2.75
ρ=2.5
ρ=2.9
ρ=2.8
ρ=3.2
-30
-20
-10
0
10
20
30
40
50
Distance(km)

Figure 7F

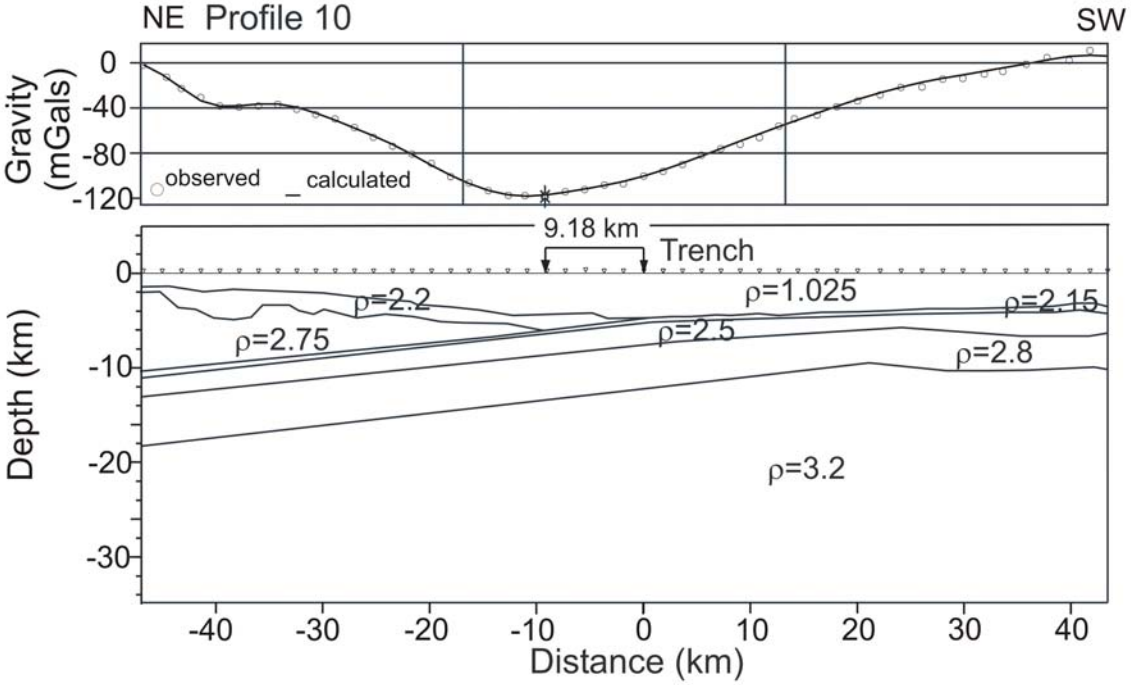
NE Profile 10
SW
Gravity (mGals)
0
-40
-80
-120
observed
calculated
9.18 km
Trench
Depth (km)
0
-10
-20
-30
ρ=2.2
ρ=1.025
ρ=2.15
ρ=2.75
ρ=2.5
ρ=2.8
ρ=3.2
-40
-30
-20
-10
0
10
20
30
40
Distance (km)

Figure 8

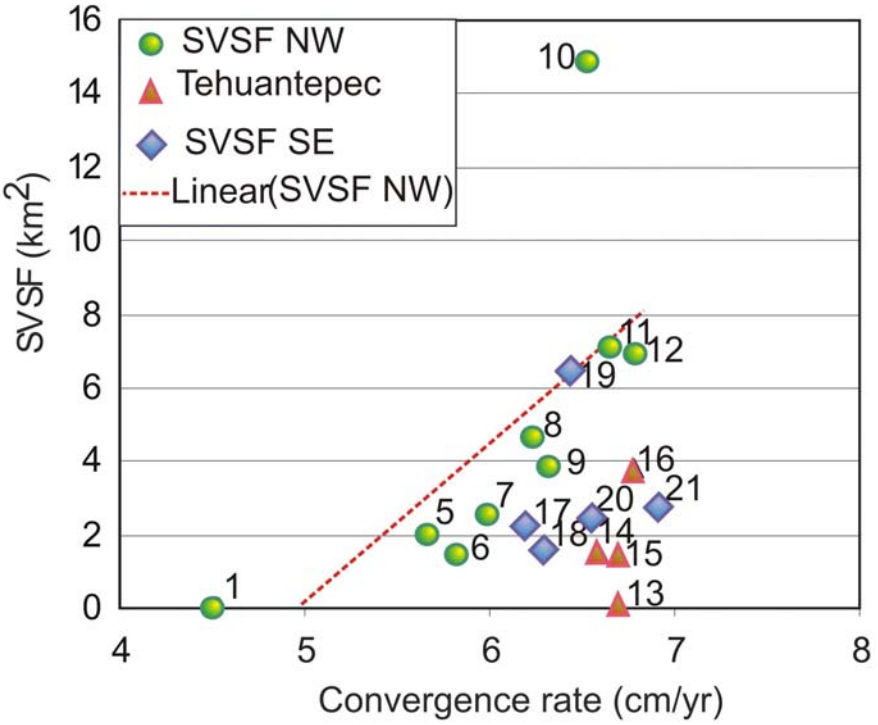
SVSF NW
Tehuantepec
SVSF SE
Linear(SVSF NW)
SVSF (km2)
Convergence rate (cm/yr)
0
2
4
6
8
10
12
14
16
4
5
6
7
8
1
5
6
7
8
9
10
11
12
13
14
15
16
17
18
19
20
21

Figure 9

III. ESPESOR ELÁSTICO DE LA LITOSFERA OCEANICA DEBAJO DE LA CORDILLERA DE TEHUANTEPEC

Accepted in Geofisica Internacional

ELASTIC THICKNESS OF THE OCEANIC LITHOSPHERE BENEATH TEHUANTEPEC RIDGE

Marina Manea[1], Vlad C. Manea[1], Vladimir Kostoglodov[1] and Marco Guzmán-Speziale[2]

[1] Instituto de Geofisica, UNAM

[2] Centro de Geociencias, UNAM, Queretaro

ABSTRACT

The relationship between bathymetry and free-air gravity is analyzed by computing response function (admittance) for 7 shipborne profiles crossing the Tehuantepec ridge (TR). The assessment of the age of the lithosphere at the time of bathymetric loading of the TR is deduced from the analysis of the experimental admittance and the elastic thickness (***Te***). We have computed the admittance, which is interpreted in terms of isotropic elastic plate thickness. The most appropriate model of isostatic compensation is one in which the oceanic lithosphere is considered to behave similar to an elastic plate. The lithosphere

beneath TR can be modeled by an elastic plate 10 ± 5 km thick. The shape of the admittance (low values at low wave-numbers) suggests that TR is isostatically compensated. The relation between the age of the oceanic lithosphere at the time of loading and Te, for a cut-off temperature of 450°C, offers an age estimation of 8 +9/-6 Ma for the oceanic lithosphere at the time of TR onset.

Keywords: Tehuantepec ridge, elastic thickness, admittance, gravity modeling.

INTRODUCTION

One of the most prominent bathymetric features in Guatemala basin is TR. The nature of this major structure and the age of its formation are still unknown. This ridge is considered bathymetrically similar to the great fracture zones of the northeastern Pacific (*Menard and Fisher, 1958*) and forms a major structural boundary, separating the Cocos plate in two regions (*Fig. 1*), tectonically distinct (*DSDP 67 – Aubouin et al., 1982; Manea et al., 2003*). Although *Klitgord and Mammerickx (1982)* proposed a difference in ages between these two compartments of ~ 12 Ma, their study confirmed that the identification of ages in the southern part has been proved to be very difficult. The low amplitude of the magnetic anomalies in Guatemala basin (*Anderson, 1974*) make problematical to obtain reliable crustal ages. *Wilson (1996)* mentioned a difference of ~ 8 Ma using paleontological dating for anomaly identification, meanwhile, Couch and *Woodcock (1981)* give an age difference of ~ 10 Ma. One hypothesis for TR formation comes from *Herron (1972)*, who considers TR the result of a hot spot trace. *Truchan and Larson (1973)* eliminate the possibility that the TR is a fracture zone continuation of the Siqueiros Transform Fault. TR is considered by *Truchan and Larson (1973)* as a hinge fault separating the Cocos Plate underthrusting the North America plate to the northwest and the Caribbean plate to the southeast. The study of *Couch and Woodcock (1981)* for this area shows discordance between the two compartments that defines the TR shape within the Cocos Plate: the northwestern compartment seems to be older and thicker than the southeastern one. They model the gravity

of a cross section normal to the TR. Unfortunately, their model is not in agreement with the estimated age of the Cocos Plate in Guatemala Basin from the relation between oceanic water depth and age (*Parsons and Sclater, 1977*): the Cocos plate lithosphere being subducted beneath the Caribbean plate is older, colder and therefore thicker than the portion of the Cocos plate being thrust under North America.

The data used in this study come from the GEODAS NGDC database (*Marine Trackline Geophysics, v 4.0*) and consist of bathymetry and free-air gravity anomaly data across TR. An estimation of the oceanic lithosphere elastic thickness beneath TR is performed using the observed data. Then we present a comparison of the results with several elastic thicknesses from theoretical models of compensation, choosing the best model. The central goal of this study is to propose a possible mechanism and an approximately age of formation for TR. In order to achieve the aim of this study, a gravity interpretation was performed using a mean profile crossing TR (*Fig. 2*) and the structure was analyzed by the means of the admittance techniques in order to infer the oceanic plate elastic thickness (***Te***) below TR.

ELASTIC THICKNESS ESTIMATION

The gravitational admittance is the wavenumber parameter that modifies the topography in order to generate the gravity anomaly. This parameter contains information on the state of isostasy for a surface feature. Variations of the sea floor bathymetry constitute a load distribution on the oceanic lithosphere, which reacts elastically (isostatic compensation) with the formation of a flexural depression, bulge and root. It has been known for some time that the spectral techniques can be used to better quantify the degree of isostatic compensation of oceanic bathymetric features (*Watts, 2001*). The theory of admittance technique is described in detail in a recent book by *Watts (2001)*. The spectral techniques employ the relationship between gravity and topography over a surface load (TR), which varies as a function of its wavelength. To determine the appropriate compensation mechanism of such a load, the frequency content (*Z(k)*-admittance) of observed gravity and topography data is compared with the spectra of the predictions for different isostatic models, such as those of Airy or Vening-Meinesz (simple flexure model). The isostatic response in the spectral domain for theoretical models depends also on the elastic thickness (***Te***) of the oceanic plate. Under the same load, a thin plate would produce a greater flexure (lower amplitude of the admittance function) than a thick slab. The best fit between the observed admittance with theoretical admittances for various ***Te***, will give us the elastic plate thickness.

Observed Admittance

We used in this study bathymetry and free-air gravity anomaly profiles from the GEODAS NGDC database (*Marine Trackline Geophysics, v 4.0*). Before applying the spectral technique, a despiking filter to remove the outliers (*Wessel and Watts, 1988*) was applied to these profiles. Then, computing the discrepancies in free-air gravity anomaly at intersecting ship tracks, we found 82 cross-over errors (COEs) with a standard deviation of 16.67 mGal. Using the algorithm of *Wessel (1989)* and *Wessel and Watts (1988)* for data adjustment, we exclude those profiles with COEs > 19 mGal, and the standard deviation dropped to 10.76 mGal. Finally, a number of 7 profiles, which cross TR were selected (*Fig. 1 - inset*). Since this spectral analysis requires a uniform data set (equally spaced and oriented), these profiles were projected perpendicular to TR.

We estimated the ***Te*** of the TR by the means of the admittance techniques using profiles projected orthogonal to the structure and with a final longitude of 482 km. A total of 512 samples of the free air gravity anomaly and bathymetry data were extracted from each profile resulting into a regularly spaced data set at intervals of 0.943 km. Wavenumbers of $0.0065 < k < 3.33$ were calculated for this wavelengths using $k = 2 \cdot \pi / \lambda$ formula**.** The trend of the data, including the mean was removed for each profile. The ends of the profiles were tapered using a cosine window on 10% of the total length of the profile (*Kogan and Kostoglodov, 1981*). Finally, the Fast Fourier Transform (FFT) of the sampled, trend-removed and

tapered gravity anomaly and bathymetry data sets was applied to calculate the spectral estimates for each pair of profiles. The complex admittance, $Z(k)^{OBS.}$, cross-spectrum , $C(k)$, power spectrum of bathymetry, $E_1(k)$, are given by:

$$Z(k)^{OBS.} = \frac{C(k)}{E_1(k)}, \quad (1)$$

$$C(k) = \frac{1}{N}\sum_{r=1}^{N} G(k)_r \cdot B(k)_r^*, \quad (2)$$

$$E_1(k) = \frac{1}{N}\sum_{r=1}^{N} B(k)_r \cdot B(k)_r^*, \quad (3)$$

where:

$G(k)$ and $B(k)$ are the Fourier transforms of the observed gravity and bathymetry data, respectively and N the number of profiles (*Tamsett, 1984*). The "*" denotes the complex conjugate.

The measure of the fraction of energy in the gravity at a particular wavenumber, which can be attributed to the bathymetry, is given by the coherence, γ^2:

$$\gamma^2(k) = (N \cdot \frac{C(k) \cdot C(k)^*}{E_0(k) \cdot E_1(k)} - 1)/(N-1), \quad (4)$$

where the power spectrum of gravimetry, $E_0(k)$, is:

$$E_0(k) = \frac{1}{N}\sum_{r=1}^{N} G(k)_r \cdot G(k)_r^* \quad (5)$$

The above admittance estimation mutually assumes that the Cocos plate across Tehuantepec ridge is all in one, but several works recognized that the ridge separates the Cocos plate in two parts with distinct tectonic regimes and age (*DSDP 66 and 84; Wilson, 1996; Couch and Woodcock, 1981; Klitgord and Mammerickx, 1982; Manea et al., 2003*). According to these papers the difference in ages ranges from 8 to 12 Ma. Therefore, in order to perform a distinct admittance analysis, the original profiles were divided into two groups across TR. One data set, situated north of the Tehuantepec ridge, is represented by 7 profiles of 187 km each, meanwhile the second data set, situated south of the Tehuantepec ridge, contains 7 profiles of 325 km length. A total of 256 samples of the free air gravity anomaly and bathymetry data were extracted from each data set resulting into a regularly spaced data set at intervals of 0.73 km ($0.0168 < k < 4.3$) and 1.27 km ($0.00967 < k < 2.47$) respectively. Then the data were processes in the same manner as for the original profiles of 483 km length.

Theoretical Admittance

The theoretical models of isostatic compensation (Airy and Vening-Meinesz) contain the plate (***Tc***) and elastic thickness (***Te***) information. The theoretical curves of admittance for Airy isostatic compensation ($Z(k)^{Airy}$) (*Fig. 3-A*) and for the simple flexure isostatic compensation model ($Z(k)^{Flex}$) (Vening-Meinesz) (*Fig. 3-B*) are based on the following equations:

$$\therefore Z(k)^{Airy} = 2\pi G(\rho_c - \rho_w)e^{-kd}(1 - e^{-kT_c}), \quad (6)$$

$$\therefore Z(k)^{FLEX} = 2\pi G(\rho_c - \rho_w)e^{-kd}(1 - \Phi_e^{'}(k)e^{-kT_c}), \quad (7)$$

where:

G - universal gravitational constant *($6.6726 \cdot 10^{-11}$ $N \cdot m^2/kg^2$),*

t - mean thickness of the crust,

ρ_c - crust density,

ρ_m - mantle density,

ρ_w - water density,

d - water depth,

Tc - oceanic crust thickness (7 km for Pacific crust),

$\Phi_e^{'}(k)$ - wavenumber parameter (*Watts, 2001*), expressed by:

$$\Phi_e^{'}(k) = \left(\frac{Dk^4}{(\rho_m - \rho_c)g} + 1\right)^{-1}, \quad (8)$$

where:

D - flexural rigidity ($D = \frac{E\boldsymbol{T}_e^3}{12(1-\nu^2)}$),

E - Young's modulus (10^{11}N/m^2),

Te - elastic thickness,

ν - Poisson's ratio (0.25).

RESULTS

The profiles of bathymetry which cross the TR zone indicate the existence of two distinct areas separated by the TR: the northwestern area characterized by depths between 3500 - 3900 m and the southeastern area (corresponding to the Guatemala Basin) with depths between 4200 - 4800 m, with a difference of ~ 1000 m between them. The gravity low of ~ -7 to -8 mGal indicates the location of the limit between the two regionss. The 2D gravity modeling performed (*Fig. 2*) is in good agreement with the age/depth and age/lithospheric thickness estimates and supports that the TR is a border between those two parts, which are thicker in the southeastern part than in the northwestern portion.

The amplitude, phase and coherence of the admittance function over the TR are shown in *Fig. 4*. The slope of the dashed line (*Fig. 4-A*) gives an estimate of the water depth of 4000 m, and the intercept of this line on the vertical axis gives a density estimate of the bathymetry of approximately 2.55 g/cm^3. For $0.0065 < k < 0.4$ ($966 > \lambda > 15$ km), the coherence is high (> 0.5) suggesting that most of the energy in the free-air gravity anomaly is caused by the bathymetry. Within the same waveband the admittance and phase are smooth (*Fig. 4-A,C*). *Fig. 3* shows the admittance estimates together with theoretical curves for Airy isostatic compensation (A) and simple flexure isostatic compensation (B) models. The error bars in the admittance coefficients are computed from the coherence (*Watts, 1978*). The decrease of the admittance at low wave numbers is caused by isostasy

suggesting that TR is isostatically compensated. The Airy model fits the observed admittance for mean crustal thickness of 20 - 40 km. These values are higher than the normal oceanic crustal thickness (7 - 8 km) and consequently the Airy model cannot be accepted as a possible isostatic compensation mechanism. A simple plate flexure model with ***Te*** = 10 ± 5 km (*Fig. 3-B*) seems to be more feasible. The side wings of the filter (which is the inverse FFT of the admittance) coefficients are negatives and do not decrease asymptotically to zero (*Fig. 5*) suggesting that the structure is isostatically compensated. To test the success of this method, the inverse FFT was applied to the product between the admittance and FFT of bathymetry in order to obtain the predicted gravity. The good correlation between the observed and predicted gravity (*Fig. 6*), is an indicator that the admittance technique is adequate for the present study.

Using the half space cooling model (*Watts, 2001*) for a cut-off temperature of 450 °C (elastic to ductile behavior transition), the age of ~ 8 +9/-6 Ma was obtained for the oceanic lithosphere at the time of TR onset (*Fig. 7*).

The results obtained by dividing the data into tow groups show a Te for the oceanic lithosphere south of the Tehuantepec ridge of 10 - 15 km (*Fig. 9-B*). As for the second data set (situated north of Tehuantepec ridge), the high dispersion of the admittance for low wavenumbers does not allow to estimate a reliable Te, likely because of the very short profiles. Here, apparently Te is 5 -10 km (*Fig. 9-A*). Also, it looks like there is less scattering for admittance at low wavelengths when we divide the data in two parts according

to TR (*Fig. 8),* suggesting that there is an important age difference, and therefore Te difference, across the Tehuantepec ridge.

According to *Watts's (2001)* studies, oceanic fracture zones are characterized by specific shapes and specific isostatic responses. Using yield strength envelopes for oceanic lithosphere for two different thermal ages in the range of 16 - 26 Ma, *Watts (2001)* obtained a difference in ***Te*** of ~ 6 km. The simple plate flexure model, which considers a continuous plate beneath the TR, gives a ***Te*** estimate of 10 ± 5 km; therefore, the application of the admittance techniques for a fracture zone with a ~ 10 Ma (~ 6 km ***Te*** difference) discrepancy between the two regions might be a good model approximation.

2D GRAVITY MODELING ACROSS TEHUANTEPEC RIDGE

Using a mean free-air gravity profile (from the 7 profiles used for observed admittance estimation) we obtained a 2-D density model (*Fig. 2*). The densities used are the same as those used by *Couch and Woodcock (1982):* 1.03 g/cm^3 for sea water, 2 g/cm^3 for sediments, 2.8 g/cm^3 for basalts and gabbros, 3.32 g/cm^3 for oceanic litosphere and 3.1 g/cm^3 for the asthenosphere. The model shows that the southeastern oceanic lithosphere is thicker (~ 50 km) than in the northwestern part (~ 38 km). Using the relationship between the thickness of the oceanic lithosphere and its age (*Turcotte and Schubert, 1982*) the southeastern part has an age of ~ 17 Ma, while the northwestern part has an age of ~ 10 Ma (age difference of ~ 7 Ma). The average crustal density of 2.55 g/cm^3 inferred from admittance analysis (Fig. 4) is lower than the density value (2.8 g/cm^3) used in the 2D density model. Nevertheless, this normal density value of 2.8 g/cm^3 for the oceanic crust is situated in the density range predicted by means of admittance (2.2 – 2.9 g/cm^3).

CONCLUSIONS AND DISCUSSIONS

A previous study in this area (*Couch and Woodcock, 1981*) gave an erroneous result regarding the structure of TR. They obtained for a profile crossing TR the same separation of the Cocos plate in two distinct parts, with the specification that the northwestern part seems to be thicker than the southeastern. This is in contradiction with other authors (*Truchan and Larson, 1973; Klitgord and Mammerickx, 1982*) and with the age/depth and age/lithospheric thickness relationship (*Turcotte and Schubert, 1982).* Using a mean free-air gravity profile over TR (from the 7 profiles used for the admittance estimation), we performed a 2D gravity model that can support the idea that the southeastern part is older, thicker and colder (with a lower thermal gradient) than the northwestern one. The mean age difference between the two regions is ~ 7 Ma.

The assessment of the elastic thickness, ***Te***, and of the lithospheric age at the time of bathymetric loading of the TR was deduced from the analysis of the experimental admittance. The best fitting model can be considered the simple flexure model with an estimated ***Te*** of 10 $\pm$ 5 km, since the Airy model gives an overestimated ***Te*** of 30 $\pm$ 10 km. Low observed admittance for low wavenumbers and also the shape of the filter coefficients show that TR is isostatically compensated. Using the estimate for ***Te*** and a half-space cooling model, the age of the oceanic lithosphere at the time of the TR onset is ~ 8 +9/-6 Ma.

Since we have an older plate on one side and a younger plate on the other side of TR, we mix together measurements of two different ***Te*** in one analysis. Probably this might be the cause for considerable data scattering at short wavelengths (4 - 6 km) (*Fig. 4*). Separating the data in two distinct parts (NW and SE of TR), the admittance for short wavelength seems to be less scattered (*Fig. 8*). This result suggests that there might be an important age difference across the TR and therefore a different ***Te***. In order to search for this difference in Te, we perform the admittance analysis both in NW and SE, independently. The results apparently show that in NW (where the crust is younger) the ***Te*** is ~ 5 - 10 km, while in SE the ***Te*** has values of ~ 10 - 15 km (*Fig. 9*). The important scattered of the admittance for the NW region (*Fig. 9-A*) is probably caused by the very limited length (187 km) of the profiles used in the analysis. On the other hand, because of the larger profiles (325 km) used in the SE part, we found a less scattered admittance for low wavenumbers and a better ***Te*** estimate (*Fig. 9-B*).

Because of the inconclusive ***Te*** estimate for the NW part we cannot assume that we have a significant difference in the ***Te*** values for that two sides. In this way, might be justified a better use of the simpler model assuming a single value of the ***Te*** across TR.

Acknowledgments

Very helpful comments and constructive suggestions by two anonymous reviewers were very important to improve the manuscript. This study was supported by G25842-T and 37293-T CONACYT grants.

REFERENCES

Aubouin, J., von Huene, R. et al., 1982. Initial Reports*. Deep Sea Drilling Project,* v. 67, Washington (U.S. Govt. Printing Office).

Couch, R., and Woodcock, S., 1981. Gravity structure of the continental margins of southwestern Mexico and northwestern Guatemala. *Journal Geophysical Research, 86*, 1829-1840.

Damon, P.E., and Montesinos, E., 1978. Late Cenozoic volcanism and metallogenesis over an active Benioff zone in Chiapas, Mexico. *Arizona Geological Society Digest, Volume XI, 155-168.*

DSDP Leg 66. Shipboard party, 1979, Middle America Trench. *Geotimes, v. 24, p. 20-22.*

DSDP Leg 84. Shipboard party, 1982, Challenger drills again off Guatemala. *Geotimes, v. 27, p. 23-25.*

Engdahl, E. R., and W. A. Rinehart, 1991. Seismicity map of North America project *in* Slemmons, D. B., E. R. Engdahl, M. D. Zoback, and D. B. Blackwell, eds., Neotectonics of North America. *Decade Map Volume 1 in The Decade of North American Geology Project series, GSA, Boulder, p. 21-27.*

GEODAS v. 4.0, Marine Trackline Geophysics. U.S. Department of Commerce, National Oceanic and Atmospheric Administration.

Herron, E.M., 1972. Sea-floor spreading and the Cenozoic history of the east-central Pacific. *GSA Bulletin, 83*, *1671-1692.*

Klitgord, K.D., and Mammerickx, J., 1982. Northern east Pacific Rise; magnetic anomaly and bathymetric framework. *Journal of Geophysical Research, 87*, *138, 6725-6750.*

Kogan, M.G., and Kostoglodov, V., 1981. Isostasy of Fracture Zones in the Atlantic Ocean. *Journal of Geophysical Research, 86*, *9248-9258.*

Manea, M., Manea, V.C., and Kostoglodov, V., 2003. Sediment Fill of the Middle America Trench Inferred from the Gravity Anomalies. *Geofisica Internacional, v. 42, no. 4, pp. 603-612.*

Menard, H.W., and Fisher, R.L., 1958. Clipperton fracture zone in the northeastern equatorial Pacific*. Journal of. Geology, 66, no. 3, 239-253.*

Parsons, B., and Sclater, J.G., 1977. An analysis of the variations of ocean floor bathymetry with age. *Journal of Geophysical Research, 82*, *803-827.*

Smith, W.H.F., and Sandwell, D.T., 1997. Global sea-floor topography from satellite altimetry and ship depth soundings. *Science, 277*, *1957-1962.*

Tamsett, D., 1984. An application of the response technique to profiles of bathymetry and gravity in the Gulf of Aden. *Geophysical Research Letters Astronomical Society, 78, 349-369.*

Truchan, M., and Larson, R.L., 1973. Tectonic lineaments on the Cocos Plate. *Earth and Planetary Science Letters, 17, 46-432.*

Turcotte, D.L., and Schubert, G., 1982. Geodynamics, Applications of continuum Physics to Geological Problems. *Wiley, New York, NY.*

Watts, A.B., 1978. An analysis of isostasy in the World's oceans. 1. Hawaiia-Emperor seamount chain. *Journal of Geophysical Research, 83*, 5989-6004.

Watts, A.B., 2001. Isostasy and Flexure of the Lithosphere. Cambridge University Press.

Wessel, P., 1989. XOVER: A Cross-over error detector for track data. *Computers and Geoscience, 15*, *333-346.*

Wessel, P., and Watts, A.B., 1988. On the accuracy of marine gravity measurements*. Journal of Geophysical Research, 93*, 393-413, Table A1.

Wilson, D.S., 1996. Fastest known spreading on the Miocene Cocos-Pacific plate boundary. Geophysical Research Letters 23, no. 21, 3003-3006.

FIGURE CAPTIONS

Figure 1.

The bathymetry (based on *Smith and Sandwell, 1997*) and location of the study area. The inset represents the magnified study area.

Inset: Location of the free air gravity anomaly and bathymetry profiles. Dashed-lines represent the original ship-tracks; solid lines indicate the profiles where the data along each track were projected perpendicular to TR. MAT – Middle America Trench.

Figure 2.

2-D density model along the mean profile from the 7 profiles used for admittance estimation. The densities are in g/cm^3 from *Couch and Woodcock (1982)*. The upper continuous curve gives the computed anomaly. The circles represent the observed free air gravity. The density of 2 g/cm^3 corresponds to a very thin layer of oceanic sediments.

Figure 3.

Amplitude of admittance for low wavenumbers k = 0.0 - 0.3. Observed admittance values (solid circles) and theoretical curves for Airy isostatic compensation **(A)** and simple flexure isostatic compensation model **(B)**. The standard error on each estimate is computed from the coherence (*Watts, 1978*).

The best fitting model is for a simple flexure elastic oceanic crust (B) with ***Te*** = 10 ± 5 km.

Figure 4.

A - Continuous line is the calculated admittance. Dashed line is the regression line for low wavenumbers. d_{med} and ρ_{med} represent the calculated mean water depth and oceanic crust density.

B - Continuous line represents the coherence, which is high (> 0.5) for low wavenumbers.

C - Continuous line shows the phase, which is close to zero for low wavenumbers.

Figure 5.

The spatial filter generated from the inverse FFT of the admittance. The shape of the filter side wings, which are not decreasing asymptotically to zero, is an indicator that TR is isostatically compensated.

Figure 6.

Observed (continuous blue line) and predicted gravity (dashed red line) for profiles A, B, C and F. The predicted gravity (or filtered bathymetry) is inferred by applying an inverse FFT to the product between the admittance and the FFT of bathymetry.

Figure 7.

Plot of ***Te*** against the age of the lithosphere at the time of loading (TR onset). The isotherms are calculated for the half-space cooling model. For a ***Te*** of 10 $\pm$ 5 km the plate age is ~ 8 +9/-6 Ma.

Figure 8.

A – Calculated admittance for profiles across TR;

B – Calculated admittance for profiles situated in the NW part of TR;

C – Calculated admittance for profiles located on the SE part of TR.

Note the less scattered in admittance estimation for short wavelengths when the analysis is done on separate datasets. The insets to the left show the location of the profiles. Isochrons are based on *Wilson (1996).*

Figure 9.

Amplitude of admittance for low wavenumbers *k* = 0.0 - 0.3 for two separated datasets. Observed admittance values (solid circles) and theoretical curves for simple flexure isostatic compensation model for NW part of TR **(A)** and for SE part of TR **(B)**. The standard error on each estimate is computed from the coherence (*Watts, 1978*). The best fitting model for the SE part is a simple flexure elastic oceanic crust with ***Te*** = 10 –15 km. For the NW part a reliable ***Te*** estimation is not possible due to a large dispersion of the observed admittance. The insets show the location of the profiles with isochrons based on *Wilson (1996).*

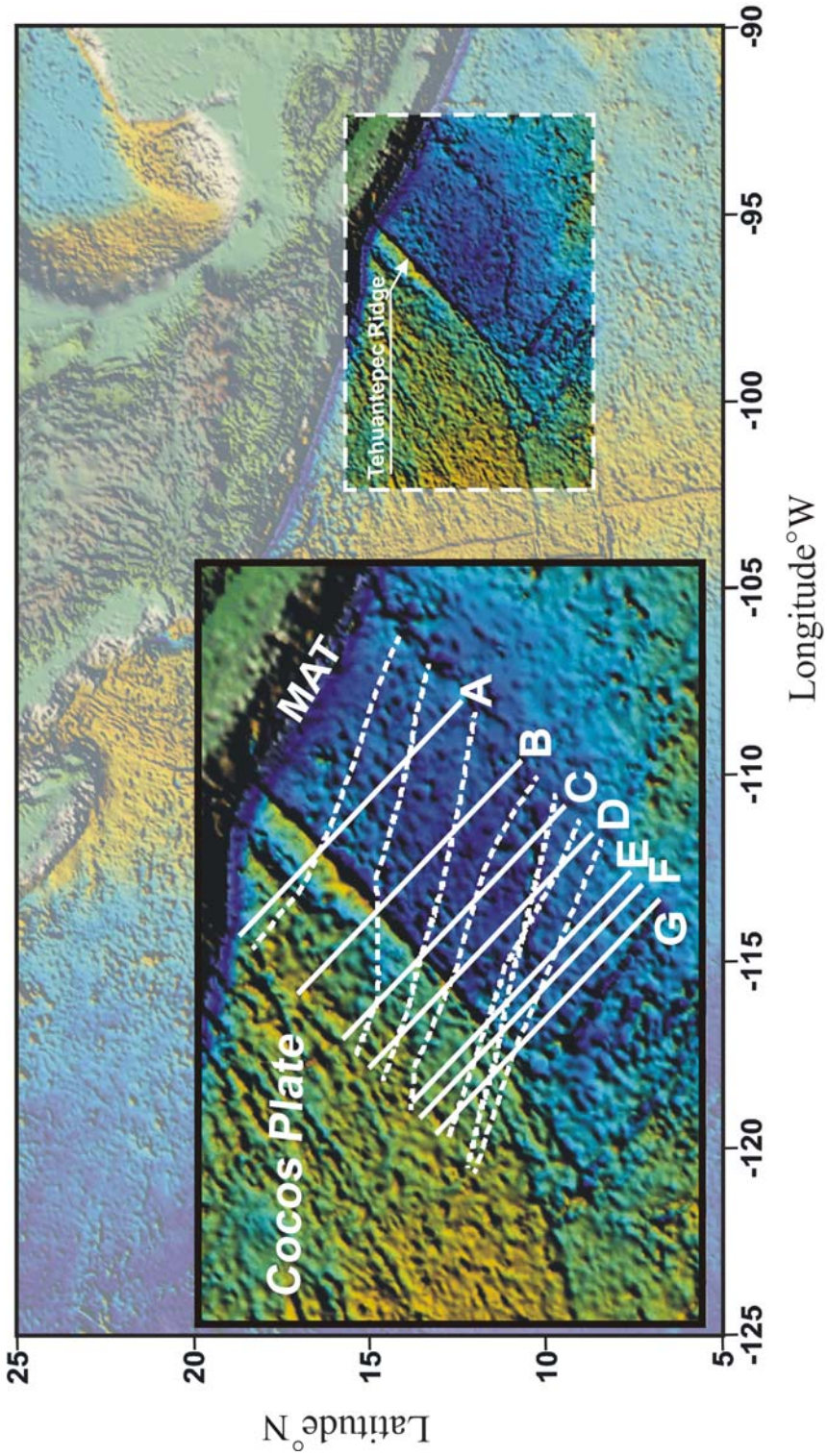
Tehuantepec Ridge
MAT
A
B
C
D
E
F
G
Cocos Plate
-90
-95
-100
-105
-110
-115
-120
-125
Longitude°W
25
20
15
10
5
Latitude°N

Figure 1

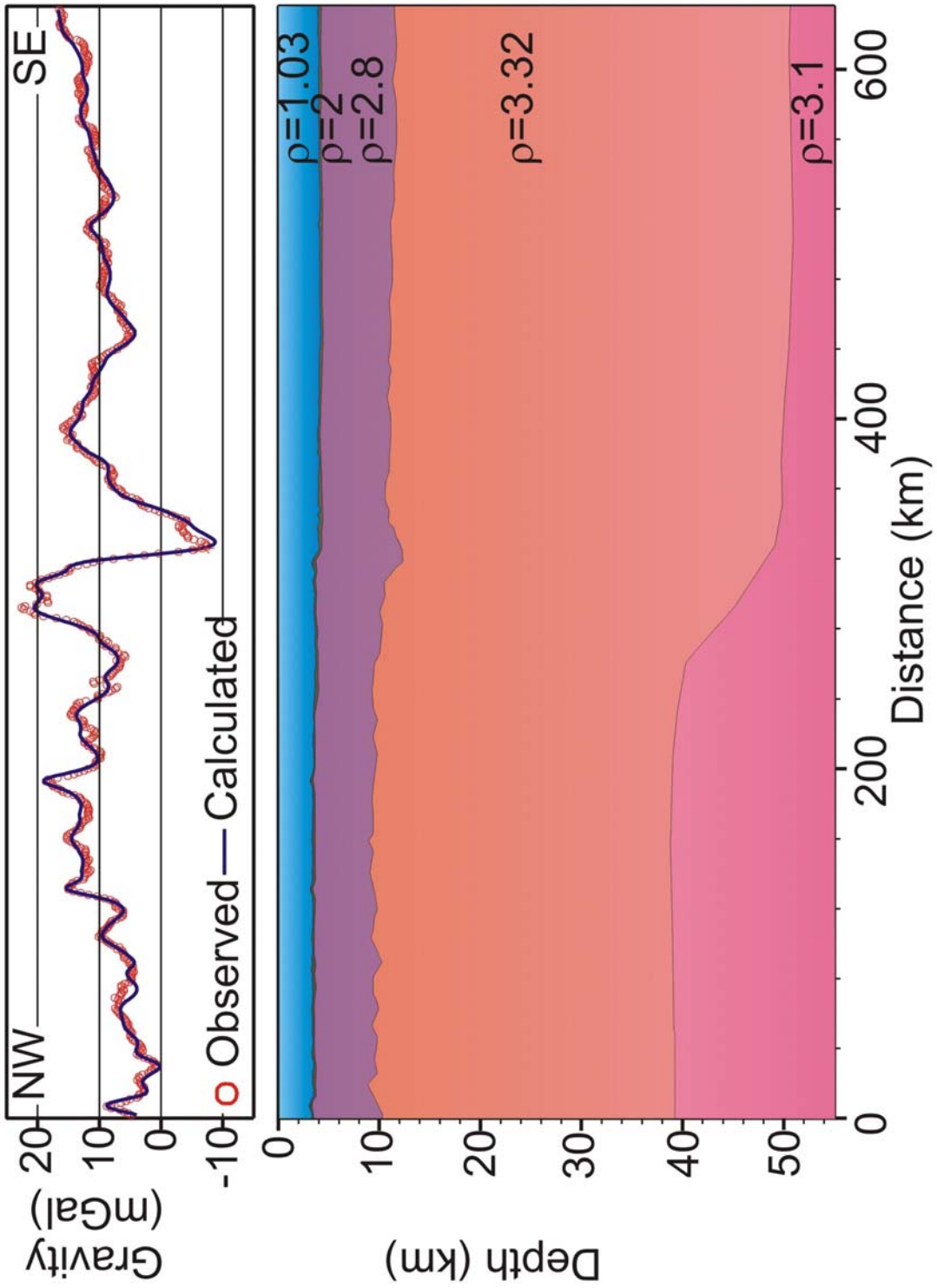
NW
SE
Gravity (mGal)
20
10
0
-10
o Observed — Calculated
Depth (km)
0
10
20
30
40
50
ρ=1.03
ρ=2
ρ=2.8
ρ=3.32
ρ=3.1
0
200
400
600
Distance (km)

Figure 2

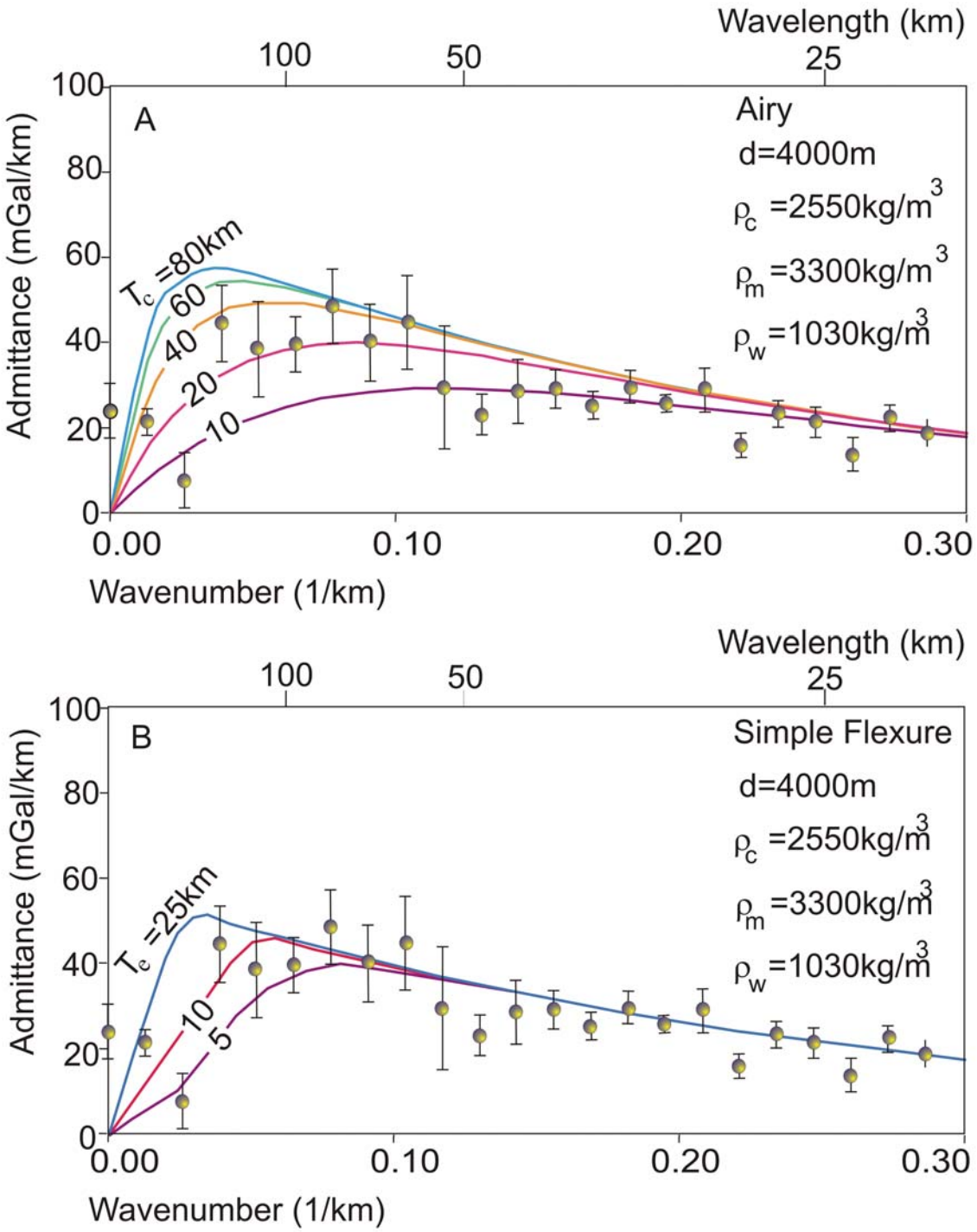
Wavelength (km)
100
50
25
A
Airy
d=4000m
ρc =2550kg/m3
ρm =3300kg/m3
ρw =1030kg/m3
Tc =80km
60
40
20
10
Admittance (mGal/km)
Wavenumber (1/km)
0.00
0.10
0.20
0.30
B
Simple Flexure
d=4000m
ρc =2550kg/m3
ρm =3300kg/m3
ρw =1030kg/m3
Te =25km
10
5

Figure 3

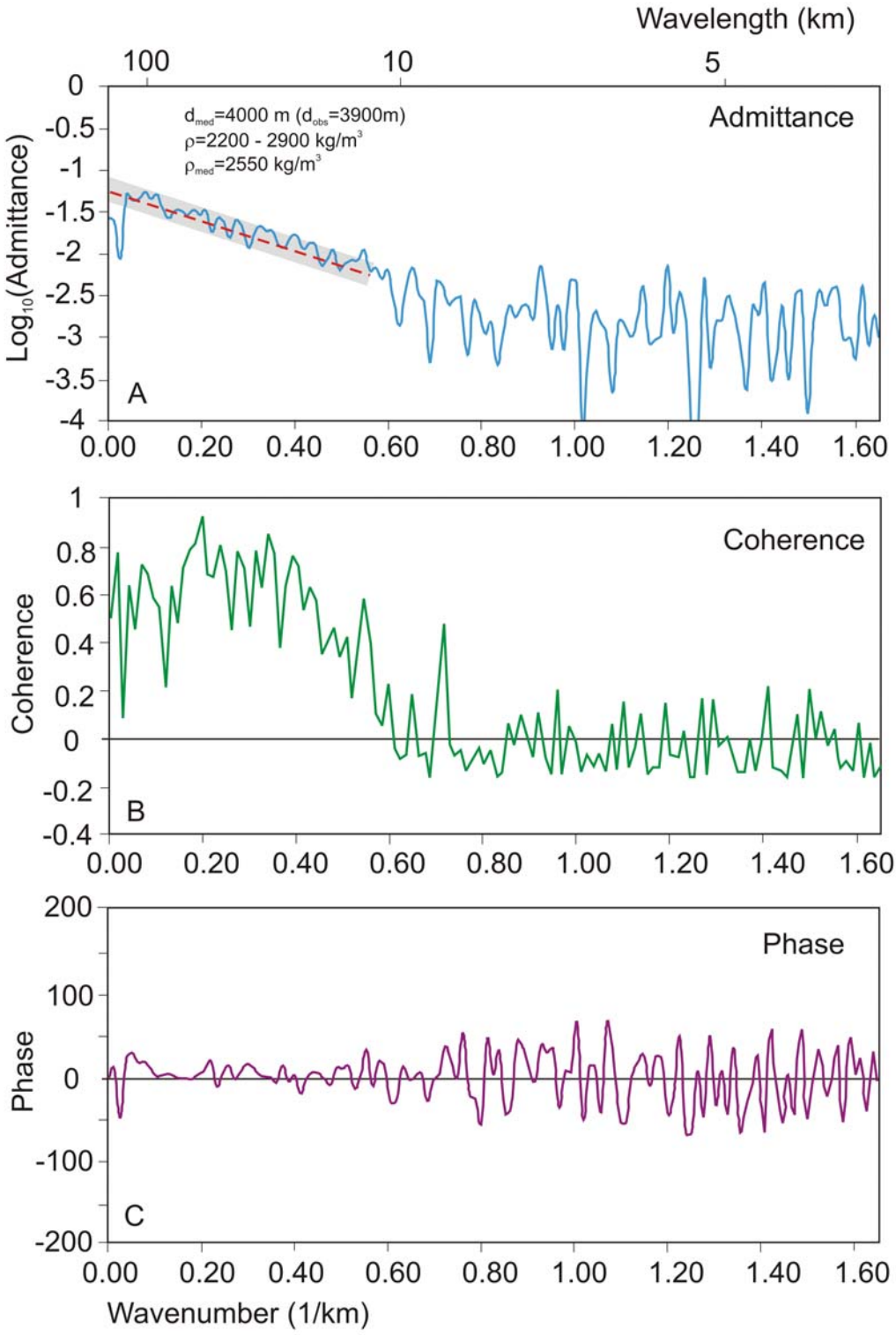
Wavelength (km)
100
10
5
Admittance
d_{med}=4000 m (d_{obs}=3900m)
ρ=2200 - 2900 kg/m^3
ρ_{med}=2550 kg/m^3
Log$_{10}$(Admittance)
A
Coherence
B
Phase
C
Wavenumber (1/km)

Figure 4

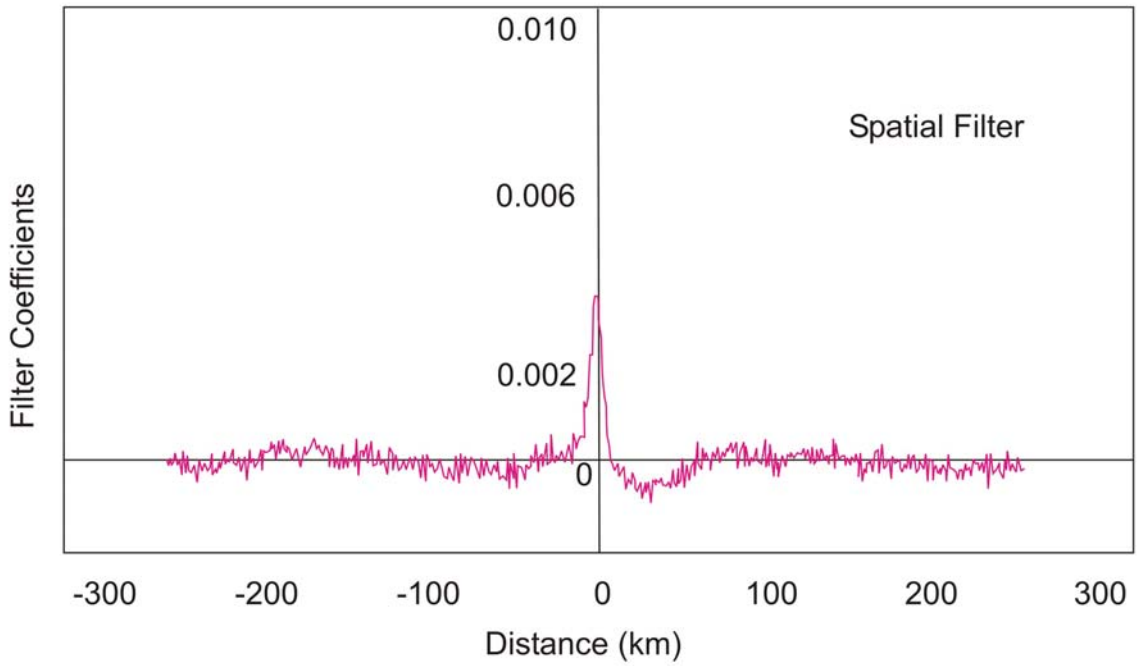
0.010
0.006
0.002
0
Spatial Filter
Filter Coefficients
-300
-200
-100
0
100
200
300
Distance (km)

Figure 5

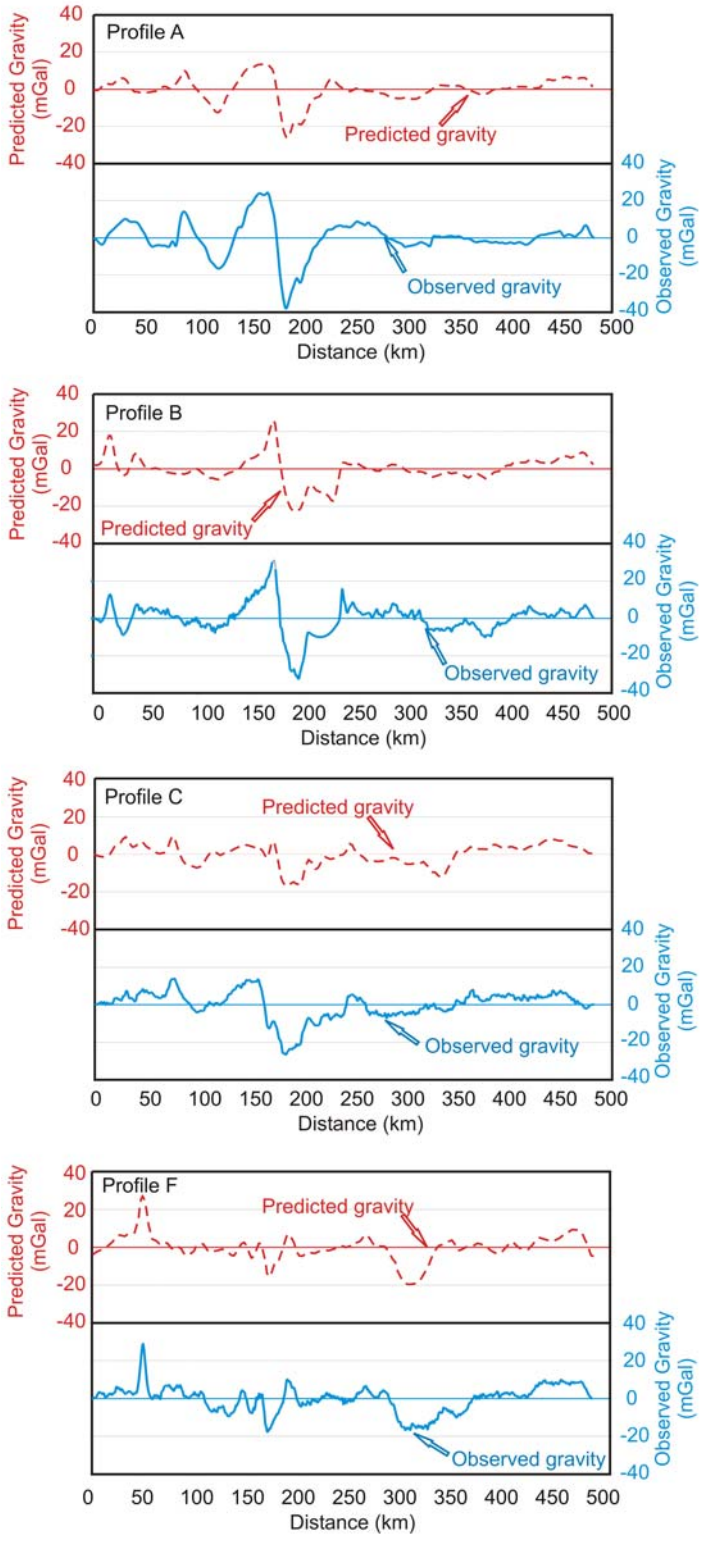
Profile A
Predicted gravity
Observed gravity
Predicted Gravity (mGal)
Observed Gravity (mGal)
Distance (km)
Profile B
Predicted gravity
Observed gravity
Predicted Gravity (mGal)
Observed Gravity (mGal)
Distance (km)
Profile C
Predicted gravity
Observed gravity
Predicted Gravity (mGal)
Observed Gravity (mGal)
Distance (km)
Profile F
Predicted gravity
Observed gravity
Predicted Gravity (mGal)
Observed Gravity (mGal)
Distance (km)

Figure 6

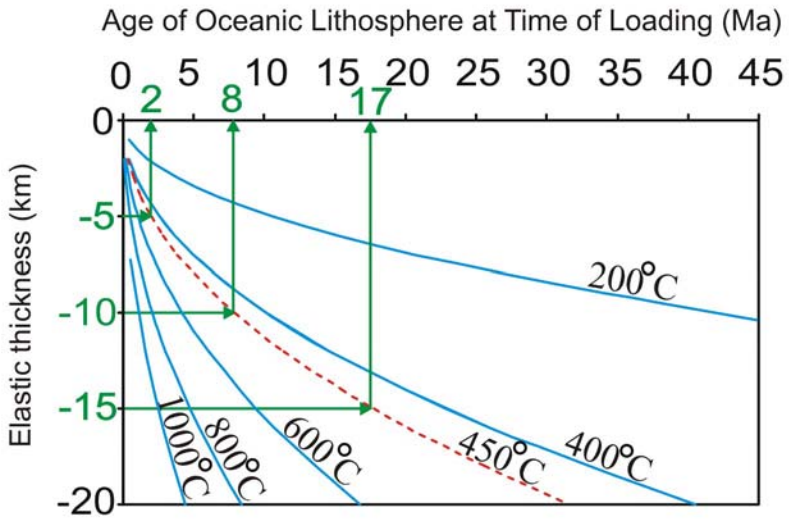
Age of Oceanic Lithosphere at Time of Loading (Ma)
0 5 10 15 20 25 30 35 40 45
2
8
17
0
-5
-10
-15
-20
Elastic thickness (km)
200°C
400°C
450°C
600°C
800°C
1000°C

Figure 7

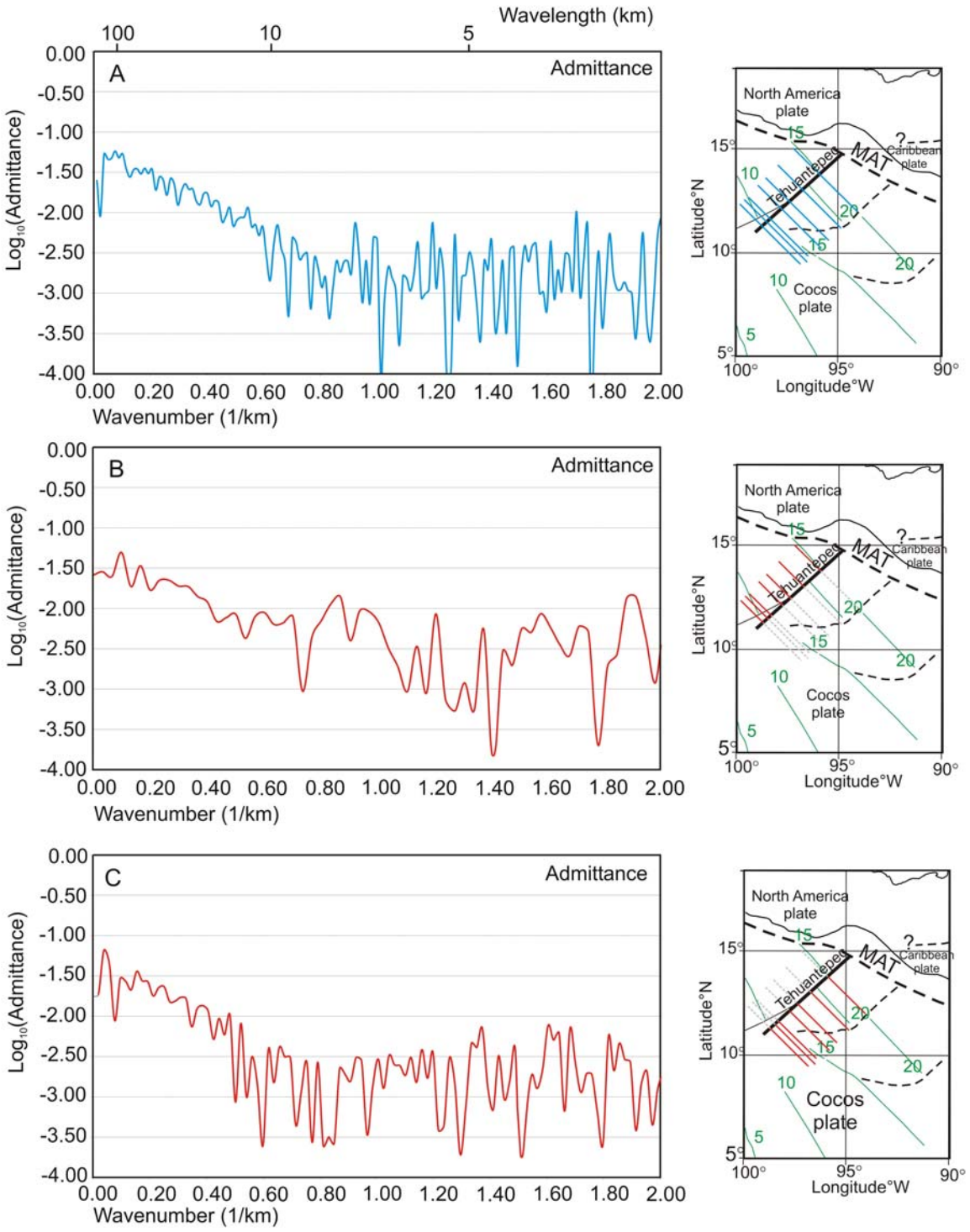
Wavelength (km)
100
10
5
A
Admittance
Log10(Admittance)
Wavenumber (1/km)
North America plate
Caribbean plate
MAT
Tehuantepec
Cocos plate
Latitude°N
Longitude°W
B
C

Figure 8

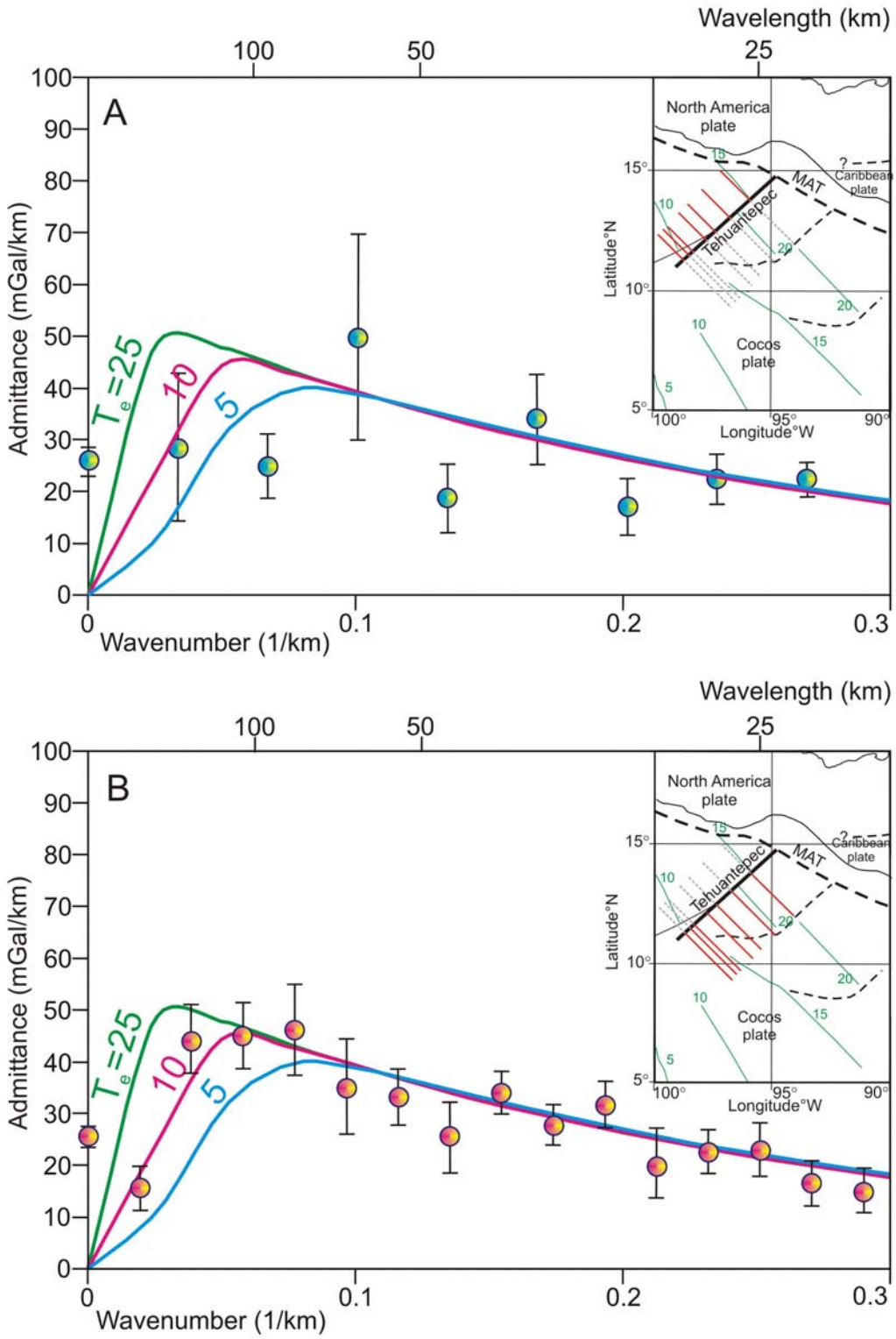
Wavelength (km)
100
50
25
A
B
Admittance (mGal/km)
Wavenumber (1/km)
0
0.1
0.2
0.3
T_e=25
10
5
North America plate
Caribbean plate
MAT
Tehuantepec
Cocos plate
Latitude°N
Longitude°W
15°
10°
5°
100°
95°
90°

Figure 9

IV. ESTRUCTURA Y ORIGEN DE LA CORDILLERA DE TEHUANTEPEC

Submitted to Earth and Planetary Science Letters

STRUCTURE AND ORIGIN OF THE TEHUANTEPEC RIDGE

Manea, M.[1], Manea, V.C.[1], Ferrari, L.[2], and Kostoglodov, V.[1]

[1]Instituto de Geofisica, UNAM, Ciudad Universitaria, Mexico

[2]Centro de Geociencias, UNAM, campus Juriquilla, Qro., Mexico

ABSTRACT

The Tehuantepec ridge is one of the most prominent lithospheric structures of the Cocos plate, yet its age and mechanism of formation have remained poorly constrained until now. Based on a morphostructural analysis of the ridge and the surrounding ocean floor in the Guatemala Basin as well as on geodynamic relations, we propose two genetic models for Tehuantepec Ridge: one in which the ridge was formed by transpression between two regions of the Cocos plate assuming a differential motion of a third microplate, and an alternative model testing the response of a fracture zone to changes in the rotation Euler pole without any differential motion of a third plate.

The first model proposes that a decrease in spreading rate at the East Pacific Rise south of the Clipperton Fracture Zone after 12 - 14 Ma would have led

to significant transpressional deformation along the fracture zone, resulting in the formation of the Tehuantepec Ridge. The estimates indicate that the position of the intersection between the Clipperton Fracture Zone and the Tehuantepec Ridge corresponds to an age of ~12 Ma, which is considered the time of initiation of transpression. The Tehuantepec Ridge subsequently developed until ~ 3.5 Ma through episodic pole shifts that also produced other secondary associated structures in the Guatemala Basin.

The second model is based on the analysis of a similar pattern along the Kane Fracture Zone in the Atlantic Ocean. This model assumes that the fracture zone existed before a clockwise change in direction of relative plate motion tooks place. The resulting structure of this model on the eastern limb of the Clipperton Fracture Zone looks remarkably similar with the Tehuantepec ridge and its associated structures.

Keywords: Tehuantepec ridge, Clipperton Fracture Zone, Guatemala Basin, Euler pole shift, Cocos plate.

INTRODUCTION

According to the classic view of Plate Tectonics, transform plate boundaries are characterized by narrow strike-slip deformation zones parallel to a small circle around the Euler pole of relative motion between the two plates. In some cases, however, deformation can deviate from pure strike-slip so that transform faults may accommodate a compressional component of deformation (e.g. *Sonder and Pockalny, 1999*). Here we analyze the case of the Tehuantepec Ridge (*Fig. 1*), located on the Cocos plate at the eastern prolongation of the Clipperton Fracture Zone. Whereas other fracture zones from the East Pacific Rise toward the Middle American Trench (i.e. Orozco, O'Gorman) present a curved shape, the Tehuantepec Ridge is characterize by its linearity (*Fig. 1*). Several works recognized that the ridge separates the Cocos plate in two parts with distinct tectonic regimes and age (*DSDP 66 and 84; Wilson, 1996; Couch and Woodcock, 1981; Klitgord and Mammerickx, 1982; Manea et al., 2003*). According to these papers the difference in ages ranges from 8 to 12 Ma. Using a mean gravity profile over TR, *Manea et al. (2004)* found a mean age difference across Tehuantepec ridge of ~ 7 Ma. By contrast the difference in age across the Clipperton Fracture Zone east of the East Pacific Rise is only 1.6 Ma (*Pockalny, 1997*) suggesting that something unusual has happed in the Guatemala Basin just south of Tehuantepec ridge. Using the spectral technique (admittance) to free-air gravity and bathymetry data over Tehuantepec ridge, *Manea et al. (2004)* found an age of 8 +9/-6 Ma for the oceanic lithosphere at the time of Tehuantepec ridge onset.

A few authors tried to explain the nature of the Tehuantepec Ridge. *Herron (1972)* considers the Tehuantepec Ridge as the result of a hot spot trace. The sharp and asymmetric morphology of the Tehuantepec ridge *(Fig. 2),* however, suggests that this is a tectonic rather than a volcanic feature. *Truchan and Larson (1973)* consider the ridge as a hinge fault separating the part of the Cocos Plate subducting beneath the North America plate to the northwest from that subducting beneath the Caribbean plate to the southeast. Subsequent seismological studies (*Ponce et al., 1992; Bravo et al., 2004*) basically support this interpretation showing that the Cocos plate increases its dip up to 45° and the depth of seismicity reaches 270 km to the east of the intersection between the Tehuantepec Ridge and the Middle America Trench. However, the absence of seismicity rules out that the ridge is the product of an ongoing deformation process. Another study of *Schilt et al. (1982)* suggests that Tehuantepec ridge initiated as a ridge-ridge transform which may have created the Clipperton fracture zone.

In this study we infer the age of the Cocos plate just south of Tehuantepec ridge and Clipperton Mountains using the relationship between the ocean depth and its age (half space cooling model). Accordingly, it is possible to infer the full spreading rate in this area (south of Clipperton fracture zone) and to compare it with the full spreading rate just north of the Clipperton fracture zone). To evaluate the success of this method we use for comparison the previous Cocos and Pacific plates age estimation in Guatemala basin from *Wilson (1996)* and *Klitgord and Mammerickx (1982).* To constrain independently the age of the Cocos plate at the trench we use the relation between the thermal parameter and the maximum depth

of seismicity (*Gorbatov et al., 1997*). A recent study of *Kanjorski (2003)* shows that the oceanic crust is uniformly increasing in age from ~ 12.3 to ~ 16.2 Ma from northwest to southeast along the trench axis between the Orozco Fracture Zone and Tehuantepec ridge. Another study of *Barckhausen et al. (2001)* shows a uniform age of ~ 24 Ma for the Cocos plate along the trench offshore Costa Rica. We compare our plate age estimation at the trench with these two estimates.

Kanjorski (2003) reports a slow down of the Cocos plate north of Tehuantepec ridge ~ 12 Ma ago. The magnetic model uses a half spreading rate of 7.8 cm/yr from 12 - 17 Ma decreasing in rate of spreading to 4.8 cm/yr between 5.5 - 12 Ma. In this work, we propose two possible models: one in which the Tehuantepec ridge may be the result of transpressional deformation due to different Euler poles for the Pacific - N. Cocos and Pacific - S. Cocos plates, and an alternative model in which the Tehuantepec ridge and its associated structures represents the severe response of an old fracture zone to a ~10° clockwise change in direction of plate motion around 12 Ma.

MORPHO - STRUCTURAL ANALYSIS

The Tehuantepec Ridge is a ~ 625 km long linear structure, making an angle of ~ 45° with the coastline (*Fig. 1*). In cross-section, the bathymetry is highly asymmetric with a difference of ~ 1,000 m between the two regions (*Fig. 2*). To the northwest, an abyssal plain with depths of approximately 3,500 - 3,900 m flanks the Tehuantepec Ridge. To the southeast of the ridge the Guatemala Basin is characterized by a rugged morphology, with depth ranging between 4,200 - 4,800 m. Approaching the Middle America Trench the difference in bathymetry across the Tehuantepec Ridge increases from ~ 400 m to ~ 1,110 m. Close to the trench the differential height diminishes again to ~ 850 m due to the bending of the plate. The ridge itself has an elevation of over 1,000 m with respect to the adjacent NW plain (*Fig. 2*), which contrasts with the small relief of the Orozco and O'Gorman fracture zones to the northwest. The asymmetric morphology suggests that the Tehuantepec Ridge may be the expression of a major compressional structure, along which an area of the Cocos plate to the northwest overthrusted the Guatemala Basin (*Fig. 2*).

The Tehuantepec Ridge intersects the Clipperton Fracture Zone near 13°N, 97°W and can be followed for about 310 km to the southwest within the Cocos plate until it disappears. The intersection between the Tehuantepec Ridge and the Clipperton Fracture Zone (point "P" in *Fig. 1 - inset*) corresponds to magnetic anomaly 5A (~ 12 Ma) (Klitgord and Mammerickx, 1982). The region located at the

southwestern end of the Tehuantepec Ridge is characterized by two other bathymetric highs (F1 and F2) with a similar morphology (*Fig. 1 - inset*). These two linear structures make an angle of ~ 10º and 20º respectively with Tehuantepec ridge. F1 is a continuous and well-defined structure with a total length of ~ 340 km that intersects the Tehuantepec Ridge at point "P1". The second linear feature (F2) is shorter (~ 260 km), discontinuous and not as well pronounced as F1. Two remarkably similar deep fractures, T1 and T2, are located in the same region at an angle of ~ 80º and ~ 70º with the Tehuantepec Ridge and F1 respectively. These deep fractures might represent scars of ridge jumps, representing one possible mode to end up with very asymmetric spreading rates. T1 and T2 point toward the end of Tehuantepec Ridge and F1, and they have a total length of ~ 250 km and ~ 280 km, respectively. With a mean depth of ~ 800 m T1 is deeper than T2, which has an average depth of ~ 500 m. Another clear structure (T3) appears at the southeastern part of the Guatemala basin. This is a trough with a mean depth of 200 - 300 m and two orientations. The part closer to the trench is parallel to the Tehuantepec Ridge whereas the rest is oblique with an angle of ~ 45º. This structure looks like a fracture zone that turned into an unstable transform offset, finally suffering an along-axis northward migration. Therefore, the western side of T3 might be a pseudofault trace. Unfortunately, a corresponding pseudofault trace on the Pacific Plate is not clearly seen. The Guatemala basin is bounded by the Tehuantepec Ridge, the Middle America Trench, T3 and T1.

To the west of the East Pacific Rise, the mirror structures of the Tehuantepec Ridge on the Pacific plate are the Clipperton Mountains (*Fig. 1*). This

mountain chain has a total length of ~ 600 km, similar to the Tehuantepec Ridge, but with heights up to 2,500 m, and is flanked by a ~ 2,000 m deep trough on its northern side.

AGE OF THE OCEANIC CRUST IN GUATEMALA BASIN

The age of the oceanic lithosphere just northwest of the Tehuantepec Ridge has been successfully obtained from magnetic anomalies, and is considered of ~ 16 Ma close to the trench (*Kanjorski, 2003; Klitgord and Mammerickx, 1982*). Unfortunately, the low amplitude of the magnetic anomalies in the northern part of the Guatemala basin (*Anderson, 1974*) prevents to obtain reliable crustal ages for this region located to the southeast of the Tehuantepec Ridge. To estimate the age of the Cocos plate in this region we used the method proposed by *Gorbatov and Kostoglodov (1997)* to estimate the age of an oceanic plate at trench, *A* (Ma), from the maximum depth of seismicity, D_m (km), and the vertical component of the convergence rate, $V_\perp$ (km/Ma). The product $\varphi = V_\perp A$ is called the "*thermal parameter*" *(Fig. 3)* and its dependence of D_m is used to infer the age of the oceanic lithosphere at the trench in Chiapas. Using the data from *Gorbatov and Kostoglodov (1997),* the best-fit polynomial curve for $D_m < 350$ km is:

$$D_m = 43.4 + 17.8 \cdot \varphi - 0.58 \cdot \varphi^2 + 0.00765 \cdot \varphi^3, \quad (1)$$

where:

$\varphi = V_\perp \cdot A$

$V_\perp = V \cdot \sin\alpha$

α - the angle of subduction.

The maximum depth of seismicity beneath Chiapas close to Tehuantepec Ridge is ~ 200 km (*Rebollar et al., 1999*), and the angle of subduction is ~ 43° (*Rebollar et al., 1999*). The convergence rate is 7 cm/yr between the Cocos and North American plates for the Chiapas subduction zone (*DeMets et al., 1994*). From equation *(1),* an age of 29 ± 4 Ma is obtained for the Guatemala Basin at the trench in Chiapas (see *Fig. 4*).

An independent way to estimate the age of the Cocos plate southeast of the Tehuantepec ridge is the half-space cooling model (*HSCM*). This equation predicts that the depth of the ocean increases with the square root of the distance from the ridge divided by spreading rate, or the square root of age of the ocean floor. The equation which gives the depth of the ocean floor, *w*, as a function of age, *t*, is the following (*Turcotte & Schubert, 2002):*

$$w = \frac{2 \cdot \rho_m \cdot \alpha_v \cdot (T_1 - T_0)}{\rho_m - \rho_w} \cdot \left(\frac{k \cdot t}{\pi} \right)^{0.5} + w_0, \qquad (2)$$

where:

ρ_m - mantle density (3,300 kg/m^3),

ρ_w - sea water density (1,030 kg/m^3),

α_v - coefficient of thermal expansion (3 x 10^{-5} °K^{-1}),

T_1 - basal temperature (1,300 °K),

T_0 - surface temperature (0 °K),

k - thermal diffusivity (1 mm^2/s),

w_0 - ridge depth (2,600 m),

t - age of the oceanic plate (years),

w - ocean depth (m).

The age of the oceanic plate is calculated for two mean depth profiles: one from East Pacific Rise toward the Middle American Trench and crossing the Guatemala Basin (*Fig. 4*) and another one on the Pacific Plate just south of the Clipperton fracture zone (*Fig. 5*). A very good correlation between the ages predicted with HSCM and magnetic anomalies for ages < ~ 6.5 Ma (*Klitgord and Mammerickx, 1982*) is obtained. Also the 20 Ma magnetic anomaly in Guatemala basin just south of Tehuantepec ridge from *Wilson (1996)* is in good correlation with our estimate of ~ 20.8 Ma (*Fig. 4*). Approaching the trench, the ocean depth decreases due to the bending of the oceanic lithosphere. Therefore an underestimated plate age is obtained and these estimates should not be used. Instead a regression line from the ages unaffected by the bending, gives an age estimate at the trench of ~ 26 Ma. This value is in good agreement with the plate age at the trench inferred from the dependence between D_m and φ (29 ± 4) Ma (*Fig. 4*). The above estimations indicate that the difference in age across the Tehuantepec Ridge at the trench is ~ 10 Ma. The age difference across Tehuantepec ridge increases from ~ 4 Ma at the southeastern edge to ~ 10 Ma at

the trench (*Fig. 4*) with a mean age discrepancy of ~ 7 Ma. This result is in good agreement with the mean age difference estimate across Tehuantepec ridge inferred from gravity modeling of ~ 7 Ma (*Manea et al., 2004*). Also, the trench age estimation of ~ 26 Ma correlates with the age of the Cocos plate at the trench offshore Costa Rica of ~ 24 Ma (*Barckhausen et al., 2001*) (*Fig. 6*).

For the second profile, also a good correlation between the ages predicted with HSCM and magnetic anomalies (*Klitgord and Mammerickx, 1982; Wilson, 1996*) for ages < ~ 6.5 Ma is obtained.

SPREADING HALF-RATES OF THE EAST PACIFIC RISE NORTH AND SOUTH OF THE CLIPPERTON FRACTURE ZONE AND TEHUANTEPEC RIDGE

The HSCM can also be used to predict the ocean bathymetry from ridge to trench, as a function of spreading rate. A reasonably good fit between the observed and predicted bathymetry is obtained using a constant half-spreading rate of 6.0 cm/yr (*Wilson, 1996*) (*Fig. 4 - dashed green line*). The best fit is obtained if we consider a period of slow half-spreading rate of ~ 2 cm/year between 9 and 14 Ma (*Fig. 4 - continuous violet line*).

On the western-flank south of Clipperton Fracture Zone, a good fit between the observed and predicted bathymetry is obtained using two half-spreading rates of 5.5 cm/yr (0 – 5 Ma) and 9.5 cm/yr (5 - 20 Ma) (*Fig. 5*). The preponderance of the asymmetric spreading between the two flanks for age > 5 Ma is obvious (*Fig. 7 - B*). However, these values of half-spreading rates (inferred from HSCM) might be used with precaution because they have large uncertainties up to 2 cm/yr. More reliable spreading rates are obtained using the magnetic anomalies, but HSCM is useful for the regions where no magnetic lineations are available.

A half-spreading rate of 6.5 cm/yr for the eastern East Pacific Rise flank, north of Clipperton Fracture is inferred from magnetic anomalies (*Wilson, 1996*). For the eastern flank, north of Tehuantepec ridge, a recent work of *Kanjorski (2003)* proposes the following half-spreading rates: 4.8 cm/yr (5.5 – 12 Ma) and 7.8 cm/yr (12 – 17 Ma). These values suggest a symmetric spreading rate rather than an asymmetric (*Fig. 7 - A*).

Within the large uncertainties in half-spreading estimations from HSCM, a comparison between the two full-spreading rates (*Fig. 7 - C*) suggests that there might be a differential full-spreading rate across the fracture zone al least for ages between 12 and 14 Ma. However, at this stage we cannot conclude that a differential full-spreading rate across Tehuantepec ridge occurred in the past, due to the lack of reliable age estimation from magnetic anomalies in Guatemala Basin.

GENETIC MODELS FOR THE TEHUANTEPEC RIDGE

The Tehuantepec Ridge as a transpressional structure

Assuming the existence of differential full-spreading rates N and S of the Tehuantepec ridge for a longer period of time (6 - 14 Ma) a tectonic model is proposed in this study. The tectonic model for the formation of the Tehuantepec Ridge (*Fig. 8*) is built on some basic constraints deduced in the previous sections: 1) the age of inception of the deformation at ~ 12 Ma; 2) the mean difference in age of about 7 Ma across the ridge; 3) the identification of a period of remarkably slow half-spreading rate for the segment of the East Pacific Rise south of the Clipperton fracture zone between ~ 14 and ~ 9 Ma (*Fig. 4*).

A cross section (A-A' in *Fig. 8*) perpendicular to the trace of the Clipperton Fracture Zone illustrates the formation of the Tehuantepec Ridge. Before 14 Ma the tectonic background is proposed to be similar with the present day situation. The two regions should have the same parallel velocity although a small difference in plate thickness must have been present because of the offset of the ridge along the Clipperton transform. At ~ 14 Ma the slowdown of spreading to the south of the Clipperton transform produces a southward jump of the Euler pole for this region (blue region on the cross-section in *Fig. 8-A*). Since the new Euler pole is now closer to the Clipperton transform, it describes a smaller circle (light blue circle, corresponding to the Pacific South-Cocos pole, in *Fig. 8-A*) than the northwestern part of the plate, which is supposed to conserve its initial pole (red dashed circle,

corresponding to the Pacific North-Cocos pole, in *Fig. 8-A*). As a consequence the plate velocities are no longer parallel but start to converge. This significant discontinuity in the velocity field at ~ 14 Ma might have generated an incipient transpressional deformation which began to build the Tehuantepec Ridge. The prominent trough of structure T3 might be a consequence of transtensional deformations between the southern Cocos plate and the deeper part in front of Tehuantepec Ridge.

In the next step of the model the Tehuantepec Ridge propagated (14 - 9 Ma) until it reaches ~ 625 km (*Fig. 8-B*). Since the southern compartment is slower, the plate becomes thicker than the lithosphere to the northwest so the depth of the ocean increases. Given that the plate velocities are now convergent and different, significant compression combined with strike-slip deformation is accommodated at the Tehuantepec Ridge. After ~ 9 Ma the difference in spreading rate decreases although it is difficult to know if this process occurs smoothly or discontinuously. Considering the plate reorganization episode proposed by *Klitgord and Mammerickx (1982)* we hypothesize that the pole shifted closer to the initial Euler pole at ~ 6.5 Ma (*Fig. 8-C*). This pole jump results in the formation of the F1 structure (*Fig. 8-C*). The T1 fracture, which points toward the end of the Tehuantepec Ridge, is likely linked with this moment of plate reorganization. Following the same tectonic scheme F1 propagates until reaching its full length of ~ 340 km (*Fig. 8-C*). Since the trace of F2 fracture is not so evident as Tehuantepec Ridge and F1, this can be attributed to a less significant pole jump somewhere between 5 and 4 - 3.5 Ma B.P, according to the last plate

reorganization period of *Klitgord and Mammerickx (1982).* This last episode can be associated with the formation of T2 fracture, which points toward the end of F1. The last episode of our model occurs in the last 4 - 3.5 Ma B.P, when the two Euler poles joined again (*Fig. 8-D*) so that transpression along the Tehuantepec Ridge ceased. The magnetic lineations for the last 4 Ma between Clipperton and Siqueiros fracture zones are well documented and indicate that spreading velocity for the two compartments bounded by the Clipperton transform was the same during this time span (although the Euler Pole changed slightly for the last 3 Ma (*Pockalny, 1997*)). A differential spreading rate of 3 cm/yr along the Tehuantepec ridge gives an amount of 150 km of strike-slip motion in 5 Ma. Indeed, the distance between the 10 Ma isochron on either side of the Tehuantepec ridge is ~ 150 km and the 10 Ma isochron just north of the Tehuantepec ridge corresponds to a ~ 15 Ma isochron in Guatemala Basin. This differential spreading rate of 3 cm/yr is in agreement with the estimate of ~ 2.5 cm/yr for ages between 14 and 12 Ma.

Although in part speculative our model explains the peculiar morphology of the Tehuantepec Ridge and adjacent Guatemala Basin as well as the significant difference in age at the trench (~ 10 Ma). The results indicate that an incipient microplate, corresponding with the deep Guatemala Basin, may have started to form out of the main Cocos plate between ~ 14 and ~ 9 Ma. In this hypothesis this microplate would have been bounded by the transpressional Tehuantepec Ridge and, possibly, by the transtensional T3 structure. Alternatively, the Cocos plate was behaving in a nonrigid fashion with the Tehuantepec Ridge and the Guatemala Basin accommodating diffuse intraplate deformation.

Response of the Tehuantepec Ridge to changes in plate motion

It has been proposed by *Menard and Atwater (1968, 1969)* that severe changes in direction of relative plate motion might change the transform and spreading-ridge orientation and also may create a new set of transform faults and short spreading ridges. One of the best examples in this case is the Kane Fracture Zone situated in the North Atlantic Ocean (*Fig. 9*). *Tucholke and Schouten (1988)* studied in detail the Kane Fracture Zone, and showed that this transform has exhibited specific structural responses to changes in relative plate motion. They proposed that during rapid change in direction of relative plate motion, the magnitude of the reorientation might be so large that a single new transform fault cannot be accommodated within the preexisting transform valley. In this case the adjustment will produce a series of short spreading centers near the existing transform valley. The trace of this readjustment on both flanks of the Middle Atlantic Ridge is represented by a series of linear structures (*Fig. 9-II-B*) very similar to the F1 and F2 structures situated at the end of the Tehuantepec ridge (*Fig. 9-III*). In this study is proposed an alternative model that might explain the fracture pattern associated with the Tehuantepec ridge. The main advantage of this model is that the fracture pattern occurred due to a change in the rotation pole and represents the adjustment in kinematics of a long-offset transform fault, between two plates, without any differential motion of a third plate (*Fig. 10*).

Two spreading ridges with a right-lateral offset represent the initial stage of the model (*Fig. 10-A*). A ~ 10° clockwise change in direction of plate motion

occurred around 12 Ma (*Fig. 10-B,C*), creating three new, short transform faults within or close to the existing transform valley and two new short spreading ridges. Surprisingly, the angle between the F1 and the Tehuantepec ridge and F1 and F2 is ~ 10°. After 12 Ma, the southern spreading ridge propagated northward, causing the end of one of the newly created short spreading centers (*Fig. 10-D*). In this way, the development of the southernmost of the three short fracture valleys on the eastern limb of the initial fracture zone ceases. The same process continues until all the short transform faults and ridges disappear, resulting the structures that we can see today (*Fig. 10-E,F,G,H,I*). The similarity between the output of this model (*Fig. 10-I*) and the actual structure on the Cocos plate is remarkable. Also the Clipperton Mountains look similar with the predicted structures on the western limb of the Clipperton fracture zone.

This model assumes that the Tehuantepec ridge existed before these severe changes in direction of relative plate motion took place. This is consistent with the model of *Klitgord and Mammerickx (1982)*, who proposed the existence of the Tehuantepec fracture zone on the former Guadalupe plate ~ 15 Ma ago. Unfortunately this model fails to explain the origin of the Tehuantepec ridge itself and the deeper bathymetry in the Guatemala Basin than in the surrounding areas. However, one of the main advantages of this model over the transpression model is a no-necessity of differential motion between N. Cocos and S. Cocos along the Tehuantepec ridge.

Acknowledgments

This study was supported by grants CONACyT G25842-T and 37293-T. Many thanks to Dr. Joann Stock whose comments and remarks improved the manuscript.

REFERENCES

Barckhausen, U., Ranero, C.R., von Huene, R., Cande, S.C., and Roeser, H.A., 2001. Revised tectonic boundaries in the Cocos Plate off Costa Rica: implication for the segmentation of the convergent margin and for plate tectonic models. *Journal of Geophysical Research, vol. 106, no. B9, pp. 19,207-19,220.*

Bravo H., Rebollar C., Uribe A., Jimenez O., 2004. Geometry and state of stress of the Wadati-Benioff zone in the Gulf of Tehuantepec, Mexico. *Journal of Geophysical Research, v. 109, 10.1029/2003JB002854.*

Couch, R. and Woodcock, S., 1981. Gravity structure of the continental margins of southwestern Mexico and northwestern Guatemala. *Journal of Geophysical Research, v. 86, p. 1829-1840.*

DSDP Leg 66. Shipboard party, 1979, Middle America Trench. *Geotimes, v. 24, p. 20-22.*

DSDP Leg 84. Shipboard party, 1982, Challenger drills again off Guatemala. *Geotimes, v. 27, p. 23-25.*

Engdahl, E. R., and Rinehart, W. A., 1991. Seismicity map of North America project in Slemmons, D. B., Engdahl, E. R., Zoback, M. D., and Blackwell, D. B., eds., Neotectonics of North America: Decade Map Volume 1 in The Decade of North American Geology Project series, *GSA, Boulder, p. 21-27.*

Gorbatov, A., and Kostoglodov, V., 1997. Maximum depth of seismicity and thermal parameter of the subducting slab: general empirical relation and its application. *Tectonophysics, v. 277, p. 165-187.*

Herron, E.M., 1972. Sea-floor spreading and the Cenozoic history of the east-central Pacific. *GSA Bulletin, v. 83, p. 1671-1692.*

Kanjorski, M.N., 2003. Cocos Plate structure along the Middle America subduction zone off Oaxaca and Guerrero, Mexico: influence of subducting plate morphology on tectonics and seismicity. *PhD thesis, University of California, San Diego.*

Klitgord, K.D. and Mammerickx, J., 1982. Northern east Pacific Rise; magnetic anomaly and bathymetric framework. *Journal of Geophysical Research, v. 87, p. 138, 6725-6750.*

Leg 206 Preliminary Report, 2003. An *in situ* section of upper oceanic crust formed by superfast seafloor spreading. *Ocean Drilling Program, Texas A&M University.*

Manea, M., Manea, V.C., Kostoglodov, V., 2003. Sediment Fill of the Middle America Trench Inferred from the Gravity Anomalies: Geofisica Internacional, v. 42, p. 603-612.

Manea, M., Manea, V.C., Kostoglodov, V., and Guzman-Speziale, M., 2004. Elastic Thickness of the Lithosphere below the Tehuantepec Ridge, *accepted Geofisica Internacional.*

Menard, H.W., and Atwater, T.M., 1968. Changes in direction of sea floor spreading. *Nature, 219, 463-467.*

Menard, H.W., and Atwater, T.M., 1969. Origin of fracture zone topography. *Nature, 222, 1037-1040.*

Pockalny, R. A., 1997. Evidence of transpression along the Clipperton transform: Implications for processes of plate boundary reorganization. *Earth and Planetary Science Letters, v. 146, p. 449–464.*

Ponce L., Gaulon R., Suarez G., Lomas E., 1992. Geometry and state of stress of the downgoing Cocos plate in the Isthmus of Tehuantepec, Mexico. *Geophysical Research Letters v. 19, p. 773-776.*

Schilt, F.S., Karig, D.E., and Truchan, M., 1982. Kinematic Evolution of the Northern Cocos Plate. *Journal of Geophysical Research, v. 87, no. B4, p. 2958-2968.*

Sonder L.J., and Pockalny R. A., 1999. Anomalous rotated abyssal hills along active transforms: distributed deformation of oceanic lithosphere. *Geology, v. 27, p. 1003-1006.*

Smith, W.H.F. and Sandwell, D.T., 1997. Global sea-floor topography from satellite altimetry and ship depth soundings. *Science, v. 277, p. 1957-1962.*

Tucholke, B.E., and Schouten, H., 1988. Kane fracture zone. *Marine Geophysical Researches, v. 10, p. 1-39.*

Turcotte, D.L., and Schubert, G., 2002, Geodynamics, 2nd edition, Cambridge University Press, New York.

Truchan, M. and Larson, R.L., 1973. Tectonic lineaments on the Cocos Plate. *Earth and Planetary Science Letters, v. 17, p. 46-432.*

Wessel, P., 1989. XOVER: A Cross-over error detector for track data. *Computers and Geoscience, v. 15, p. 333-346.*

Wilson, D.S., 1996. Fastest known spreading on the Miocene Cocos-Pacific plate boundary. *Geophysical Research Letters, v. 23, p. 3003–3006.*

FIGURE CAPTIONS

Figure 1.

Bathymetry (based on *Smith and Sandwell, 1997*) and location of the study area. The inset represents an enlargement of the study area and associated tectonic features: Tehuantepec Ridge, F1 and F2 (red continuous lines) and the two ending fractures oblique to Tehuantepec Ridge (T1 and T2); P = intersection point between Clipperton fracture zone (white dashed line) and Tehuantepec Ridge, P1 is the intersection between F1 and Tehuantepec Ridge, P2 is the intersection between F2 and F1; T1, T2 and T3 (yellow continuous lines) are deep fractures in Guatemala basin. The pink line AA' represents the cross-sections over the Tehuantepec Ridge bathymetry shown in *Fig. 2*.

Figure 2.

Bathymetry profile AA' from *Fig. 1*. Note the sharp and asymmetric morphology of the Tehuantepec ridge.

Figure 3.

The maximum depth of seismicity (*Dm*) in subduction zones is related with temperature and pressure conditions in the oceanic lithosphere sinking into the mantle. The age of oceanic plate at trench (*A*) can be inferred from the maximum depth of seismicity and the vertical component of the convergence rate (*V*) (*Gorbatov and Kostoglodov, 1997*). The product is called "*thermal parameter*" and

its dependence of *Dm* is used to infer the age of the oceanic lithosphere at the trench.

Figure 4.

Half Space Cooling Model used to predict the ocean bathymetry from ridge to trench, as a function of half-spreading rate, and also to predict the oceanic plate age in Guatemala Basin as a function of ocean depth. Using a constant spreading rate of 6 cm/yr (*Wilson, 1996*) a reasonably good fit between the observed and predicted bathymetry is obtained (dashed green line). The best fit is obtained with a slower half-spreading rate of ~ 2 cm/yr between 9 and 14 Ma.

Figure 5.

Half Space Cooling Model used to predict the ocean bathymetry at west of East Pacific Rise and south of Clipperton Fracture Zone, as a function of half-spreading rate, and also to predict the oceanic plate age on the Pacific plate as a function of ocean depth. The best fit is obtained with a half-spreading rate of 7 cm/yr between 0 and 5 Ma and 9.5 cm/yr between 5 and 20 Ma.

Figure 6.

Age map of the Cocos plate and corresponding regions of the Pacific plate. Green isochrons at 5 Ma intervals are from *Wilson (1996.* Red isochrons are from ODP Leg 206, Preliminary Report (2003). Blue lines are from Barckhausen et al. (2001). Brown arrows represent Cocos plate ages at the Middle America Trench

from *Kanjorski (2003).* Selected DSDP and ODP sites that reached basement are indicated by circles. The ages inferred from HSCM in the present study are in violet.

Figure 7.

Half and full spreading rates for North Pacific and North Cocos and South Pacific and South Cocos areas (right lower inset):

A – red-dashed line represents the half-spreading rate for North Pacific (from HSCM); blue continous line represents the half-spreading rate for North Cocos (*Kanjorski, 2003*) and green continous line is the full spreading rate for North Pacific-North Cocos;

B – red-dashed line represents the half-spreading rate for South Pacific (from HSCM); blue continous line represents the half-spreading rate for South Cocos (from HSCM) and green continous line is the full spreading rate for South Pacific-South Cocos (note the preponderance of asymmetric spreading);

C – comparison between the full spreading rate for North Pacific-North Cocos and the full spreading rate for South Pacific-South Cocos.

Figure 8.

Schematic diagram showing the tectonic reconstruction for Tehuantepec Ridge formation (magnetic lineations from *Klitgord and Mammerickx, 1982*):

A – At about 14 Ma a pole jump, only for the southeastern part of the CFZ, is proposed to be the mechanism to initiate the Tehuantepec Ridge structure. The

Euler pole for the northwestern part of CFZ remained the same. Due to the differences in velocity direction and magnitude (v1 < v2) a transpression occurs along the newly formed Tehuantepec Ridge.

B – The main part of the Guatemala Basin slow down period ceased around ~ 9 Ma and during this time another fracture F1 is formed in the same manner as Tehuantepec Ridge.

C – F1 propagates until it reaches its total length of ~ 340 km and the two Euler poles become closer.

D – The final step when the both Euler poles become one, and no more transpression occurs along Tehuantepec Ridge.

Figure 9.

I. Bathymetric map of the Kane Fracture Zone based on *Smith and Sandwell (1997)*

II. A-B The offset in flowline represents the response in relative plate motion 92 Ma.

III. Bathymetric map of the Tehuantepec Ridge based on *Smith and Sandwell (1997).* Note the similarity of structures from *II.B.* and those associated to Tehuantepec Ridge.

Figure 10.

A-G Model summarizing the severe response of a fracture zone to a approximatelly 10º clockwise change in direction of plate motion around 12 Ma.

Continuos red lines are transforms valleys. Thin parallel lines are spreading axis. Dashed twin paired lines are abandoned spreading axis. Dashed single lines represent old crust.

H-I. Resulting structures of the western and eastern limbs of the Clipperton Fracture Zone. Note the similarity of the resulting structures with FI, F2 structures associated with the Tehuantepec Ridge.

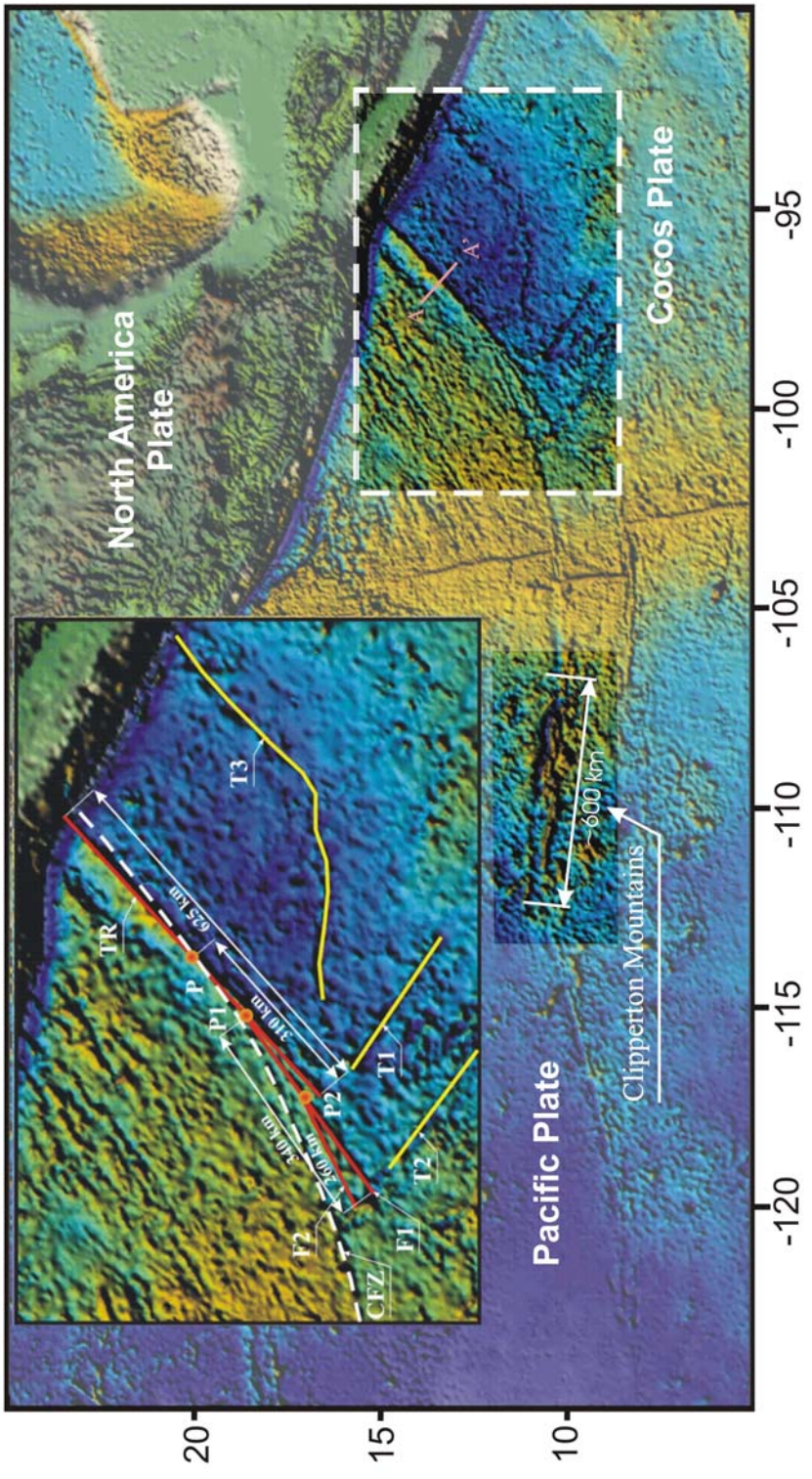
North America Plate
Cocos Plate
Pacific Plate
Clipperton Mountains
600 km
A
A'
TR
P
P1
P2
T1
T2
T3
F1
F2
CFZ
625 km
310 km
340 km
-95
-100
-105
-110
-115
-120
20
15
10

Figure 1

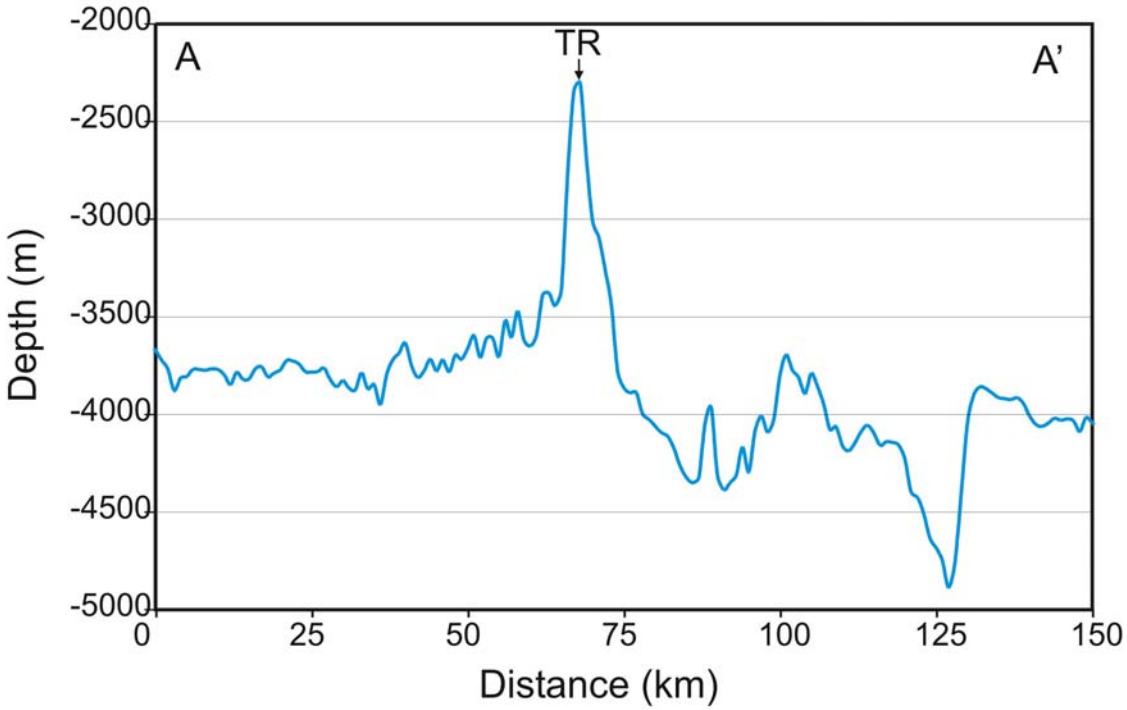
A
TR
A'
-2000
-2500
-3000
-3500
-4000
-4500
-5000
Depth (m)
0
25
50
75
100
125
150
Distance (km)

Figure 2

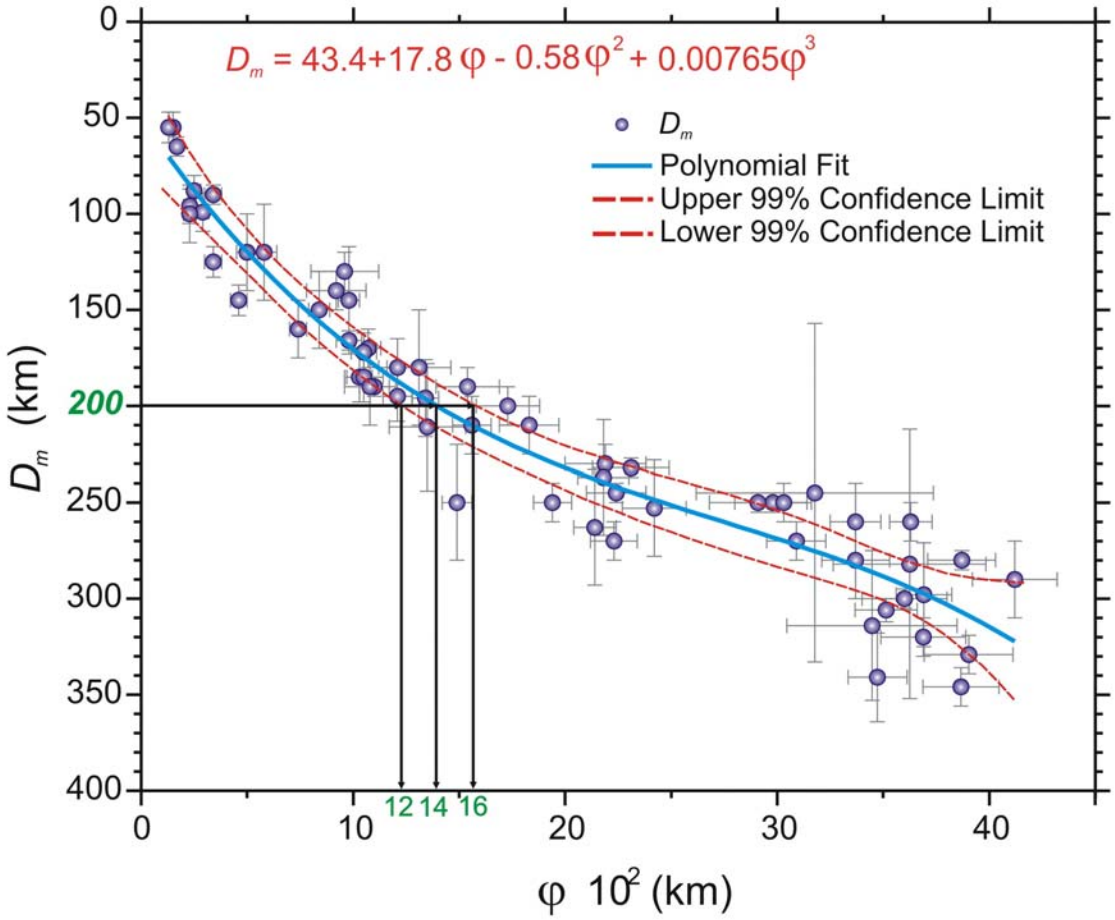
$D_m = 43.4+17.8\,\varphi - 0.58\,\varphi^2 + 0.00765\varphi^3$
D_m
Polynomial Fit
Upper 99% Confidence Limit
Lower 99% Confidence Limit
D_m (km)
0
50
100
150
200
250
300
350
400
12 14 16
0
10
20
30
40
φ 10^2 (km)

Figure 3

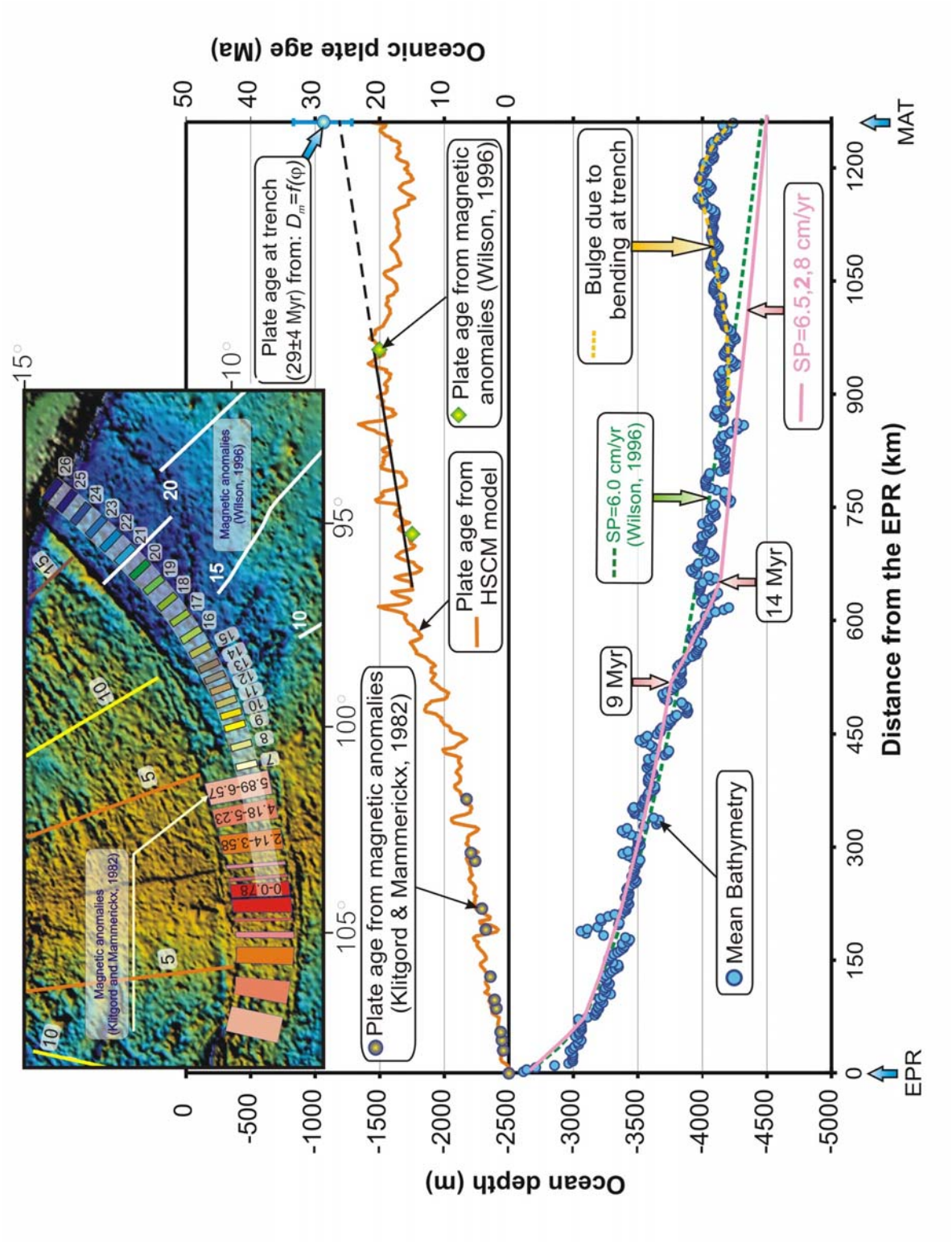
Oceanic plate age (Ma)
Ocean depth (m)
Distance from the EPR (km)
EPR
MAT
Plate age at trench (29±4 Myr) from: $D_m=f(\varphi)$
Plate age from magnetic anomalies (Klitgord & Mammerickx, 1982)
Plate age from HSCM model
Plate age from magnetic anomalies (Wilson, 1996)
Bulge due to bending at trench
SP=6.0 cm/yr (Wilson, 1996)
SP=6.5,2,8 cm/yr
9 Myr
14 Myr
Mean Bathymetry
Magnetic anomalies (Klitgord and Mammerickx, 1982)
Magnetic anomalies (Wilson, 1996)

Figure 4

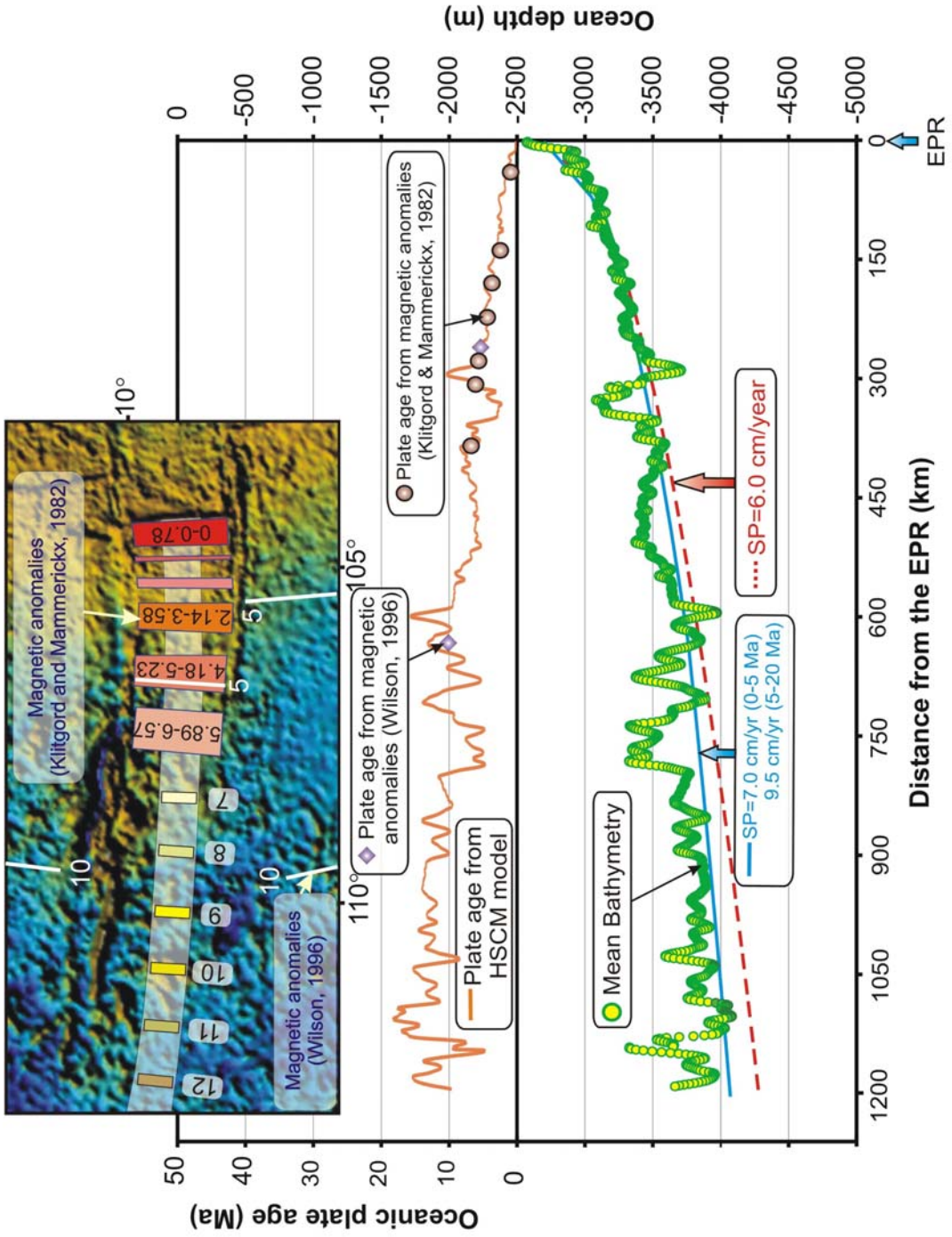
Ocean depth (m)
0
-500
-1000
-1500
-2000
-2500
-3000
-3500
-4000
-4500
-5000
EPR
0
150
300
450
600
750
900
1050
1200
Distance from the EPR (km)
Plate age from magnetic anomalies (Klitgord & Mammerickx, 1982)
Plate age from magnetic anomalies (Wilson, 1996)
Plate age from HSCM model
Mean Bathymetry
SP=6.0 cm/year
SP=7.0 cm/yr (0-5 Ma)
9.5 cm/yr (5-20 Ma)
Oceanic plate age (Ma)
50
40
30
20
10
0
110°
105°
10°
Magnetic anomalies (Klitgord and Mammerickx, 1982)
Magnetic anomalies (Wilson, 1996)
0-0.78
2.14-3.58
4.18-5.23
5.89-6.57
5
7
8
9
10
11
12

Figure 5

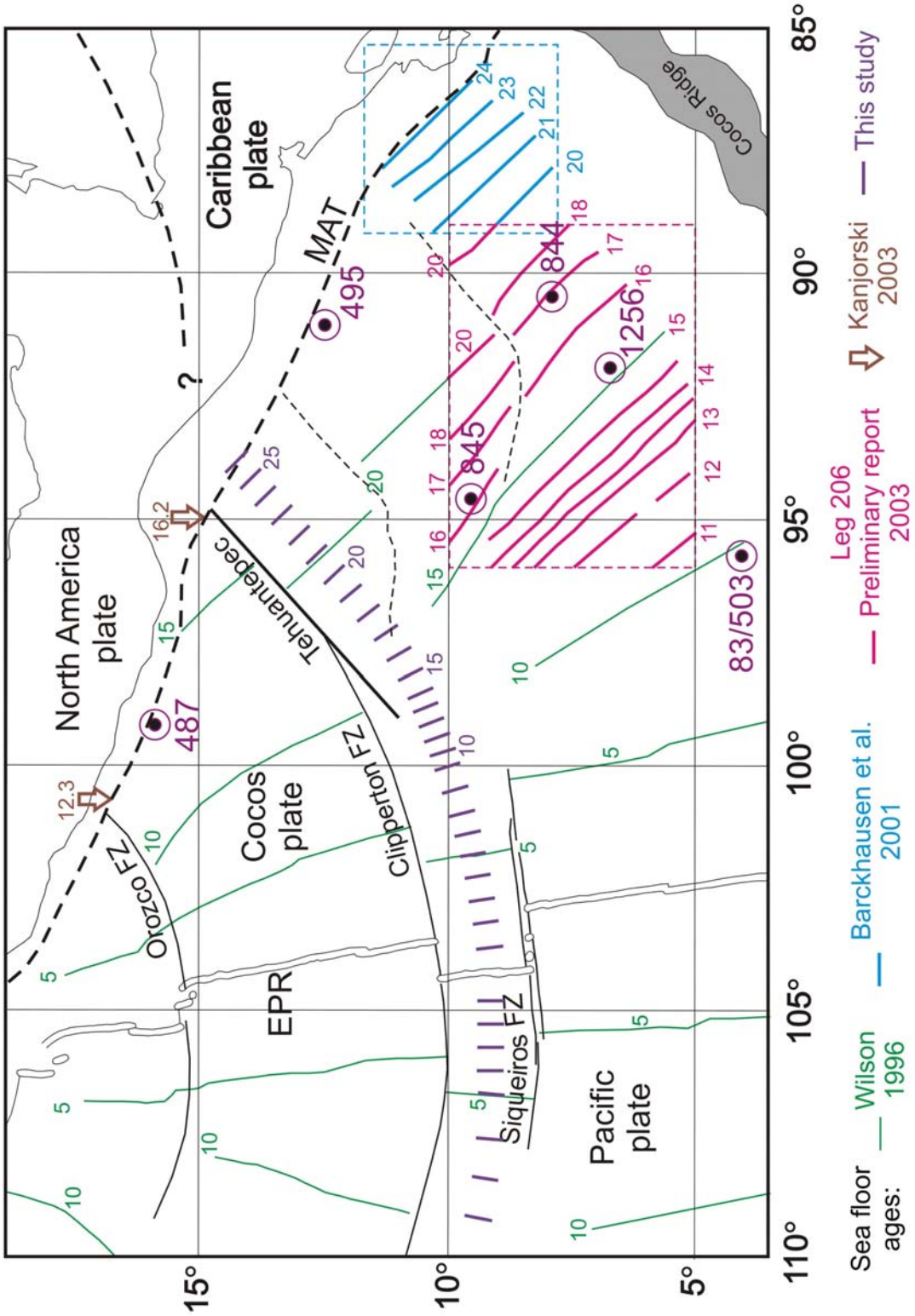
North America plate
Caribbean plate
Cocos plate
Pacific plate
MAT
Tehuantepec
Orozco FZ
Clipperton FZ
Siqueiros FZ
EPR
Cocos Ridge
487
495
844
845
1256
83/503
?
15°
10°
5°
85°
90°
95°
100°
105°
110°
Sea floor ages:
Wilson 1996
Barckhausen et al. 2001
This study
Leg 206 Preliminary report 2003
Kanjorski 2003

Figure 6

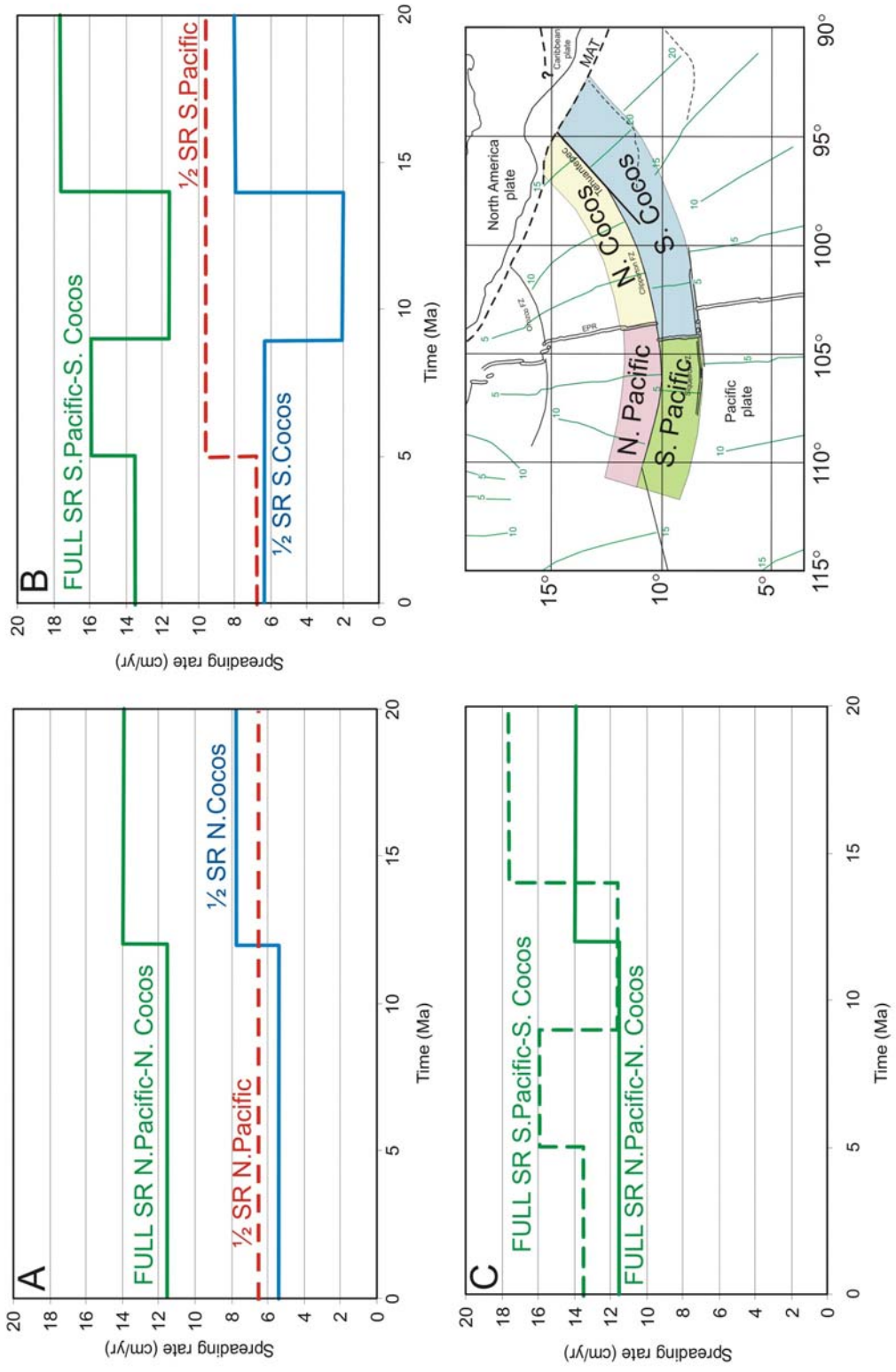
B
FULL SR S.Pacific-S. Cocos
½ SR S.Pacific
½ SR S.Cocos
Spreading rate (cm/yr)
Time (Ma)
A
FULL SR N.Pacific-N. Cocos
½ SR N.Cocos
½ SR N.Pacific
C
FULL SR S.Pacific-S. Cocos
FULL SR N.Pacific-N. Cocos
North America plate
Caribbean plate
MAT
N. Cocos
S. Cocos
N. Pacific
S. Pacific
Pacific plate
15°
10°
5°
115°
110°
105°
100°
95°
90°

Figure 7

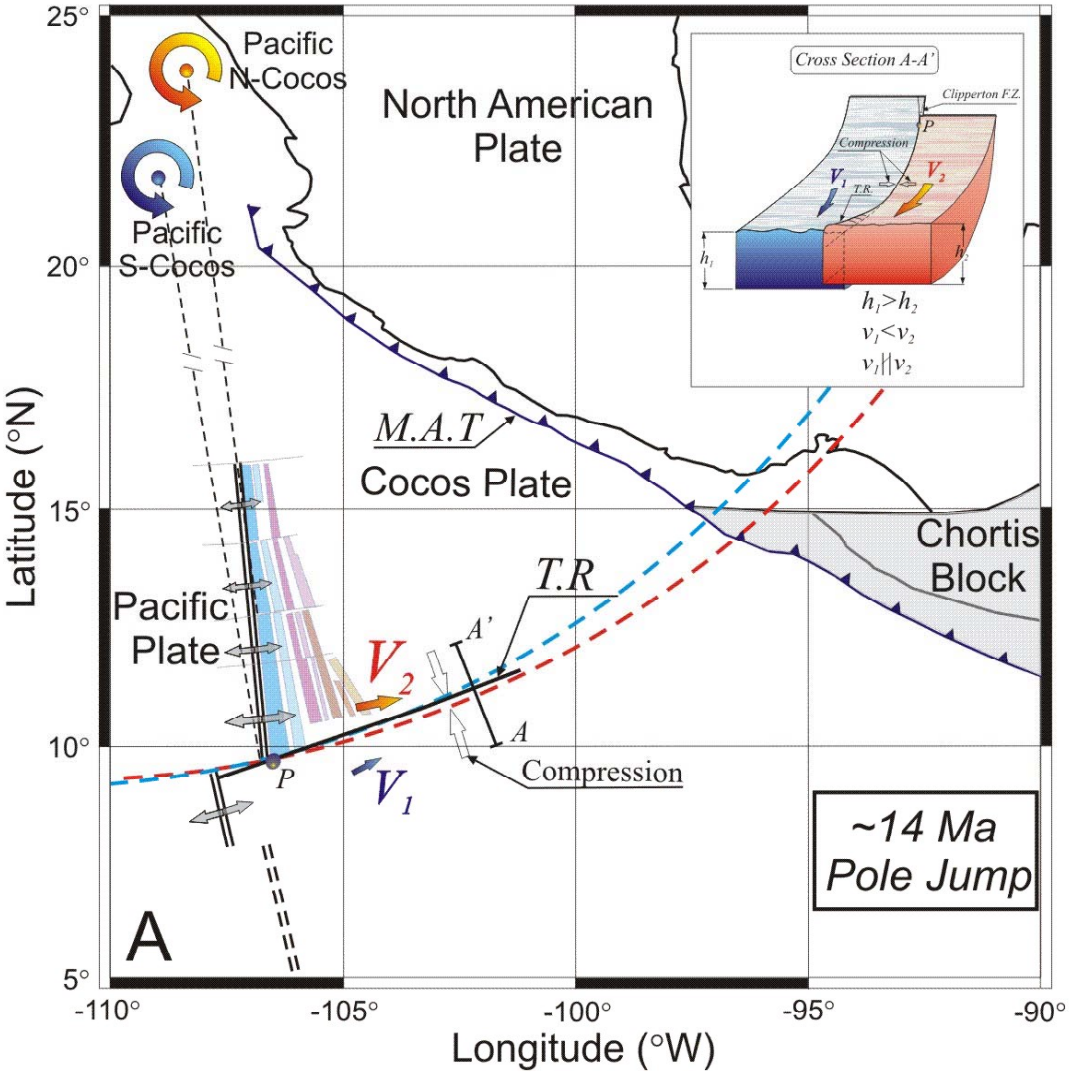
Pacific
N-Cocos
Pacific
S-Cocos
North American
Plate
Cross Section A-A'
Clipperton F.Z.
P
Compression
V_1
T.R.
V_2
h_1
h_2
$h_1>h_2$
$v_1<v_2$
$v_1 \| v_2$
M.A.T
Cocos Plate
Chortis
Block
T.R
Pacific
Plate
V_2
A'
A
Compression
P
V_1
~14 Ma
Pole Jump
A
25°
20°
15°
10°
5°
-110°
-105°
-100°
-95°
-90°
Latitude (°N)
Longitude (°W)

Figure 8 A

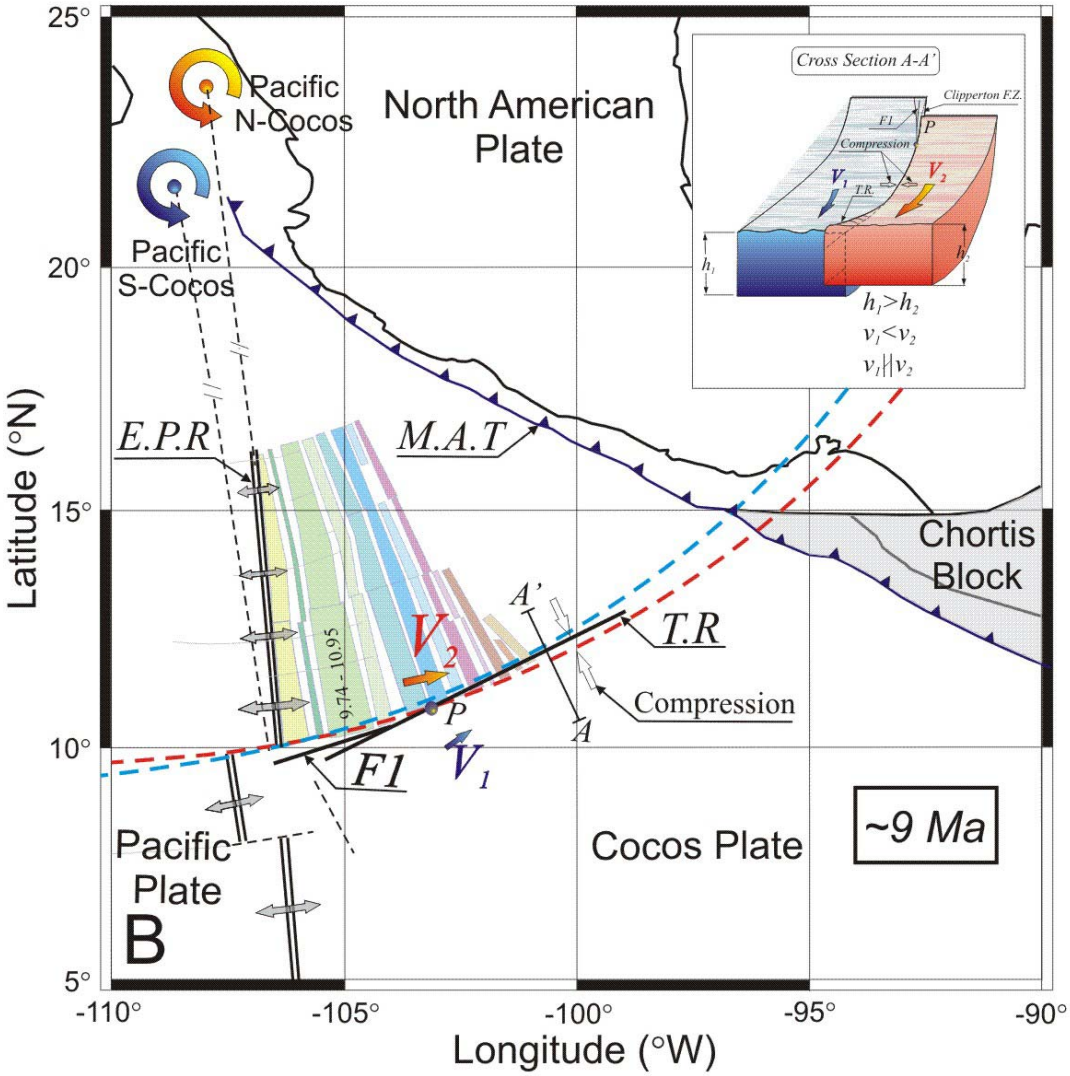
Pacific
N-Cocos
Pacific
S-Cocos
North American
Plate
Cross Section A-A'
Clipperton F.Z.
F1
P
Compression
V1
T.R
V2
h1
h2
h1>h2
v1<v2
v1||v2
E.P.R
M.A.T
Chortis
Block
A'
T.R
V2
9.74 - 10.95
P
Compression
A
F1
V1
Pacific
Plate
B
Cocos Plate
~9 Ma
25°
20°
15°
10°
5°
-110°
-105°
-100°
-95°
-90°
Latitude (°N)
Longitude (°W)

Figure 8 B

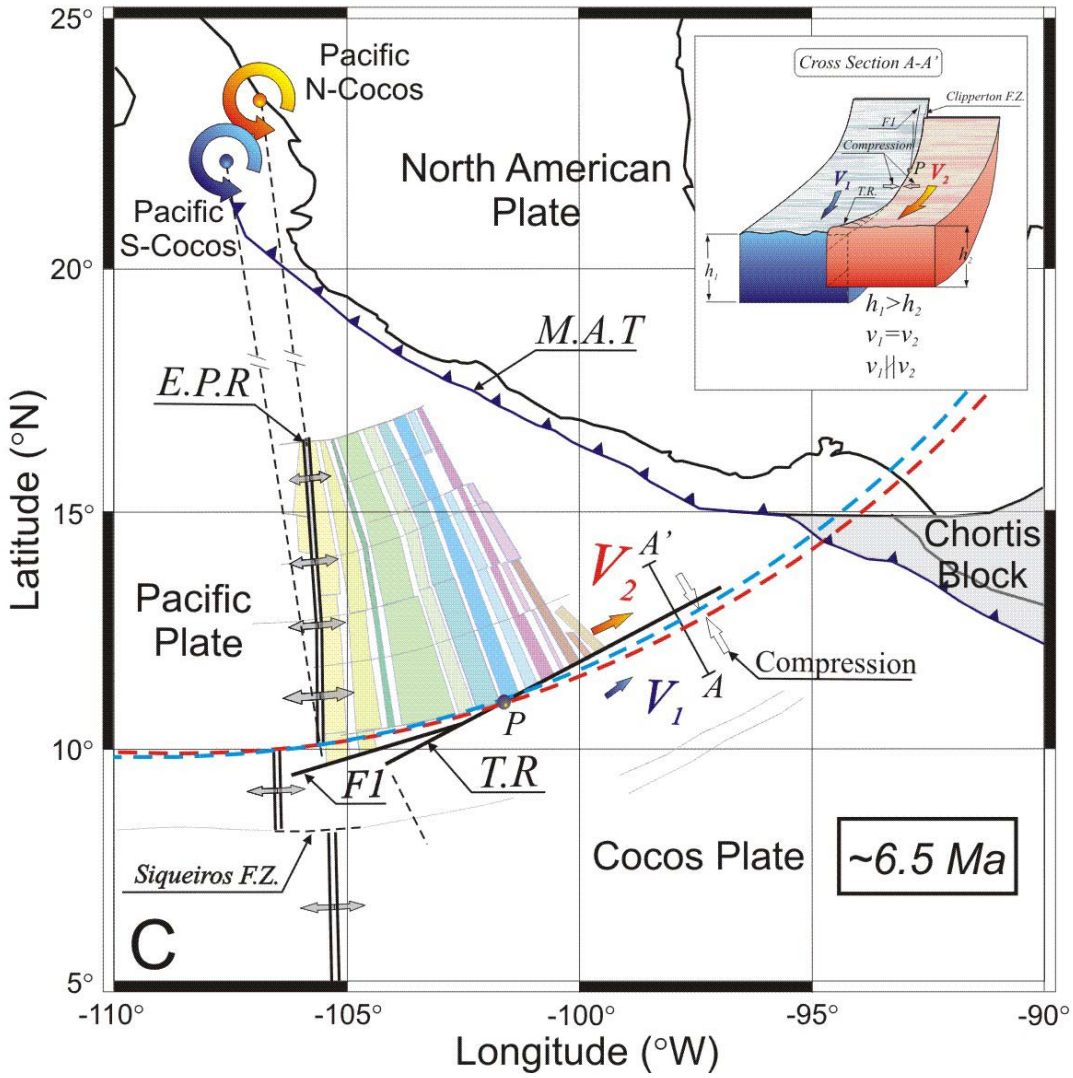
Pacific
N-Cocos
Pacific
S-Cocos
North American
Plate
M.A.T
E.P.R
Pacific
Plate
Chortis
Block
Cocos Plate
~6.5 Ma
Compression
F1
T.R
P
A'
A
Siqueiros F.Z.
C
Cross Section A-A'
Clipperton F.Z.
Compression
$h_1>h_2$
$v_1=v_2$
$v_1 \| v_2$
25°
20°
15°
10°
5°
-110°
-105°
-100°
-95°
-90°
Latitude (°N)
Longitude (°W)

Figure 8 C

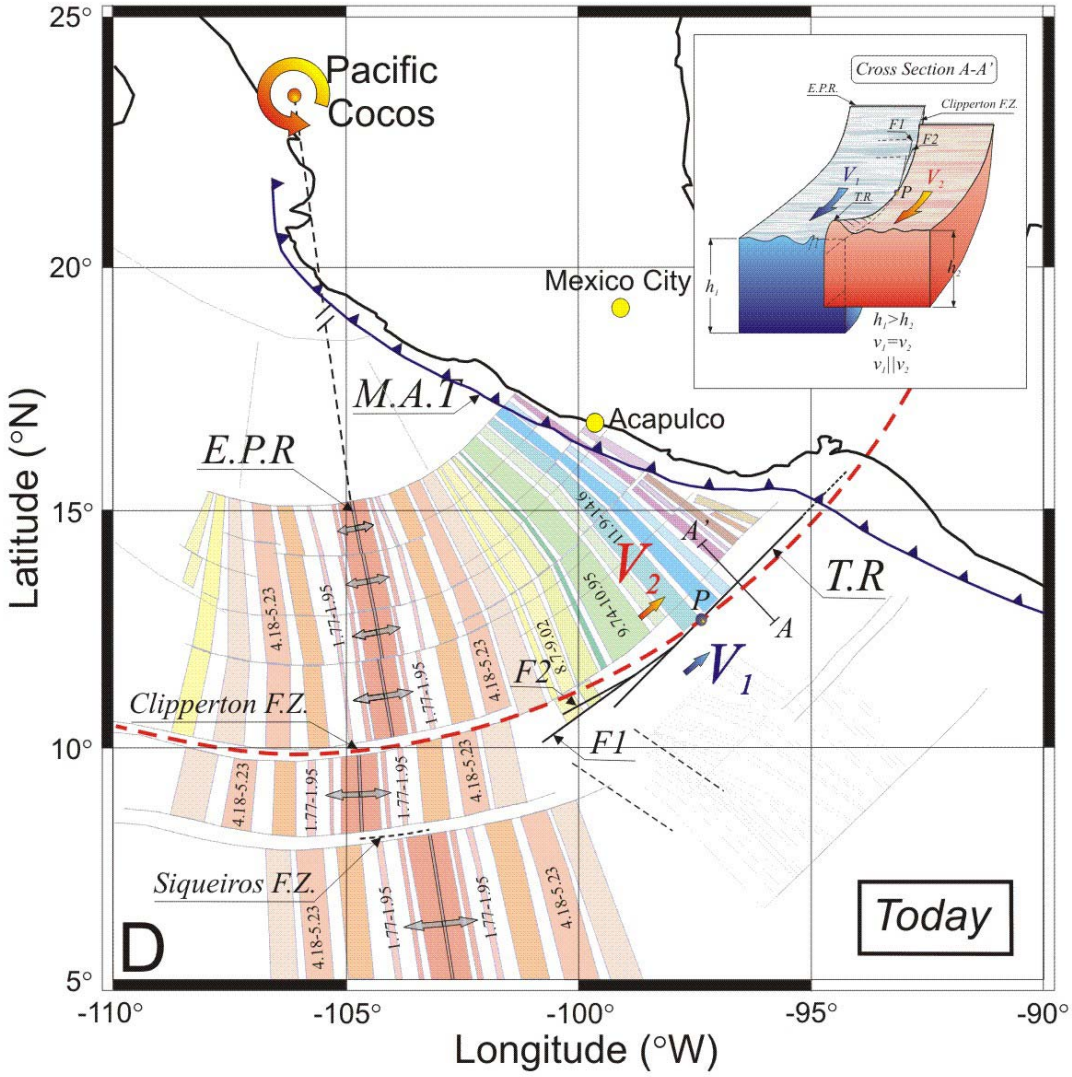
Pacific
Cocos
Mexico City
Acapulco
M.A.T
E.P.R
Clipperton F.Z.
Siqueiros F.Z.
F1
F2
T.R
A
A'
P
V1
V2
D
Today
Cross Section A-A'
E.P.R.
Clipperton F.Z.
F1
F2
TR
h1>h2
v1=v2
v1||v2
25°
20°
15°
10°
5°
-110°
-105°
-100°
-95°
-90°
Latitude (°N)
Longitude (°W)

Figure 8 D

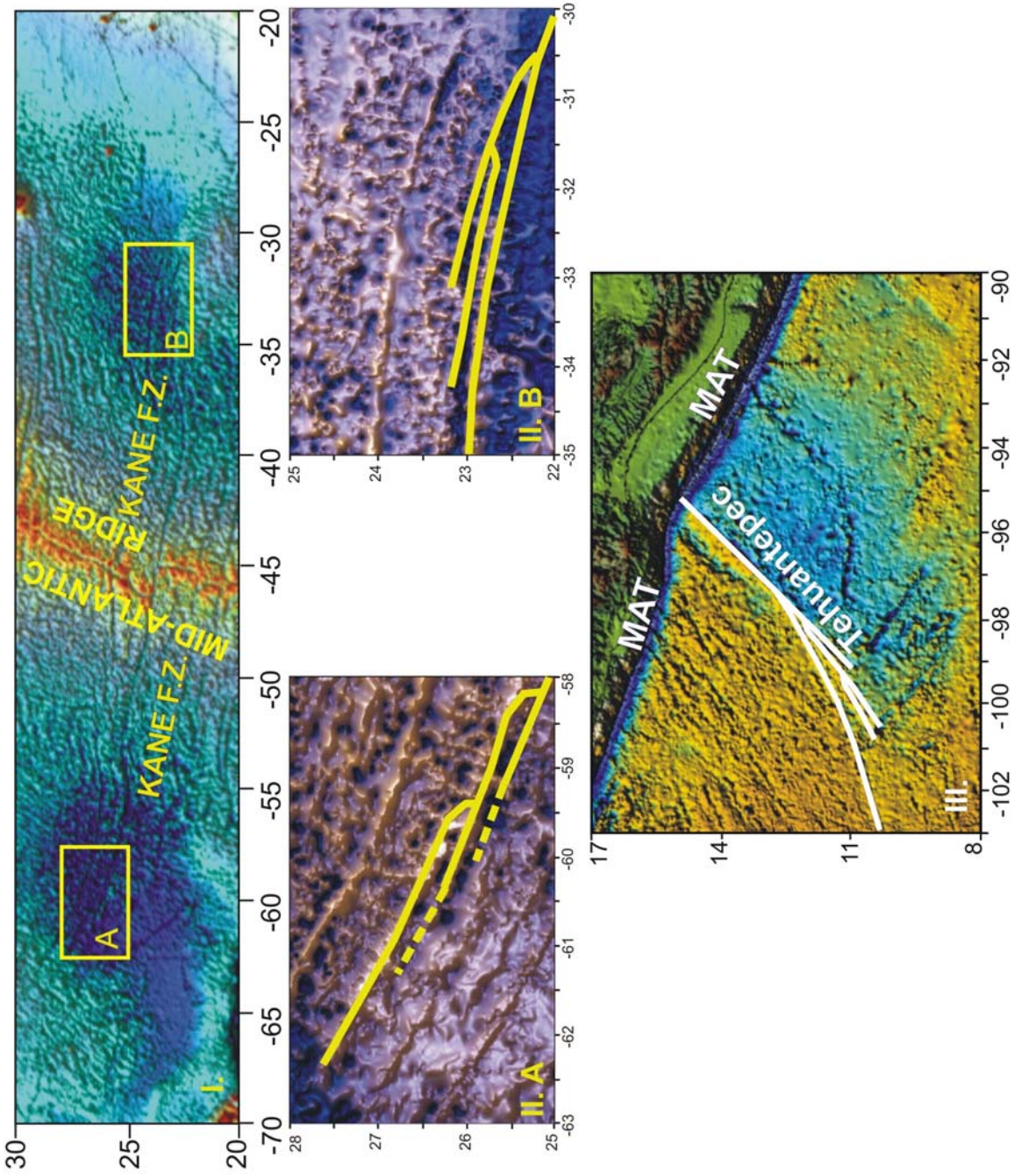
I.
A
B
MID-ATLANTIC RIDGE
KANE F.Z.
KANE F.Z.
II. A
II. B
III.
MAT
MAT
Tehuantepec
30
25
20
-70
-65
-60
-55
-50
-45
-40
-35
-30
-25
-20
28
27
26
25
-63
-58
-59
-60
-61
-62
24
23
22
-30
-31
-32
-33
-34
-35
17
14
11
8
-102
-100
-98
-96
-94
-92
-90

Figure 9

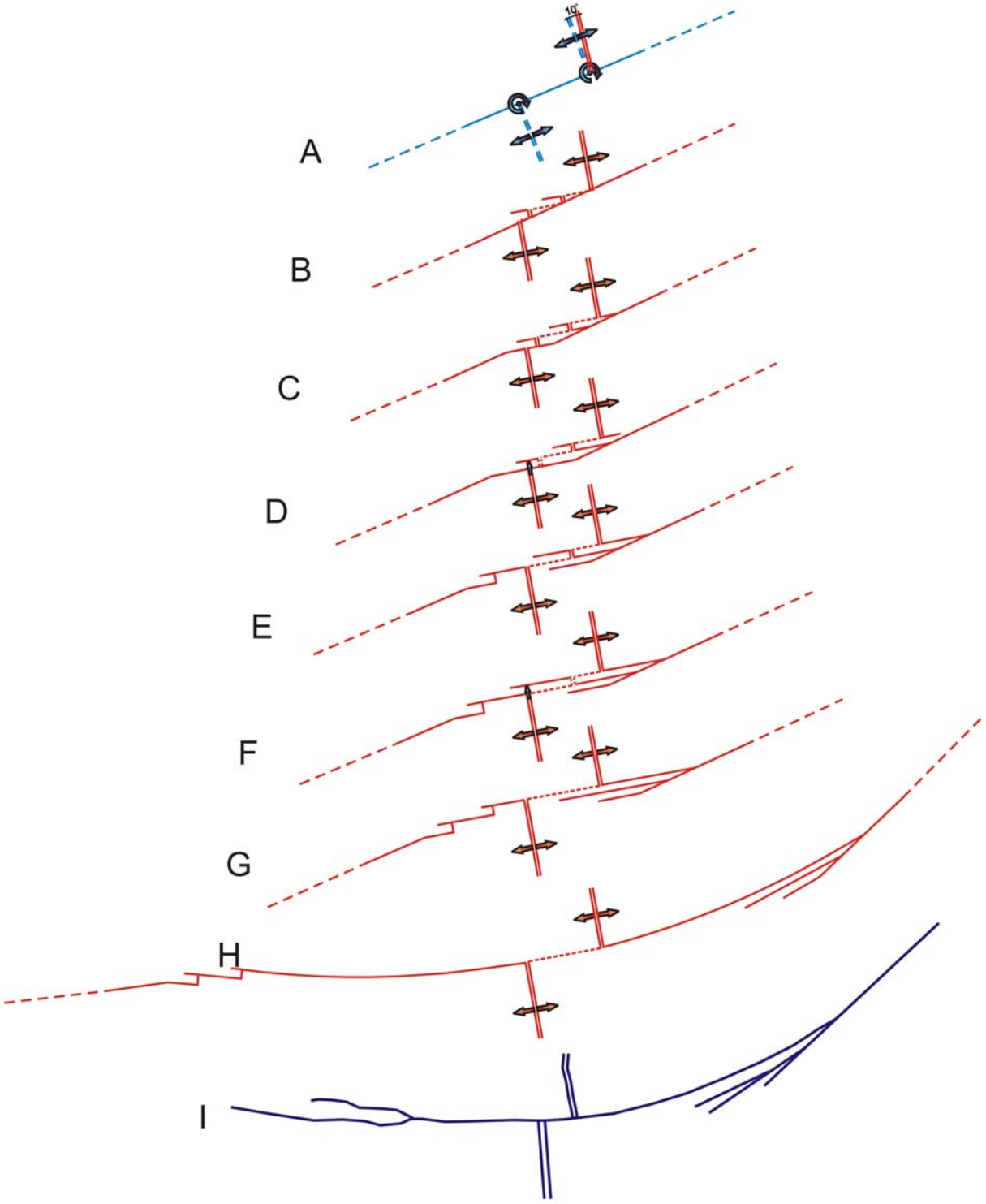

Figure 10

V. DISCUSIÓN Y CONCLUSIONES

El volumen específico del relleno sedimentario en la trinchera mesoamericana ha sido analizado usando perfiles batimétricos y gravimétricos que cruzan la trinchera.

El mínimo de la anomalía de gravedad de aire libre a lo largo de la trinchera mesoamericana no coincide con el mínimo batimétrico. Esta diferencia es pequeña ξ = 0.44 - 0.80 km para la parte noroeste de la trinchera (Jalisco y Michoacán). La diferencia aumenta de una manera sistemática en la parte central de la trinchera hasta ξ = 2.05 - 9.19 km (Guerrero y Oaxaca), para que después, enfrente de la Cordillera de Tehuantepec disminuya otra vez llegando a ξ = 0.5 - 2.18 km. A continuación, enfrente de la cuenca de Guatemala, esa diferencia se mantiene aproximadamente constante a lo largo de la trinchera (ξ = 2.73 - 4.80 km), exceptuando algunos perfiles con gran contribución terrígena. Lo mismo pasa en la parte noroeste, en donde la contribución terrígena de algunos ríos, como el Rió Verde, trae consigo una desviación de la tendencia general de los volúmenes específicos estimados.

El volumen específico del relleno sedimentario y la edad de la litosfera en la trinchera para la cuenca de Guatemala, no cambian mucho. Este volumen específico es más bajo que en la parte noroeste de la trinchera mesoamericana.

La dependencia entre el volumen específico como función de la velocidad de subducción muestra una tendencia general de aumento del volumen con la tasa de convergencia. Esta tendencia se nota más en la parte noroeste de la

trinchera que en la parte sureste (enfrente de la cuenca de Guatemala, en donde los bordes entre las placas de Norte-América y Caribe y la tasa de convergencia no son bien conocidos).

Los resultados de este estudio muestran que es posible que estos dos segmentos de la trinchera (noroeste y sureste) delimitados por la cordillera de Tehuantepec tengan regímenes sedimentarios distintos. La tasa de sedimentación terrígena promedio, S_t, en la trinchera enfrente de la cuenca de Guatemala se espera que sea más baja que en la parte noroeste debido a un cambio dramático en la distancia entre la costa y la trinchera marcado por la presencia de la cordillera de Tehuantepec. La distancia más grande determina una disminución en la tasa de sedimentación terrígena en la trinchera.

Una diferencia en el acoplamiento de la placa puede ser considerada como otro factor aceptable, que pudo haber afectado la erosión y la acreción de los sedimentos de la placa oceánica subducida. Se puede esperar un acoplamiento más grande entre las placas en la parte noroeste de la cordillera de Tehuantepec, en donde la placa de Cocos es relativamente joven (A < 16 Ma).

Un valor relativamente pequeño estimado por medio del modelado de las anomalías de gravedad de aire libre es la mejor explicación para la subducción de sedimentos. Los volúmenes de los sedimentos estimados en este estudio son menores a los volúmenes calculados en la hipótesis de que todos los depósitos transportados por la litosfera oceánica hacia la trinchera hubieran sido acrecionados. De todos modos, una evaluación del balance de los sedimentos subducidos/ acrecionados no es posible todavía en la trinchera mesoamericana

(incluso en una escala global) debido a la falta de datos confiables. Para una mejor evaluación del volumen especifico del relleno sedimentario se necesitan algunos perfiles sísmicos perpendiculares a la trinchera para proporcionar las profundidades de la superficie del basamento acústico y el espesor de los depósitos.

Los perfiles batimétricos que cruzan la zona de la cordillera de Tehuantepec indican la existencia de dos áreas distintas separadas por esta cordillera: el área noroeste, caracterizada por profundidades entre 3,500 – 3,900 m y el área sureste (que corresponde a la cuenca de Guatemala) con profundidades entre 4,200 – 4,800 m. Entre las dos áreas hay una diferencia de ~ 1,000 m. Un mínimo gravimétrico de ~ -7 - -8 mGal muestra la ubicación del límite entre las dos áreas. El modelo gravimétrico 2D da una imagen que está de acuerdo con las estimaciones edad/ profundidad y edad/ espesor de la litosfera y muestra que el Tehuantepec es un límite entre estas dos partes (la parte sureste que tiene un espesor mayor que la parte noroeste).

Un método muy útil en la análisis de las grandes estructuras formadas sobre las placas oceánicas es el método espectral de la admitancia. Para calcular la admitancia se han procesado 7 perfiles batimétricos y gravimétricos que cruzan la cordillera de Tehuantepec. Los resultados muestran para $0.0065 < k < 0.4$ una coherencia mayor de 0.5 sugiriendo que gran parte de la energía de la anomalía de gravedad es causada por la batimetría.

La disminución de la admitancia para números de onda pequeños es producida por la isostasia, sugiriendo que la cordillera está compensada

isostáticamente. Asimismo, las alas laterales del filtro de los coeficientes (que es el inverso de la FFT de la admitancia) son negativas y no tienden asimtóticamente hacia el valor de cero indicando que la estructura está compensada. Para comprobar que el método ha sido aplicado con éxito se hizo una comparación entre la gravedad observada y la gravedad predicha. La gravedad predicha ha sido obtenida aplicando la transformanda rápida inversa de Fourier (IFFT) al producto entre la admitancia y la FFT de la batimetría. La comparación muestra que la técnica de la admitancia es la apropiada para este estudio.

Al comparar las curvas teóricas para la compensación isostática de Airy con los datos de admitancia observados, se nota que este modelo ajusta bien para un espesor de la corteza oceánica de 20 - 40 km. Estos valores son mayores que los valores aceptados para el espesor de una corteza oceánica (7 - 8 km). Como consecuencia, el modelo de Airy no puede ser aceptado como mecanismo de compensación isostática para la cordillera de Tehuantepec. En cambio, el modelo de compensación por la flexura de una placa, con un espesor elástico Te = 10 ± 5 km, es mejor.

Usando el modelo de enfriamiento de la placa oceánica con la edad para una temperatura de corte de 450 °C (la transición entre el comportamiento elástico a uno dúctil) ha sido obtenida una edad de ~ 8 +9/-6 Ma para la formación de la cordillera de Tehuantepec sobre la placa de Cocos.

El modelo gravimétrico para un perfil promedio que cruza la cordillera de Tehuantepec nos da una imagen sobre la separación de la placa de Cocos en dos

partes distintas. La parte de noroeste más joven tiene un espesor menor que la parte sureste, esto estando de acuerdo con las estimaciones entre edad/ profundidad y edad /espesor elástico de la litosfera.

Por la razón de tener una placa más vieja de un lado y otra más joven del otro lado de la cordillera de Tehuantepec las mediciones de dos diferentes ***Te*** se mezclaron en una análisis. Probablemente esto seria la razón por la dispersión considerable para longitudes de onda cortas (4 - 6 km). Separando los datos en dos partes distintas (NW y SE de la cordillera), la admitancia para longitudes de onda corta parece tener menos dispersión. Este resultado sugiere que podría ser una diferencia importante en la edad de un lado y de otro de la cordillera y por eso tener diferentes ***Te***. Para encontrar esta diferencia se calculó la admitancia para ambos lados, en NW y SE, por separado. Los resultados aparentemente muestran que en la parte NW (en donde la placa e s más joven) el ***Te*** es 5 - 10 km, mientras en la parte SE el ***Te*** es ~ 10 - 15 km. La importante dispersión en la admitancia para la región de NW podría ser causada por la longitud muy limitada de los perfiles (187 km) utilizados en la análisis. En cambio, en la parte SE, por los perfiles más largos (325 km), se ha encontrado menos dispersión para números de onda bajas y estimaciones mejores del ***Te.*** Por las estimaciones inconcluyentes del ***Te*** para la parte NW no podemos concluir que hay una diferencia importante en el ***Te*** para los dos lados de la cordillera. De este modo se justifica el uso de un modelo sencillo que supone un único valor para el ***Te*** debajo del Tehuantepec.

Para la estimación de la edad de la placa de Cocos en la trinchera, frente a la cuenca de Guatemala, se usó la relación entre la profundidad máxima de los

sismos y la componente vertical de la velocidad de convergencia. La edad promedia en la trinchera que se obtuvo usando este método es de ~ 29 ± 4 Ma.

Un método independiente de estimación de la edad de la placa de Cocos en la cuenca de Guatemala es el modelo del enfriamiento de la placa oceánica con el tiempo. La ecuación de este modelo predice que la profundidad del océano aumenta con la raíz cuadrada de la edad de la placa oceánica. Los resultados muestran una diferencia promedio de edad a ambos lados de la cordillera de Tehuantepec de 6 - 7 Ma. Este resultado está en buena correlación con el modelado gravimétrico 2D, que muestra una diferencia de espesor de la litosfera oceánica de ~ 10 km (~ 6 Ma). También se ha obtenido una buena correlación entre las edades estimadas con el modelo del enfriamiento de la placa y las edades obtenidas a través de las anomalías magnéticas disponibles (para edades menores de 6.5 Ma). Asimismo, se ha obtenido una edad de ~ 27 Ma para la trinchera, valor que está dentro del rango de edades (29 ± 4 Ma) inferidas a través de la profundidad máxima de los terremotos y la tasa de convergencia.

El modelo de enfriamiento de la placa con la edad se puede usar para predecir la batimetría del océano desde la dorsal hacia la trinchera, como función de la tasa de expansión. Se ha obtenido una buena correlación entre la batimetría predicha y la observada, usándose una tasa de expansión por la mitad de 6 cm/ año. El mejor modelo se obtuvo considerando un periodo de ~ 5 Ma (entre 9 y 14 Ma), cuando pudo haberse producido un alentamiento en la tasa de expansión por la mitad bajando hasta ~ 2 cm/ año.

Finalmente en este estudio se proponen dos modelos genéticos para la formación de la cordillera de Tehuantepec.

El primer modelo trata de ofrecer una hipótesis sobre el origen de la cordillera de Tehuantepec y la cuenca de Guatemala, asimismo sobre la diferencia de edad entre las dos áreas de la placa de Cocos. Los resultados muestran que pudo haber existido una microplaca, que corresponde a la cuenca de Guatemala. Esta microplaca se pudo haber formado de la placa de Cocos entre ~ 14 y ~ 3.5 Ma. En este escenario, la placa de Cocos pudo haberse comportado de una manera no rígida y como consecuencia, la cordillera de Tehuantepec y la cuenca de Guatemala se acomodaron como una zona de deformación intraplaca difusa.

El modelo alternativo propone una posible explicación para la formación de las estructuras asociadas a la cordillera de Tehuantepec. Esta explicación podría ser relacionada con unos cambios importantes en la dirección de movimiento relativo de las placas que pudo haber causado cambios en la orientación de la falla transformante y del spreading-ridge y que pudo haber creado nuevas fallas y spreading-ridge cortos. Este modelo supone que la cordillera de Tehuantepec existió antes de estos cambios importantes en la dirección en cual ocurrió el movimiento relativo de las placas. Desgraciadamente, este modelo no puede explicar el origen de la misma cordillera de Tehuantepec y la mayor profundidad que se encuentra en la cuenca de Guatemala comparándola con las de la placa de Cocos. De todos modos, la mayor ventaja de este modelo es que no necesita un movimiento diferencial entre las parte N y S de la placa de Cocos a lo larga de la cordillera de Tehuantepec.